

# **HYDROGEN RESPONSE OF PALLADIUM NANOPARTICLES AND SURFACE MODIFIED FILMS**

*Thesis submitted in fulfillment for the requirement of the degree of*

**DOCTOR OF PHILOSOPHY**

*in*

**PHYSICS**

*by*

**DIKSHITA GUPTA**

**[Enrollment No.-126901]**



DEPARTMENT OF PHYSICS & MATERIALS SCIENCE

JAYPEE UNIVERSITY OF INFORMATION TECHNOLOGY WAKNAGHAT  
SOLAN (H.P)-173234, INDIA

JUNE 2016



**JAYPEE UNIVERSITY OF INFORMATION TECHNOLOGY**  
(Established by H.P. State Legislative vide Act No. 14 of 2002)  
Waknaghat, P.O. Dumehar Bani, Kandaghat, Distt. Solan – 173234 (H.P.) INDIA  
Website : [www.juit.ac.in](http://www.juit.ac.in)  
Phone No. (91) 07192-257999 (30 Lines)  
Fax: (91) 01792 245362

Date: June 11, 2016

## **DECLARATION**

This is to certify that the work reported in the Ph.D. thesis entitled **“HYDROGEN RESPONSE OF PALLADIUM NANOPARTICLES AND SURFACE MODIFIED FILMS”**, is an authentic record of my work carried out under the supervision of Dr.P.B.Barman and Dr. S.K Hazra. I have not submitted this work elsewhere for any other degree or diploma.

*Dikshita*

**Dikshita Gupta**  
Department of Physics & Materials Science  
Jaypee University of Information Technology, India.



# JAYPEE UNIVERSITY OF INFORMATION TECHNOLOGY

(Established by H.P. State Legislature vide Act No. 14 of 2002)

P.O. Waknaghat, Teh. Kandaghat, Distt. Solan - 173234 (H.P.) INDIA

Website : [www.juit.ac.in](http://www.juit.ac.in)

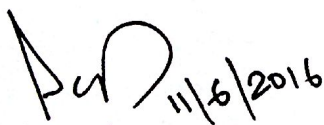
Phone No. +91-01792-257999 (30 Lines).

Fax: +91-01792-245362

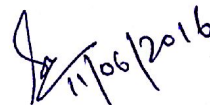
Date: June 11, 2016

## CERTIFICATE

This is to certify that the work reported in the Ph.D. thesis entitled, "**HYDROGEN RESPONSE OF PALLADIUM NANOPARTICLES AND SURFACE MODIFIED FILMS**", submitted by **Ms. Dikshita Gupta** at **Jaypee University of Information Technology, Waknaghat, India**, is a bonafide record of her original work carried out under our supervision. This work has not been submitted partially or wholly to any other University or Institute for the award of this or any other degree or diploma.

 11/6/2016

(Signature of Supervisor)  
Dr. P.B. Barman  
Professor and Head  
Deptt. of Physics & Materials Science

 11/06/2016

(Signature of Co-Supervisor)  
Dr. S.K. Hazra  
Assistant Professor  
Deptt. of Physics & Materials Science

## **ACKNOWLEDGEMENT**

Research is very interesting and challenging venture considering the tremendous amount of input necessary for its completion and contribution of various people in this endeavor. So it is indeed my moral duty to acknowledge sincere gratitude and thanks to all those who encouraged, guided and helped me in completing and presenting of the present work.

I wish to express my deepest appreciation to Dr. Surajit Kumar Hazra and Dr. P.B.Barman, as my supervisors. Their guidance has made my research an enjoyable and rewarding journey. Heartiest thanks to Dr. Surajit Kumar Hazra for spending countless hours reading my manuscripts.

I would like to thank my DPMC members Dr. Ghanshyam Singh, Dr. Sunil Kumar Khah, Dr. Ragini Raj Singh to listen to my semester progress presentations and to give valuable suggestions. I extend my warm and sincere thanks to all the faculty members of the Department of Physics & Materials Science.

In addition, I owe my thanks to Dr. Pankaj Sharma for providing assistance in UV-vis spectroscopic analysis. I want to acknowledge SAIF, Punjab University for providing instrumentation facility like TEM, Jadavpur University for XRD, AFM, and hydrogen sensing facility.

Over the past 3 and half years, I have received support and encouragement from a great number of individuals. Firstly, I am greatly fortunate to have my loving parents and an extremely supporting husband who have always been a source of comfort and hope when I needed it. I could not have completed this milestone without the support and patience of my husband, Mr. Sunny Gupta and my in-laws. No words or phrases can convey my gratitude to my parents for all they have done for me all these years. Many thanks to my parents for giving me a push to get this PhD started and get completed. I can never forget to remember my sister Ms. Deepika whose healthy criticism and motivation always boosted me to achieve something bigger and better in my life.

I would like to thank my colleagues and friends for their support-Abhishek Kandwal, Pawan Thakur, Hitanshu Minhas, Jai Vardhan, Sarita Kango, Rajinder Kumar, Rajinder Singh, Bandna Thakur, Prashant Thakur, Rohit Thakur, Neha Kondal, Johnny Dhiman, Asha Sharma.

Many thanks to my roommates Ira Vashisht, Tamanna Sharma, Neha Sharma, Priya Panigrahi and Mansi Sharda. They have been friends in listening to all my problems and frustrations. Their encouragement was also very helpful in the completion of this Ph.D.

Many more persons participated in various ways to ensure my research succeeded and I am thankful to them all. Last but not the least, I am thankful to those who helped me directly or indirectly during the course of this research and who are un-named. Still I hope, they shall understand and accept my sincere thanks.

Dated: June 11, 2016

*Dikshita*  
(Dikshita Gupta)

Abstract	xiii-xiv
List of Publications	xv
List of Figures	xvii-xix
List of Tables	xx

<b>CHAPTER</b>	<b>CONTENTS</b>	<b>Page No.</b>
<b>1</b>	<p style="text-align: center;"><b>Introduction</b></p> <p>1.1 Chemical sensors in general and response parameters.  1.1.1 Gas sensing mechanism of chemical gas sensors.</p> <p>1.2 Palladium and its versatile properties.</p> <p>1.3 Palladium-hydrogen system.</p> <p>1.4 Surface Modifications of metal oxides by metal particles.</p> <p>1.5 Motivation of the present work.</p> <p>1.6 Organisation of the thesis.</p>	<b>1-16</b>
<b>2</b>	<p style="text-align: center;"><b>Synthesis of pure palladium nanoparticles, palladium film, AZO:Pd films and their characterizations</b></p> <p>2.1 Polyol synthesis of palladium nanoparticles.</p> <p>2.2 Experimental analysis of palladium nanoparticles  2.2.1 TEM (Transmission Electron Microscopy).  2.2.2 UV-Vis spectroscopy.</p> <p>2.3 Palladium thin film preparation on glass substrates.</p> <p>2.4 Experimental analysis of palladium films  2.4.1 GIXRD (Glancing Incident angle X-Ray Diffraction).  2.4.2 AFM (Atomic Force Microscopy).</p> <p>2.5 Deposition of Al doped ZnO films by sputtering.</p> <p>2.6 Surface modification of Al doped ZnO films by chemical dip method.</p> <p>2.7 Experimental analysis of AZO:Pd film</p>	<b>17-34</b>

	<p>2.7.1 GIXRD</p> <p>2.7.2 AFM</p>	
<b>3</b>	<p><b>Fabrication of sensor device and electrical measurements</b></p> <p>3.1 Resistive device fabrication based on:</p> <p>3.1.1 Pure palladium nanofilm device with interdigitated electrodes.</p> <p>3.1.2 AZO:Pd nanofilm device with two parallel electrodes.</p> <p>3.2 Importance of substrate.</p> <p>3.3 Sensor setup and electrical measurements.</p>	<b>35-42</b>
<b>4</b>	<p><b>Hydrogen response results and discussions</b></p> <p>4.1 Response studies of pure Pd NPs devices in H<sub>2</sub>/N<sub>2</sub> ambient.</p> <p>4.2 Response studies of pure Pd NPs devices in H<sub>2</sub>/air ambient.</p> <p>4.3 Response studies of surface modified devices (AZO:Pd films) in air ambient.</p>	<b>43-58</b>
<b>5</b>	<b>Adsorption kinetics on solid surfaces and theoretical interpretation of the sensor data</b>	<b>59-71</b>
<b>6</b>	<b>Summary, conclusions and future scope</b>	<b>73-79</b>
	<b>References</b>	<b>81-109</b>

## LIST OF FIGURES

Figure No.	Caption	Page No.
Figure 1.1:	Schematic of sensor setup.	8
Figure 1.2:	Arrangement of palladium nanoparticles array on glass substrate. $P_1, P_2, \dots, P_n$ represents the number of conducting paths. (a) Palladium film without hydrogen exposure (b) Palladium film with hydrogen exposure.	12
Figure 1.3:	Phase diagram showing relation of $\beta$ phase and $\alpha + \beta$ phase of $PdH_x$ with hydrogen to palladium (H/Pd) ratio at room temperature.	12
Figure 1.4:	Phase diagram showing hysteresis loop during absorption/desorption of hydrogen in palladium. Shaded part is hysteresis area.	13
Figure 2.1:	Schematic diagram of top down approach and bottom up approach to prepare nanoparticles.	19
Figure 2.2:	Protection of metal nanoparticles by PVP molecules.	22
Figure 2.3:	Reaction of PVP and metal.	22
Figure 2.4:	Schematic diagram of polyol synthesis of palladium nanoparticles.	24
Figure 2.5:	Carbon coated 400 mesh copper grid.	25
Figure 2.6:	(a) TEM image of pure palladium nanoparticles (b) Size distribution.	26
Figure 2.7:	Absorption and transmission of light through cuvette containing sample.	26
Figure 2.8:	UV-Vis spectra of pure palladium nanoparticles.	28
Figure 2.9:	Palladium film preparation on glass substrate by drop method.	28
Figure 2.10:	(a) Conventional XRD, (b) GIXRD.	29
Figure 2.11:	GIXRD of prepared palladium nanofilm.	30
Figure 2.12:	AFM images of palladium nanoparticles at different areas.	32



Figure 2.13:	Schematic of chemical dip method.	33
Figure 2.14:	GIXRD of Pd modified AZO nanofilm (AZO:Pd).	33
Figure 2.15:	AFM topography (scale length 200 nm) (a) unmodified AZO surface, (b) Pd nanoparticle modified AZO surface.	34
Figure 3.1:	Schematic of sensor device (Pure Pd).	37
Figure 3.2:	Sensing device connected to digital multimeter.	37
Figure 3.3:	Schematic of sensor device (AZO:Pd).	38
Figure 3.4:	Block diagram of sensor setup.	40
Figure 3.5:	General response pattern.	41
Figure 3.6:	Reproducible sensor response.	42
Figure 4.1:	Transient response of palladium nanoparticle sensor in hydrogen mixed with nitrogen at (a) 35°C, (b) 40°C, (c) 50°C, and (d) 60°C and 75°C.	46
Figure 4.2:	Schematic of geometric effect. $P_1, P_2, \dots, P_n$ are the number of conducting pathways.	47
Figure 4.3:	Hydrogen sensing mechanism of palladium nanoparticles.	48
Figure 4.4:	Transient response of palladium nanoparticle sensor in hydrogen mixed with air at 40°C and 50°C.	49
Figure 4.5:	Shift in baseline resistance by changing the ambient atmosphere from nitrogen ( $N_2$ ) to air.	51
Figure 4.6:	(%) Response, response time and recovery time of the palladium nanoparticle sensor for sensing hydrogen (a) mixed with nitrogen and (b) mixed with air.	52
Figure 4.7:	Response of palladium nanoparticle sensor to 1% methane in air.	52
Figure 4.8:	(a)–(g) Transient response of AZO:Pd devices in different concentrations of hydrogen mixed with air in the temperature range 40°C–150°C. (h) Variation of (baseline) device resistance with temperature in air ambient.	54
Figure 4.9:	Sensing mechanism of AZO:Pd devices (AZO resistors are only temperature dependent, whereas Pd resistors depend both on temperature and adsorbed hydrogen).	55

Figure 4.10:	(a) Response time, (b) recovery time, (c) response (%), and (d) temperature windows, of AZO:Pd devices in different concentrations of hydrogen mixed with air in the temperature range 40°C–150°C.	56
Figure 4.11:	Repeated cycle transient response of AZO:Pd devices in different concentrations of hydrogen mixed with air at (a) 60°C (b) 125°C.	57
Figure 4.12:	(a) Selectivity study of AZO:Pd devices. (b) Stability study of AZO:Pd devices.	58
Figure 5.1:	Schematic of (a) tetrahedral geometry, (b) octahedral geometry, (c) tetrahedral interstitial site, and (d) octahedral interstitial site. Green circle represents the interstitial site.	61
Figure 5.2:	Schematic arrangement of host and guest atoms in (a) Tetrahedral configuration (b) Octahedral configuration.	62
Figure 5.3:	Adsorption isotherms for various models below and above the transition temperature (~100°C).	68
Figure 5.4:	Variation of activation energy with hydrogen gas concentration.	70

## LIST OF TABLES

<b>Table No.</b>	<b>Caption</b>	<b>Page No.</b>
Table 1.1:	Characteristics of chemical gas sensors.	6
Table 2.1:	Materials used in the synthesis of palladium nanoparticles.	23
Table 4.1:	Response (%), Response and Recovery times (for 90% change) of the palladium nanoparticle sensor for sensing hydrogen (a) mixed with nitrogen and (b) mixed with air at 50°C.	50
Table 5.1:	$r^2$ values of the adsorption fits. t: temperature; L: Langmuir; and F: Freundlich. (The deviation from Langmuir type with temperature is indicated in bold).	68
Table 5.2:	Constants obtained from the activation energy versus concentration fitted curves.	71
Table 6.1:	Comparative picture of the devices.	78

## ABSTRACT

The interest in hydrogen sensors arises due to the safety concerns of flammable hydrogen gas. Hydrogen gas is highly flammable if its concentration exceeds 4% in air. Thus hydrogen sensors are required that can detect minimal concentration of hydrogen (below its limit of detection) and operate at wide range of temperatures (low and high) needed for automotive, aerospace and fuel cell applications. The advancement in developing palladium and palladium-modified devices as hydrogen gas sensors has accelerated over the past two decades. Palladium based devices have shown excellent hydrogen sensing properties with high sensitivity and selectivity whose response varies with the hydrogen concentration and operating temperature. In the present work, efforts have been made to fabricate a hydrogen sensing device that is simple, compact, highly sensitive towards hydrogen, selective, reproducible, stable and has wide operational temperature range compatibility.

Uniform 9.5 nm sized palladium nanoparticles (PdNPs) have synthesized by polyol method by reducing sodium tetrachloropalladate at 100°C with the help of ethylene glycol in the presence of polyvinylpyrrolidone (capping agent). This method employs simple beaker chemistry that owes to the high purity product. Thin film of palladium has prepared by solution drop method on glass substrates. Palladium nanoparticles and palladium films have been characterized by Transmission Electron Microscopy (TEM), UV-vis spectroscopy, Glancing Incident angle X-Ray Diffraction (GIXRD), Atomic Force Microscopy (AFM) to reveal the information on size, crystallinity and surface morphology.

Aluminium doped Zinc Oxide (AZO) film has prepared by sputtering technique on glass substrates. The surface of AZO film has modified with palladium by solution dip method. The AZO:Pd film is characterized by GIXRD and AFM to know the crystallinity and surface morphology. The porosity of film is important for gas sensing which has been observed in AFM images.

The sensor devices have fabricated by patterning conducting silver electrodes over the film and connecting the contact pads of electrodes with multimeter to note the change in resistance of film on hydrogen exposure. A detailed hydrogen sensing studies have been performed at different

hydrogen concentrations and different operating temperatures. Sensor response has been measured as the change in resistance of the devices on hydrogen exposure.

The variation of electrical conductivity of AZO is coupled with the catalytic property of palladium for the fabrication of hydrogen sensor. Pd device reveals high sensitivity towards hydrogen at hydrogen concentrations 0.1% to 1% in temperature range from 35°C to 50°C whereas AZO:Pd films shows dual hydrogen response in the temperature range 40°C to 150°C. Reproducibility, selectivity and stability test has been done for both Pd and AZO:Pd devices. A detailed analysis of the sensor results along with possible mechanism has been presented. The work presented here has profound applications for wide temperature range hydrogen sensors.

The response data has been modeled by various adsorption isotherm models to understand the solid-gas interactions and gas adsorption characteristics on solid surface.

# **CHAPTER 1**

## **Introduction**



**CHAPTER 1****INTRODUCTION**

As its name entails, sensor is a device that senses the presence or absence of a visible or invisible entity. For more betterment, a sensor is a device that receives a signal and responds to it changing its output characteristics. A sensor is a sensitive device that responds to some input, makes electrical, chemical or mechanical changes and produces a quantitative output signal in the form of an electrical signal (in terms of conductance/resistance/potential difference) or optical signal (color change) or in the form of heat. An interesting example of a sensor is the human body. There are five recognized sensors in the human body-eyes, nose, tongue, ears, and skin. Eyes have capability to view, focus and differentiate the images in visible light. Eyes are categorized under optical sensors. Ears have ability to feel and hear the sound vibrations within the range of 20 Hz to 20 KHz [1]. The tongue senses the entities (bitterness, sweetness, sour, etc.) through a sensory organ called as taste buds. A nose is a sensory organ that has potential to smell. The nose is an extraordinary sensor that can detect and differentiate the odor of entities. Some gases have a distinct smell due to which the nose smells them and distinguish. For example, the nose can directly sense the leakage of highly flammable gas, LPG (used daily in homes) and can avoid an accident. While in case of odorless gases like hydrogen, nitrogen, ethane etc., a laboratory sensor is required. Skin is a specialized receptor for heat, pain, allergy, pressure, current etc. All receive signal from surroundings and send a signal to the brain and then the brain performs different functions. In our daily life, sensors are employed in thermometers, CCD cameras, motion detectors, smoke detectors, refrigerators, street lights and many more. The classification of sensors is unlimited of which few has accounted below:

**Optical sensors** - Optical sensor responds to the light and converts the useful information (amplitude, wavelength, frequency, polarization, etc.) into an output signal (fluorescence, reflectance, absorbance, current *etc.*). Optical sensor includes fiber optic sensor, photo detector [2-3], LED [4], infrared detector [5], CCD image sensor [6-7] *etc.* A very interesting application is smart phones. The automatic brightness control of the screen and face detection is possible due to the presence of optical sensors fitted [8]. The advantages of optical fibers have gained the attention of many researchers for the fabrication of optical sensors [9-11]. Graphene has recently led to new material to be used in LED, photodetector, solar cells *etc.*



due to its unique properties [12-16]. Infrared detector has become a boon to security systems, especially in the dark. In military areas, when the sun sets (no visible light), it becomes difficult to see the enemy crossing the area. Since every object emit infrared radiations, when an enemy enters the restricted area the infra-red radiations emitted by their body can be recorded through the infrared detector.

**Magnetic sensors** - Magnetic sensors measure magnetic flux and provide relevant information in the form of analog or digital signal. For example, magnetometer, magnetic compass, etc. Magnetometer can also be used as a metal detector. An innovative research is going in many universities to develop a magnetic sensor with superior performance at a relatively low commercial price [17-20]. Researchers at National University of Singapore have developed a combination of graphene and boron nitride that respond to a magnetic field uniquely with high sensitivity that could replace the sensors used in vehicles (interlocks, flow meters *etc.*) [21]. An ultra-low magnetic field sensor has developed in Technical Research Centre of Finland [22].

**Temperature sensors**- Temperature sensors give the temperature measurements (like temperature gradient, climate change, degree of hotness and coolness, etc.) in the form of analog or digital output. For example, thermometer [23-25], heat flux sensor [26-27], thermistor [28], thermocouple [29-31], humidity sensors [32-33]. Thermometer is an everyday product used in refrigerators, ovens, air conditioners, geysers, *etc.* Thermometer contains a sensitive heat sensor, mercury, filled in a capillary tube that undergoes volume expansion when exposed to heat. The raised mercury level gives the present temperature. Mercury thermometer has a temperature range of  $-37^{\circ}\text{C}$  to  $356^{\circ}\text{C}$ . To measure ultra-low temperatures, alcohol thermometers are used and for high temperatures, pyrometers are used. The advanced technology has fitted temperature sensors in our smart phones also.

**Radiation sensors**- These types of sensors are employed for detecting nuclear radiations (alpha, beta and gamma radiations) and gives radiation level measurements. It comprises of a chamber filled with ionizing gas. This ionizing gas gets ionized when exposed to some radiation, releasing free electrons. These free electrons lead to conducting output, which can be recorded. For example, Geiger counter [34], scintillation detector [35], Cerenkov detectors [36] *etc.* Radiation detectors can identify the presence of different radiations in the

environment and living things. For many years, nuclear scientists have focused on preparing new materials like CdTe, CdZnTe *etc.* for radiation sensing applications [37-39].

**Motion sensors** - These types of sensors detect the positional change of an object. Motion sensors include speed sensors (speedometers) [40], radar [41-43], *etc.* The common use of a motion detector is at the doors of houses, malls and offices. The basic principle of motion sensor lies in the interruption of the path of waves by an obstacle. Write on materials. When a person walks near the sensor, he can be detected by his body temperature, his positional change, or sound produced by him. This property of the motion sensor can be explored to save electricity in homes by turning off the light when there is nobody in the room.

**Chemical sensors** – Chemical sensor is a device that consists of converting the chemical information into the electrical or optical output signal. This type of sensor includes gas sensor [44-49], electronic nose [50-51], pH glass electrodes [52-53], smoke detector [54] *etc.* Smoke detector contains two electrodes of opposite charges. When smoke particles reach the electrodes, they chemically react with the electrode material resulting in the transfer of electrons that leads to flow of current. The resulting current is compared with the initial current (without smoke) and if difference comes, the alarm is triggered. A detailed discussion on chemical sensors is figured out in this section later.

**Biosensors** – It is a device to detect and quantify microorganisms, antibodies, biomolecules [55], nucleic acids, blood cells *etc.* Lot of research is going in the field of biological sensors. Medically, the purpose of preparing biosensors aims to reduce pain during diagnosis. A simple example is pricking fingers every time to check blood sugar level questions about accuracy and skin irritation. Thus, Echo Therapeutics has developed a needle free glucose monitoring device that is painless, gives high accuracy measurements and easy to use [56]. California researchers have recently developed a biosensor tattoo for glucose monitoring that is easy to wear and is flexible [57]. Till now, cancer is the most incurable disease, but incurable never mean untreated. A lot of research is going to develop a biomarker (tumor marker) that could possibly detect growth of cancer cells in the initial stage [58].

## 1.1 CHEMICAL SENSORS IN GENERAL AND RESPONSE PARAMETERS

Chemical sensor is a sensitive device that gives the information about the effect of chemical interaction between the sample and elements of a sensor that transforms into the change in the electrical signal at the output. It is beyond the objective of this thesis to detail every

chemical sensor; a description of the simplest chemical sensor *i.e.* gas sensor will be specifically discussed. Chemical gas sensors based on nanomaterials are promising due to the large surface area of nanocrystals and morphology of nanocrystals can alter the properties of the sensor.

A gas sensor is a chemical sensor that detects the presence of distinct gases and can measure its concentration. The development of gas sensor was concerned for the safety purposes. There are many gases that are silent killers to the environment as well as living things. These gases are generally CO, SO<sub>2</sub>, NO<sub>2</sub>, *etc.* The extensive use of gas sensors is in chemical industries. Most of the gases are invisible and odorless, thus cannot be detected by human eyes, but their exposure to the environment is hazardous. Application of gas sensor includes detection of toxic and flammable gases (in case of leakage), for air quality monitoring, to check food quality, *etc.* The characteristics of chemical gas sensors are similar to any sensor including sensitivity, selectivity, packaging size, response time, durability and reproducibility as listed in Table 1.

Table 1.1: Characteristics of chemical gas sensors.

S.No.	Sensor parameters	Definition	Expectations
1.	Sensitivity	Rapid response towards target gas or a small change in the output of the device to change in input. $\text{Sensitivity} = \frac{\text{change in resistance (gas loaded)}}{\text{resistance (no gas)}}$	Sub-ppb
2.	Response time	Time required to reach 90% of saturation value or time required to respond to target gas.	Less than one second
3.	Recovery time	Time required to reach 90% of the baseline value	Less than one second
4.	Selectivity	Unresponsive to gases other than target gas.	High
5.	Reproducibility	Ability of sensor to produce same results after repeated use.	High
6.	Stability	Degree to which sensor properties remain constant with time.	High

Mostly, all the parameters are strongly dependent on the surface to volume ratio of particles. For example, sensitivity is highly dependent on surface-to-volume ratio (SA/V ratio). Higher

surface area means more number of atoms or molecules are exposed to the surface. The surface to volume ratio inflexibly depends on the shape and geometry of the material. Thus, higher the ratio more is the sensitivity. Let us illustrate the case of a sphere and the cube. Surface area of a cube of side 'a' is  $6a^2$  and volume is  $a^3$ . Thus SA/V ratio is  $6/a$ . Surface area of a sphere of radius 'a' is  $4a^2$  and volume is  $\frac{4}{3}a^3$ . Thus the ratio becomes  $3/a$ . Therefore, we found that SA/V ratio of cube is more than a sphere with the same value of 'a'. Similarly, we can calculate this ratio for other structures also. SA/V ratio is also inversely proportional to dimensions indicating that small sized particles have more surfaces to volume ratio. The high surface area is related to more exposure to gas molecules and thus materials are more reactive at their surfaces as compared to the bulk. Surface roughness of the material increases the surface active sites and enhances the surface to volume ratio.

When the surface of a material is exposed to some gas, the gas molecules get adsorbed on the surface either by chemical bonds or by any intermolecular force that attracts the molecules towards the material. The gas sensing behavior of any material strongly depends on the surface reactions. These surface reactions influence the sensitivity and selectivity of the sensor and strongly depend on the surface energy. The surface energy is directly proportional to the surface area and is given by following formula:

$$\gamma = \frac{1}{2} n_b \epsilon \rho_a$$

where  $\gamma$  is surface energy,  $n_b$  is the number of surface broken chemical bonds,  $\rho_a$  is the number of atoms per unit area, and  $\epsilon$  is the bond strength.

When a material is exposed to gas, it gets either absorbed or adsorbed on the surface of material. Adsorption relates the interaction of gas atoms with the surface sites only and absorption refers to the diffusion of atoms in the crystal lattice of material. The amount of gas absorbed/adsorbed on the surface of solid depends on surface morphology; the gas concentration, pressure and temperature. Further details of the adsorption phenomenon can be explained on the basis of adsorption isotherms [59-60]. The rate of adsorption/desorption is related to following formulas:

$$\text{Rate of adsorption} = k_1 p (1 - \theta)$$

$$\text{Rate of desorption} = k_2 \theta$$

where  $k_1$  is rate constant of adsorption and  $k_2$  is rate constant of desorption,  $p$  is gas pressure,  $\theta$  refers to sites occupied by gas molecules, and  $(1-\theta)$  refers to vacant sites. At equilibrium, rate of adsorption=rate of absorption. Many other theories have been proposed to explain the interaction of gas and solid material [61-65].

There are plenty of gas sensors available in the market made from materials such as ZnO [66-75], SnO<sub>2</sub> [76-85], TiO<sub>2</sub> [86-91], Palladium (Pd) nanostructures [92] *etc.*

### 1.1.1 Gas sensing mechanism of chemical gas sensors

The nanosized chemical sensors are good option to utilize in various applications but here we will be discussing about chemical gas sensors only. When a chemical gas sensor is exposed to gas, the molecules of the gas chemically adsorb on the sensor surface. This solid-gas interaction alters the surface properties of device and this change yields the sensor response. Gas sensors are grouped as resistance based gas sensor, capacitance based gas sensors, optical gas sensors *etc.* All the gas sensors are based on the interaction of solid (sensing material) and gas. The detection principle of resistance based gas sensor relies on the change in electrical conductance of the sensing film when it is exposed to some gas molecules. In case of capacitance based gas sensors, detection principle includes the change in dielectric constant of the film as a function of gas concentration. In case of optical gas sensors, the change in refractive index, absorbance and fluorescence properties are measured. Basic schematic of the sensor setup is illustrated in Figure 1.1. Typically a sensor consists of a sensitive layer (sensing material) printed on a substrate with two electrodes on either side of sensing material and finally connected to the measuring device. The majority charge carriers (electrons or holes) of sensitive material lead to conductivity. The interaction of the gas atoms with the surface of material leads to change in carrier charge density of the material. This change alters the conductivity of the material.

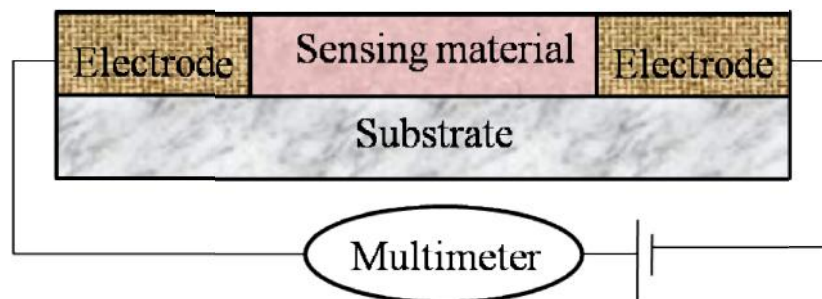


**Figure 1.1:** Schematic of sensor setup.

The difference in conductance between two electrodes is read by the multimeter. For example, for n-type semiconductors, electrons are majority carriers. A reducing gas increases the conductivity and oxidizing gas decrease the conductivity of the n-type material. The reducing gas interacts with the oxygen ions at the surface of material and oxygen gives back the electrons to the semiconductor. This decreases the depletion layer width and hence conductivity increases. For p-type semiconductor, where majority carriers are holes, reverse phenomenon occurs.

The thesis mainly discusses the metal-oxide (MO) gas sensors and metal hydrides ( $MH_x$ ) gas sensor. The sensing mechanism depends upon the change in conductivity of metal oxide semiconductor ( $ZnO$ ,  $SnO_2$ ,  $TiO_2$  *etc.*) during adsorption/absorption of gases on their surface. In the presence of air, oxygen atoms get adsorbed on the MO surface. These oxygen atoms capture electrons from the conduction band of semiconductor and forms  $O^-$ ,  $O^{2-}$ ,  $O^{2-}$  species at the surface. A space charge layer is created that increases the resistivity of the semiconductor. When a reducing gas is passed through the semiconductor,  $O^-$  ions are absorbed by the gas atoms and releases electrons from the space charge layer back to MOS (metal oxide semiconductors) that increases the conductivity of a semiconductor.

## 1.2 PALLADIUM AND ITS VERSATILE PROPERTIES

Palladium (Pd) belongs to the platinum group metals family. Palladium metal was found by William Hyde Wollaston in early 1800's while purifying platinum ores. Palladium is found in abundant in the countries like South Africa and Russia. Due to its catalytic nature, it converts harmful gases like carbon monoxide, nitrogen dioxide and hydrocarbons into harmless components like carbon dioxide, nitrogen and water molecules [93-96].

Palladium is 10<sup>th</sup> group element of the periodic table with atomic number 46 and molecular weight 106.42. Palladium has fascinating shiny silvery white metallic appearance. It has open electronic shell configuration  $[Kr]4d^{10}5s^0$ . Its ionic radius, atomic radius and covalent radius is 0.137 nm, 0.21 nm and 0.31 nm respectively. Palladium has a face centered cubic crystal structure with exposed (111), (100), (220) and (311) planes out of which (111) and (100) are most prominent [97].

The following chemical properties of palladium illustrate its advantages over other materials:

- **Catalytic converter:** Palladium catalytic property is useful in promoting hydrogenation and dehydrogenation reactions. It converts almost 90% of harmful gases like carbon monoxide, nitrogen oxide, hydrocarbons into less harmful gases like carbon dioxide, water vapor *etc* [98]. In chemistry point of view, its catalytic properties are useful in Suzuki Cross-Coupling reactions [99-100], Heck's reaction [101-103], Negishi coupling [104], Buchwald-Hartwig reaction [105], C-C cross-coupling reactions [106-107], and alcohol oxidation reaction [108]. Palladium can also be used as antimicrobial material to control the bacterial growth [109].
- **Corrosion and oxidation resistance:** Palladium is corrosion resistant. Palladium reduces the corrosion rate of titanium to make it resistant to corrosion in non-oxidizing acids (hydrochloric acid, hydrofluoric acid *etc.*) [110]. Electroplating palladium on stainless steel shows better corrosion resistance in corrosion medium [111].
- **Strong affinity of palladium towards H<sub>2</sub> absorption:** Palladium has ability to selectively absorb hydrogen atoms in a reversible manner. Due to catalytic property of palladium, hydrogen molecule first dissociates into hydrogen atoms and these hydrogen atoms occupy interstitial sites of FCC structure of palladium resulting in displacement of metal atoms from their actual sites. Thus, there is volume expansion of palladium. The reversible hydrogen absorption on palladium makes it efficient to use as a hydrogen storage device, hydrogen purifier, and hydrogen detector.

### 1.3 PALLADIUM-HYDROGEN SYSTEM

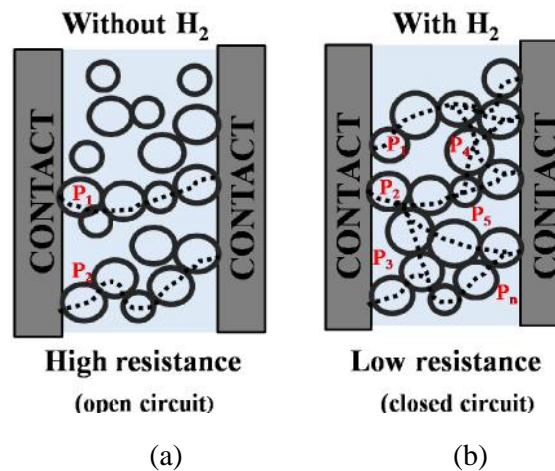
T.Graham in 1866, noticed the absorption of hydrogen in palladium for the first time [112]. Until then, researchers performed many experiments to figure out the applications of palladium as hydrogen detector and hydrogen purifier [113-116]. Palladium has been extensively used as a hydrogen sensing material due to its unique response to hydrogen [117-119]. The salient feature of palladium is its capacity to absorb large amount of hydrogen rapidly even at room temperature. This phenomenon has led researchers to utilize palladium as a hydrogen storage material or hydrogen sensing device. A catalytic surface increases the rate of chemical reactions occurring near its surface. The Pd-H interaction involves the interaction of hydrogen molecules and atoms on the surface of palladium.

The interaction of hydrogen with palladium is governed by four basic processes. As an initial step, hydrogen molecules are adsorbed on the surface of palladium (at some hydrogen pressure). The catalytic behavior of palladium, then dissociates the hydrogen molecule into its atomic form. These dissociated hydrogen atoms get diffused into the tetrahedral and octahedral interstitial sites of palladium FCC crystal structure [120-121] and leads to the formation of palladium hydrides (Binding energy of Pd-H is 2.34 eV [122] and bond length is 0.154 nm, bond length of H-H is 0.086 nm). The displacement of palladium atoms on hydrogen incorporation results in volume expansion of palladium. Volume of palladium nanoparticle expands, providing more conducting paths forming a highly conductive film. The chemical bonding process modifies the electrical properties of palladium (resistivity, work function) and provides an output signal in the form of conductance or resistance (as shown in Figure 1.2).

The thin film of palladium consists of palladium nanoparticles arranged in some array with some gaps between each nanoparticle. This volume expansion decreases the interparticle gap. Consequently, the resistivity of the film decreases. This resistivity change attributes to sensor response. The resistivity change of the film on hydrogenation is determined by the amount of hydrogen impinging on the surface of a palladium film. Thus, it is concluded that the influence of hydrogen with palladium changes its structural, mechanical, and electronic properties. The hydrogen concentration dissolved in palladium is also proportional to the partial pressure of gas *i.e*  $c=c_0 \sqrt{p}$  where  $c$  is the concentration of hydrogen gas and  $p$  is the partial pressure of gas. This is called Sievert's law and  $c_0$  is the Sievert's constant [123]. The absorption/desorption of hydrogen on palladium film can also be explained by Sievert's law [124].

Incorporation of hydrogen atoms leads to electron scattering process that increases the resistivity of the film. This electronic effect usually occurs at low H/Pd ratio. When the H/Pd ratio rises to 0.6, palladium lattice expands due to a sufficient amount of hydrogen in the palladium FCC lattice. This expansion reduces the interparticle gap, thereby decreasing the resistivity of the film. This is geometric effect [119].

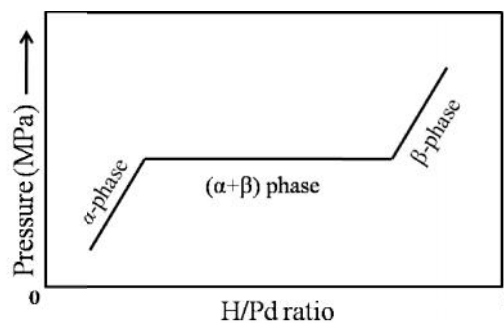




**Figure 1.2:** Arrangement of palladium nanoparticles array on glass substrate.  $P_1, P_2, \dots, P_n$  represents the number of conducting paths. (a) Palladium film without hydrogen exposure (b) Palladium film with hydrogen exposure.

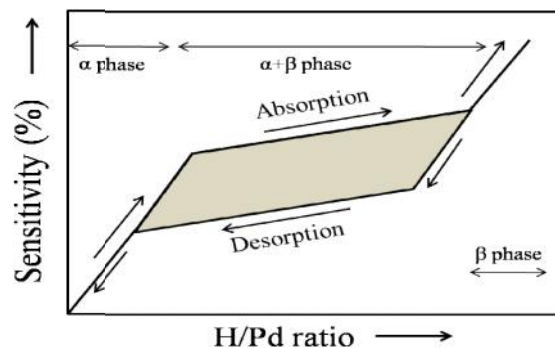
Absorption of hydrogen on palladium leads to three different phases-  $\alpha$  phase,  $\beta$  phase and a mixed  $\alpha + \beta$  phase (Figure 1.3).  $\alpha$  phase corresponds to low concentration of hydrogen in palladium lattice ( $H/Pd=0.03$ ),  $\beta$  phase corresponds to high occupation of hydrogen atoms in palladium lattice ( $H/Pd>0.7$ ) and mixed phase  $\alpha + \beta$  corresponds to  $0.3 < H/Pd < 0.7$  [125].  $\beta$ -hydride phase is considered as over hydrogenated phase.

Figure 1.3 shows the ideal case of the phase diagram at room temperature. When it comes to study response of palladium device towards hydrogen practically, the system becomes reversible in the  $\alpha$  and  $\alpha + \beta$  phase and irreversibility is observed in the  $\beta$  phase. This irreversibility of palladium hydride gives rise to lattice embrittlement owing to irregular variations in conducting properties of palladium. Thus, the output resistance response develops a hysteresis behavior over time.



**Figure 1.3:** Phase diagram showing relation of  $\alpha$  phase and  $\alpha + \beta$  phase of  $PdH_x$  with hydrogen to palladium ( $H/Pd$ ) ratio at room temperature.

Figure 1.4 shows the hysteresis in absorption-desorption process at constant pressure. This degrades the performance of the sensor-sensitivity, response %, and reproducibility. Also, on repeated hydrogenation/dehydrogenation process, palladium is susceptible to mechanical stress, cracking, and delamination. In other words, hydrogen loading-deloding weakens the mechanical strength of palladium film during phase transition. This decreases the long term stability of the sensor which is not acceptable commercially. From a commercial point of view, sensitivity and selectivity are the most appreciated characteristic of any sensor.



**Figure 1.4:** Phase diagram showing hysteresis loop during absorption/desorption of hydrogen in palladium. Shaded part is hysteresis area.

This problem can be resolved by increasing the temperature of the film to suppress the area of hysteresis loop (Figure 1.4). Ceasing the formation of  $\text{-PdH}_x$  plays an important role in improving the sensitivity of the sensor. Another is to introduce some foreign metal in palladium lattice with a similar crystal structure (to avoid lattice mismatch) and similar atomic size.

#### 1.4 SURFACE MODIFICATIONS OF METAL OXIDES BY METAL PARTICLES

Surface modification is usually done to tune the physical, chemical, mechanical, and surface properties of nanomaterial. This can be done by either roughening its surface or by coating some other compatible material at the surface. Surface modification of nanomaterials is rather an exercise to employ in many applications. A range of methods are present in order to modify the surface properties of materials, for example, dip coating method [126-127], sputtering [128], plasma treatment [129-130], photoreduction method [131-132], spin coating method [133], solution growth method [134] *etc.* The advantage of dip coating and solution

growth method over others is that in these methods no such heavy and complicated equipment is required and consumes very less time to deposit depending on wetting properties of adsorbent and adsorbate. In dip coating method, solution of the material to be deposited is prepared and a cleaned substrate (with or without film of different material) is dipped in it for different time intervals (depending on the requirement of thickness). In solution growth method, two solutions of different materials are prepared and then are mixed to grow nanoparticles simultaneously over one another. When solution is ready, the modified nanoparticles are deposited either by spin coating or dip coating method.

Here we are focused on making an efficient hydrogen sensing material with good sensing characteristics. The sensitivity, selectivity and other sensing parameters rely on the surface reactions of sensing material. The participation of a catalyst on the surface of metal oxides could increase the rate of reaction and surface reactions increase, which leads to high sensitivity [135-138]. The catalytic materials can be Pd, Au, Pt, Ag *etc.*

Metal oxide sensors have gained attention due to its ability to detect number of gases with good sensing properties [139-142]. A broad research has been done towards the hydrogen sensing properties of metal oxides like ZnO, TiO<sub>2</sub>, SnO<sub>2</sub>, MnO<sub>2</sub> *etc.* In general, metal oxide hydrogen sensors have been classified depending on the sensing mechanisms: work function based or resistance based. The key principle is based on the chemical reactions taking place between semiconductor surface and target gas. Metal oxides contain a high density of oxides atoms at the surface sites of metal. The fundamental mechanism of semiconductors based sensors is the change in resistance due to the space charge layer on the surface. ZnO is the most popular semiconductor material for hydrogen detection. Oxygen atoms (highly electronegative) on the surface of semiconductor capture electrons from conduction bands of semiconductor. This results in an increase in the current density barrier that increases the resistance. On hydrogen exposure, hydrogen atoms give the electrons to the conduction band of semiconductor to decrease the current density barrier. This change in resistivity of semiconductor on hydrogenation gives the sensor signal. But the majority of them are incompetent in terms of sensitivity and selectivity. To solve this problem, a number of strategies have been implemented such as doping or surface modification of the metal oxides for gas detection. Catalytic active material like palladium enhances the rate of interaction of gases and metal oxides. This effectively increases the sensitivity and selectivity of the sensor, resulting in fast response and recovery time.

### 1.5 MOTIVATION OF PRESENT WORK

The hazardous results of hydrogen leakage bring the hydrogen safety as an important issue. The colorless and odorless property of hydrogen requires an innovative sensing device that could detect its presence below its explosion limit to avoid the explosion risks. Thus, there is a pressing need to fabricate a fast, compact, low cost, and efficient hydrogen sensing device. There are many hydrogen sensors available but they compromise either the good sensing properties or their limited operational temperature range. Nanoparticles have high surface area, which is boon for effective gas sensing. Nanoparticles based gas sensors are potentially faster, has lower limit of detection, and operate at lower temperatures. Palladium nanoparticles have high sensitivity and selectivity towards hydrogen at room temperature. The limitation of palladium based hydrogen sensor is the failure of device performance at relatively higher temperatures ( $>50^{\circ}\text{C}$ ). Narrow operational temperature range bounds the device to work in a particular region, not universally. Thus to widen the operational temperature range with no compromise with the sensitivity and selective behavior, there is need to introduce some other material with highly sensitive palladium nanoparticles. Aluminium doped zinc oxide (AZO) is thermally stable and conducting at high temperatures. Thus, the Pd decorated AZO devices are useful for both low and relatively high temperature applications.

Thus, our motivation is to develop a hydrogen sensing device that is hydrogen specific, highly sensitive (to detect concentrations below its flammable limit), reproducible, stable, low cost and has wide operational temperature range. The use of glass substrates and simple fabrication processes lowers the cost of sensor device.

### 1.6 ORGANISATION OF THE THESIS

The thesis is organized as follows:

- Chapter 1 begins with the basic concept of sensors followed by the elaboration of chemical sensors. A summary of palladium and palladium based devices with remarkable applications has been explained. The chapter ends with the motivation of the present work.
- Chapter 2 includes the synthesis of pure palladium nanoparticles, palladium films and AZO:Pd films and their characterizations-GIXRD, TEM, AFM, and UV-vis

spectroscopy. This chapter includes general information about the synthesis method and experimental analysis of prepared nanostructures.

- Chapter 3 is devoted to the fabrication of sensor devices based on prepared films and their electrical measurements useful to calculate sensing parameters.
- Chapter 4 provides the results of hydrogen response of pure palladium and surface modified device including sensing mechanism of both the devices.
- Chapter 5 contains the theoretical interpretation of obtained sensor data.
- Chapter 6 summarizes and concludes the work contained in the thesis along with future perspectives of this work.

## **CHAPTER 2**

**Synthesis of pure palladium  
nanoparticles, palladium film, AZO:Pd  
film and characterizations**



## CHAPTER 2

SYNTHESIS OF PURE PALLADIUM NANOPARTICLES, PALLADIUM FILM,  
AZO:Pd FILMS AND THEIR CHARACTERIZATIONS

Synthesis is an important step to start with nanoparticles. Synthesis of nanoparticles provides a platform for producing nanostructures and opens prospects to explore their nanoscale properties in various applications. In the bulk material, the physical properties are independent of size. However, at the nanoscale, the physical and chemical properties become dependent on particle size and density of atoms at the surface of material. There are dozens of synthesis methods of nanoparticles including sol gel method [143-145], wet chemical method [146-147], combustion method [148-149], ball milling method [150-151] *etc.* All techniques are differentiated based on two approaches; Top-down approach and Bottom up approach (Figure 2.1) [152-153]. Bottom up approach is mostly preferred for fabrication of nanostructures with narrow size distribution and less surface defects as compared to the former approach. This approach is divided into liquid phase synthesis, vapor phase synthesis and gas phase synthesis.

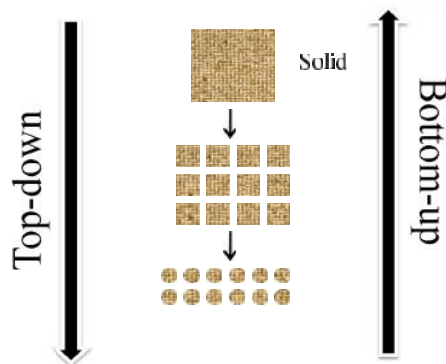


**Figure 2.1:** Schematic diagram of top down approach and bottom up approach to prepare nanoparticles.

The crystal formation of nanoparticles consists of two important steps-nucleation and growth [154]. Nucleation is a phenomenon in which a nucleus or seed initiates the crystallization. Adding more atoms to the surface of nucleating crystals leads to growth in specific directions. The criteria for the formation of mono dispersed nanoparticles are to increase the nucleation rate and to reduce growth rate. Nucleation and growth are the building blocks of synthesizing the nanoparticles. Size and shape of nanoparticles are dependent on the synthesis parameters, capping agents and surfactants. Size of the nanoparticles determines the



surface to volume ratio and surface energy. More is the surface to volume ratio; more is the reactivity. Small sized nanoparticles comprise more surface energy than larger sized nanoparticles. Thus, there are more chances for smaller nanoparticles to agglomerate. Shape determines the surface structure and can be modified and controlled by adding capping agents or surfactants.

Several size-reducing mechanisms have been proposed to prepare palladium nanoparticles such as polyol method [154-155], solvothermal method [156-157], single pot method [158], electrochemical method [159-162], hydrothermal method [163] *etc.* Among all these techniques, polyol method has been used in practice for centuries to prepare metal nanoparticles with monodispersity, agglomeration free and controlled reaction rate. They have quality control over the particle size, distribution, purity, and morphology. The choice of solvent, metal precursor, reducing agent, surfactants *etc.* plays an important role to achieve good quality metal nanoparticles. In the past few decades, the palladium nanoparticles are synthesized in a rich variety of shapes [164-169,]. These different morphologies are attained by the manipulation of either the thermodynamics of the system or by the kinetics involved in crystal growth.

### **2.1 POLYOL SYNTHESIS OF PALLADIUM NANOPARTICLES**

Polyol method is procedurally simple and monodispersed nanoparticles are readily formed with good size and shape uniformity. This chemical method consists of reduction of metal from its precursor by using ethylene glycol or poly (ethylene glycol) as reducing agent as well as solvent [155]. Polyol synthesis technique is non-aqueous method where glycol is adsorbed on surface of nanoparticles preventing oxidation problem and reduces the problem of hydrolysis of fine metal particles that often occur in aqueous solvent. Thus, this cost-effective method well suited to prepare metallic nanoparticles [170-176]. Among various other methods, the chemical reduction method is most popular one being used by researchers because of its easy process and inexpensive production. The polyol method has capability of producing nanoparticles with uniform size and shape, as always required. As its name implies, polyol contains single or multiple hydroxyl functional groups (OH) and are served as solvent as well as reducing agent in the synthesis. The optimized concentration of metal precursor, reaction temperature, reaction time and amount of capping agent yields nanoparticles with controlled size and shape.

- **Metal Precursors:** Selecting a precursor is the first route of preparing nanoparticles. Palladium has dozens of precursors like  $\text{Na}_2\text{PdCl}_4$  (sodium palladium tetrachloride) [177-179],  $\text{Pd}(\text{C}_2\text{H}_3\text{O}_2)$  (palladium acetate) [180-181],  $\text{H}_2\text{PdCl}_4$  (dihydrogen tetrachloropalladate) [182-183], dimethylpalladium [184],  $\text{PdCl}_2$  (palladium chloride) [185-187],  $\text{Pd}(\text{NO}_3)_2$  (palladium nitrate)[188] *etc.* The concentration of precursor is important to make a supersaturated solution to start nucleation.
- **Solvent and reducing agent:** Once the precursor is picked, an appropriate solvent is needed with high dissolution property with respect to the precursor. Solvents may be polar organic, non-polar organic or simply may be distilled water. In polyol method, the dual role of alcohol emerged the interest in polyol methods for metal reduction. For example, ethylene glycol is served as a solvent as well as reducing agent. Moreover, it leads to very few by-products after metal reduction that can be easily removed.  
In polyol method, the particle size distribution strongly depends upon nature and reduction potential of reducing agent [189]. Choice of the reducing agent depends on nature of metal, which is to be reduced, and stabilizing agent is chosen according to the application of the metal nanoparticles. High molecular weight of glycols, reaction rate is accelerated which speeds up nucleation and growth and situations becomes uncontrollable. This leads to inhomogeneity in size and shape of nanoparticles. Reducing agent like sodium borohydrate with low reduction potential allows the reaction to go slowly so that no free ions are left in the reaction [190]. Thus, sodium borohydride results in formation of amorphous palladium nanoparticles and weak reducing agent like ethanol forms crystalline palladium nanoparticles [190].
- **Stabilizer:** Stabilizer modifies the kinetics of atoms that are responsible for the shape change. Stabilizers are generally polymers and are selected depending on their molecular weights as per requirement. They are proficient to inhibit clumping of particles that generally occur at high temperature and large reaction time. Stabilizers guarantee to control the growth of nanoparticles by controlling particle size at initial stage during synthesis, and by controlling the growth rate. They control aggregation by two phenomenon-Electrostatic stabilization and steric stabilization. There always exist some forces of attraction between two particles and when this force of attraction increases, aggregation of particles takes place. So to stop the particles to come closer, an electrical layer of same charges on the surfaces of neighboring particles is created (either by physical adsorption of charged ions on surface or by dissociation of surface charged

species) such that there exist a force of repulsion between them. This is known as electrostatic stabilization. Layering the surface of nanoparticle with a bulky material is known as steric stabilization. Polymers keep two particles away from each other under certain conditions due to polymer and particle surface interaction. Polymer molecules are adsorbed on the surface of particles by forming chemical bonds between them.

PVP (polyvinylpyrrolidone) is one of common stabilizer widely used to protect nanoparticles from agglomeration. It stabilizes the nanoparticles as shown in Figure 2.2. PVP has structure of polyvinyl skeleton with two polar groups attached to it; O (oxygen) and N (nitrogen). Mechanism of protection of metal nanoparticles by PVP can be discussed as follows: The lone pairs from both N and O make coordinate bond with the metal that forms a complex compound M-PVP (metal-PVP).  $M^{n+}$  in  $M^{n+}$ -PVP complex is then reduced to pure metal by gaining  $n$  electrons from reducing agent. The mechanism of formation of coordinate bond between metal and PVP molecule is shown in Equations 2.1, 2.2. Thus, the PVP performs as size controller and capping agent.

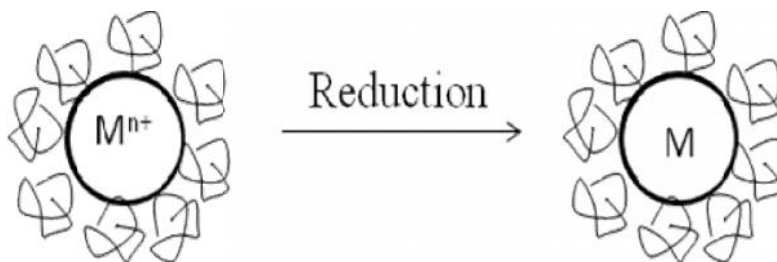


Figure 2.2: Protection of metal nanoparticles by PVP molecules.

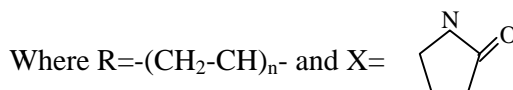
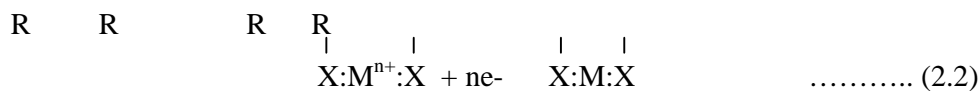
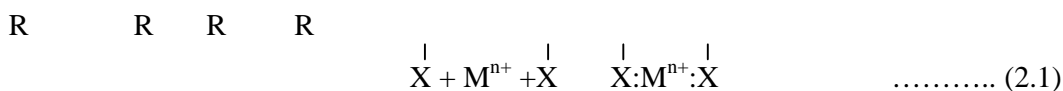


Figure 2.3: Reaction of PVP and metal.

Growth rate can be controlled by selective adhesion of stabilizers on nanoparticle surface. Other capping agents used to prepare agglomeration free palladium nanoparticles are CTAB (Cetyl Trimethyl Ammonium Bromide) [191-193,], thiols [194-195], citrate [196] *etc.*

- **Synthesis temperature and reaction time:** Synthesis temperature is important to trigger the reaction mechanisms. Usually, particles formed at low temperature are smaller than produced at high temperature. Reaction time includes the time given to complete the chemical reaction. Both parameters are connected with the reaction rate. Less reaction time could lead to incomplete reduction of metal ions due to which the reaction becomes unstable and limits the complete formation of nanoparticles. Reaction rate increases with increase in synthesis temperature.

### Experimental synthesis of palladium nanoparticles:

**Table 2.1** Materials used in the synthesis of palladium nanoparticles

Material	Purpose	Molecular formula	Appearance	Company
Sodium tetrachloropalladate (IV)	Precursor	$\text{Na}_2\text{PdCl}_4 \cdot 3\text{H}_2\text{O}$	Solid red-brown powder. MW=346 g/mol	Alfa-Aesar
Polyvinylpyrrolidone	Capping agent	$-(\text{C}_6\text{H}_9\text{NO})_n-$	Solid white powder. MW=8000	Alfa-Aesar
Ethylene Glycol	Reducing agent and solvent	$\text{OH}-\text{CH}_2-\text{CH}_2-\text{OH}$	Transparent liquid. MW=62.07 g/mol	Alfa-Aesar

The palladium nanoparticles were synthesized by the polyol method using liquid polyol, ethylene glycol (EG) [155][197] as shown in Figure 2.4. The chosen palladium precursor was sodium tetrachloropalladate(II) ( $\text{Na}_2\text{PdCl}_4 \cdot 3\text{H}_2\text{O}$ ). 5 ml of EG was heated in a dust free clean volumetric flask at 100°C under constant stirring for one hour. 0.0165 g of  $\text{Na}_2\text{PdCl}_4 \cdot 3\text{H}_2\text{O}$  and 0.0031 g of polyvinylpyrrolidone (PVP) were added simultaneously in hot EG under stirring condition. PVP is used as a capping agent to prevent the agglomerated growth of the metal nanoparticles. The red brown solution turned dark brown within few minutes of the addition. This change in color is an indication of the initiation of reduction of palladium

precursor to metallic palladium. The temperature and stirring was maintained for another one hour and then the content of the flask was centrifuged at 5000 rpm to yield desired clean precipitates (washed with ethanol several times to remove organic components). The reduction reactions are as follows:

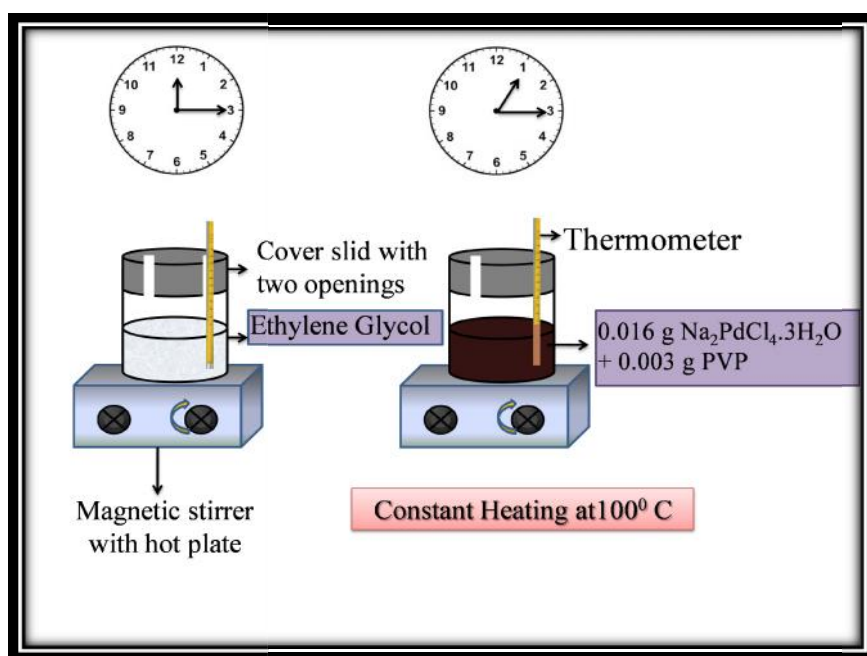
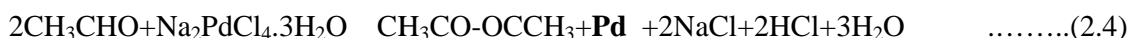


**Figure 2.4:** Schematic diagram of polyol synthesis of palladium nanoparticles.

## 2.2 EXPERIMENTAL ANALYSIS OF Pd NANOPARTICLES

The studies of properties of nanoparticles are of paramount importance. It is important to know how the prepared nanostructures look like (morphology), the composition (elemental, chemical and phase), surface impurities, how it interacts with surroundings (surface area, surface charge, surface reactivity) and its stability. High precision characterization techniques are required to observe the properties of nanomaterials at their atomic scale. There are many approaches to study the properties such as size, shape, structure, phase, energy levels *etc.* associated with nanoparticles. Here we will discuss the electron microscopic analysis and optical analysis of prepared palladium nanoparticles.

### 2.2.1 Transmission Electron Microscopy (TEM)

Transmission electron microscopy is a microscopy technique where an energetic beam of electrons (emitted from electron gun or cathode) is transmitted through an ultrathin specimen. An image is formed from the interaction of the electrons transmitted through the specimen. Then the image is magnified, focused and captured by a camera. TEMs are capable of imaging at a significantly higher resolution, owing to the small de-Broglie wavelength of electrons. Transmission electron microscopy gives information about size-shape of particles and their distribution.

#### **TEM analysis of pure palladium nanoparticles:**

##### **Sample preparation:**

For the TEM measurement, the eppendorf tube containing palladium precipitates and supernatant was mechanically shaken for uniform mixing by ultrasonication for one hour. Then two drops were taken out of the solution and dropped on carbon coated 400 mesh copper grid (Figure 2.5).



**Figure 2.5:** Carbon coated 400 mesh copper grid.

TEM images were obtained using Hitachi-7500 operating at 100 kV. TEM image of chemically prepared nanoparticles at 100°C is shown in Figure 2.6. An overall uniformity in particle size is evident from the TEM micrograph. The average particle size is  $\sim 9.5 \pm 0.5$  nm. The shapes of the synthesized palladium nanoparticles were nearly spherical with some polyhedron shaped particles. Clusters seen in the images are because of insufficient period of sonication.

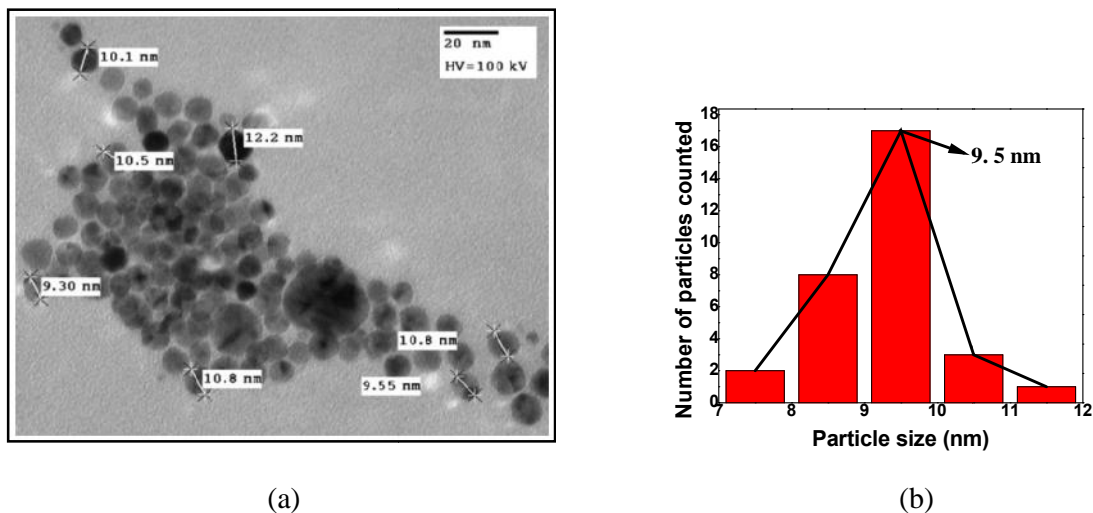


**Figure 2.6:** (a) TEM image of pure palladium nanoparticles (b) Size distribution

### 2.2.2 UV-Vis Spectroscopy

When a beam of incident light (200-700 nm) is passed through a solution containing nanoparticles, it is absorbed, transmitted or is scattered. In UV-Vis spectroscopy, the absorption and transmission of light are considered at the molecular and atomic level. Solution containing test sample is filled in a cuvette and is irradiated by a broad spectrum of UV-vis light (200-700 nm) (Figure 2.7). The wavelength at which absorption occurs is recorded by an optical spectrometer along with the degree of absorption. The absorption of light by the solution contains the electronic transitions in the molecules of the solution. Absorption leads to the movement of electrons from lower energy molecular orbital to higher energy molecular orbital. This leads to the electronic transitions of the molecules of the solute. If the atoms of the sample match the energy of a certain band of UV-vis light, there occurs electronic transitions and photons of that particular wavelength get absorbed. The spectrometer records the wavelength of incident radiation when maximum absorption occurs.

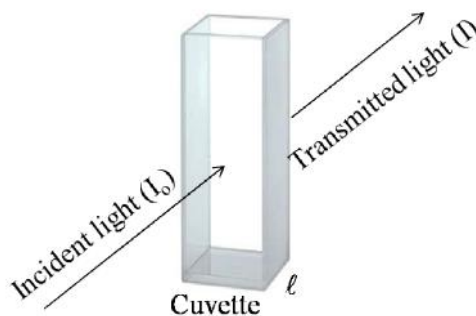


**Figure 2.7:** Absorption and transmission of light through cuvette containing sample.

The absorbance of light by a solution follows Lambert-Beer law which states that absorption is directly proportional to the concentration of solution (c) (mol/l) (Beer's law) and the width of cuvette (l) (cm) (path length of light inside cuvette) (Lambert's law). This can be formulated as:

$$A = \epsilon \cdot l \cdot c$$

where  $\epsilon$  is the absorption coefficient (probability of absorbance of light by solution)

$$\text{Also } A = \log \frac{I_0}{I}$$

where  $I_0$  is the intensity of incident light and  $I$  is the intensity of transmitted light.

When  $I < I_0$ , it means light is partially absorbed by the solution.

If  $I_0 = I$ , then  $\log \frac{I_0}{I} = 0$ , it means no absorbance occurs, light is completely transmitted.

Absorbance is very high in concentrated solution due to presence of comparatively more number of molecules than a dilute solution.

In case of metal nanoparticles, the absorption of incident radiations takes place by Surface Plasmon Resonance phenomenon [198-202].

### **UV-Vis analysis of pure palladium nanoparticles:**

To prepare sample for UV-vis study, 5 $\mu$ l of palladium precipitate solution is dropped in quartz cuvette containing ethylene glycol and is shaken well to dissolve palladium precipitates uniformly. SPR absorption band depends on the particle size, concentration of solution, and nature of metal. We used PerkinElmer Lambda 750 UV photo spectrometer for UV-vis analysis of palladium nanoparticles. The working range of this equipment is 190-800 nm. The spectrometer was equipped with suitable software to record the data. Baseline correction was done by using quartz cuvette containing ethylene glycol solution. The recorded numerical data was plotted in Origin 8 software.



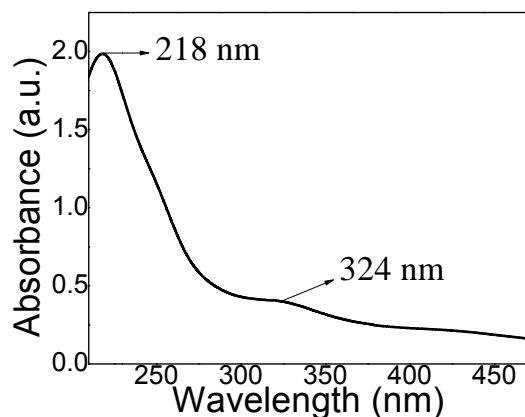


**Figure 2.8:** UV-Vis spectra of pure palladium nanoparticles.

The plotted Absorbance vs Wavelength data in Figure 2.8 shows the maximum absorption peak at 218 nm.

### 2.3 PALLADIUM THIN FILM PREPARATION

Thin film deposition is about coating a very thin layer of material (thickness in nanometer range) over a substrate. Deposition of film on substrate is a challenging task to achieve a continuous film with overall uniformity and to be corrosion resistant and strong adhesion to substrate. Numerous techniques are present to deposit palladium thin film which are broadly categorized under two main techniques- Chemical methods [203-212] and Physical methods [213-219]. Every method has its own advantages and disadvantages. Here, we use solution drop method because of its simplicity, requires no expensive or messy equipment and film forms within minutes with good surface roughness (required for sensor studies).

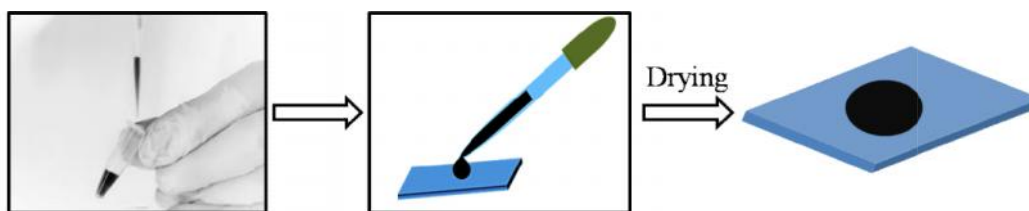


**Figure 2.9:** Palladium film preparation on glass substrate by drop method.

To prepare palladium nanofilms, two drops of the cleaned precipitates (preparation is discussed in Figure 2.4) were placed on the cleaned ultra-thin glass cover slips (thickness  $\sim 0.7$ mm) and allowed to dry at room temperature (Figure 2.9). Cover slips were cleaned by acetone followed by ethanol and distilled water and were dried in dust free environment.

## 2.4 EXPERIMENTAL ANALYSIS OF PALLADIUM FILMS

### 2.4.1 Grazing Incident angle X-Ray Diffraction (GIXRD)

The very basic characterization in nanoscale world is XRD. The XRD graphs give the partial confirmation of the formation of nanoparticles by matching the diffracted planes with the standard JCPDS data. X-Ray diffraction technique is a non-destructive technique which gives information about the internal crystal structure of crystalline solid that includes the lattice parameters of unit cell, interplanar spacing, Bragg's angle (diffraction angle), phase identification, orientation of crystallites *etc.* All crystalline solids have long range order of periodic arrangement of atoms, molecules or ions forming a crystal lattice. In a crystal, all unit cells are symmetric with no gaps and lie in all crystallographic directions. The systematic arrangement of atoms gives rise to certain planes. The lattice planes and family of directions are generally described by miller indices. Thus, basically XRD shows the fingerprint of the sample. XRD normally distinguishes between amorphous, crystalline and polycrystalline material. For amorphous materials, the XRD graph shows no peak. The crystalline and polycrystalline materials can be distinguished on the basis of the number of diffracting peaks. More number of planes, more number of peaks. Thus polycrystalline material shows more diffraction peaks as compared to crystalline material. XRD is not suitable for ultrathin films and multilayered thin films because of large penetration depth. Thus to study thin films of few nanometer thickness, GIXRD is used. Difference between the XRD and GIXRD is that in GIXRD, X-rays are incident on the surface of film at very low incident angle (usually less than  $10^\circ$ ). In GIXRD, incident angle is kept fixed, the incident and diffracted angle is varied by moving the detector arm only. GIXRD increases the pathway of incident rays inside the film and is used to minimize the contribution of substrate as illustrated in Figure 2.10. It can be seen from Figure 2.10,  $L_2 > L_1$  i.e penetration path is longer in GIXRD as compared to XRD which is beneficial to collect more information of surface properties of crystallographic thin films without interference of substrate.

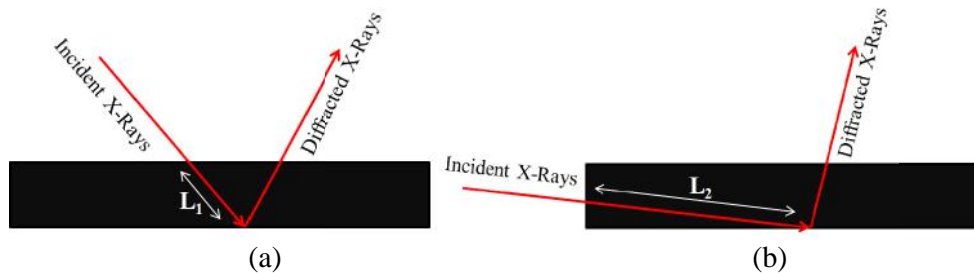


**Figure 2.10:** (a) Conventional XRD, (b) GIXRD.

**GIXRD analysis of prepared palladium nanofilm:**

The GIXRD patterns were collected by a Bruker diffractometer with  $\text{CuK}_{\alpha 1}$  radiation at a fixed  $3^\circ$  grazing incidence angle. The  $2\theta$  detector scan was performed in the range  $20^\circ$ - $80^\circ$  that was sufficient to capture all important palladium peaks. As shown in Figure 2.11, the most intense palladium peak (111) is obtained at  $2\theta \sim 40.26^\circ$  followed by (200) and (220) reflections (JCPDS card: 050681). These three peaks clearly indicate the face centered cubic (FCC) structure of the particles.

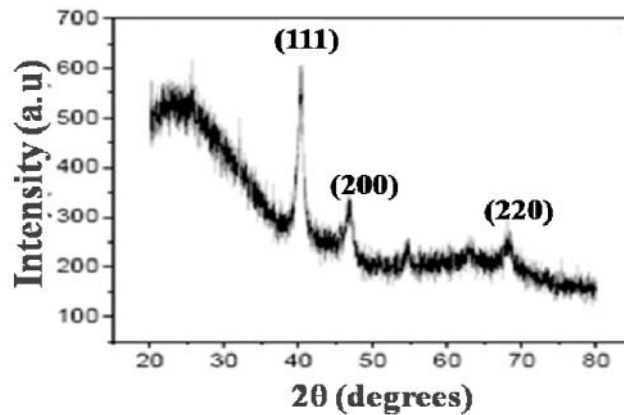


**Figure 2.11:** GIXRD of prepared palladium nanofilm.

In general, minimum number of XRD peaks contributes to the presence of highest symmetry crystals i.e of cubic structure. Thus, Figure 2.11 indicates the FCC structure owing to the most intense (111) reflection. The presence of FCC lattice structure can also be confirmed by the selection rule for miller indices i.e. [220]

Allowed reflections=  $h, k, l$  all odd or all even.

Forbidden reflections=  $h, k, l$  mixed odd and even.

The absence of other peaks eliminates the existence of other phases and impurities in the system.

The size of crystallite ( $d$ ) is estimated from the peak width of the most intense (111) reflection using the Scherrer's formula which is [221-222]:

$$d = \frac{0.9\lambda}{\beta}$$

where  $\lambda = 1.54059$  (wavelength of  $\text{CuK}_{\alpha 1}$  radiation),

$\beta$  is the Full Width at Half Maximum (FWHM), and

is the Bragg's angle of the considered peak.

The (111) reflection peak from the experimental data is fitted with a smooth curve and the calculated 'd' was 11.6 nm.

#### **2.4.2 Atomic Force Microscopy (AFM)**

AFM produces a three dimensional image-horizontal X-Y and vertical Z. In AFM, the resolution in Z direction is more than in XY direction giving the information of thickness of film. AFM normally works at three modes; contact mode, non-contact mode and tapping mode. AFM uses a spring like cantilever with small and sharp tip probe to scan the surface of film over a region of interest. A laser beam is used to detect the movements of cantilever over the surface. These movements of cantilever will change the direction of reflected beam which are tracked by the position sensitive photodiode detector.

##### **AFM analysis of prepared palladium nanofilm:**

AFM (non-contact mode) was used to study the surface morphology of the palladium films prepared on glass substrates. A porous surface morphology of the films can be seen with high surface to volume ratio in Figure 2.12. The scan has been done for four different areas *viz.* (2 $\mu\text{m}$ ×2 $\mu\text{m}$ ), (1 $\mu\text{m}$ ×1 $\mu\text{m}$ ), (500 nm×500 nm), and (100 nm×100 nm) to check the porosity of the surface of prepared palladium nanofilm. Figure 2.12 shows that the surface is highly porous with high surface to volume ratio. This porous morphology is favorable for good adsorption of gases indicating the potential applications as gas sensors. The z-scale attached with each AFM scan illustrates that the maximum depth of the porous sensing layer is ~516 nm.

From TEM analysis (discussed in section 2.2.1), the average particle size was observed to be ~10 nm. Thus, it can be said that the sensing layer consists of a stack of ~51 layers of palladium nanoparticles arranged in some array.

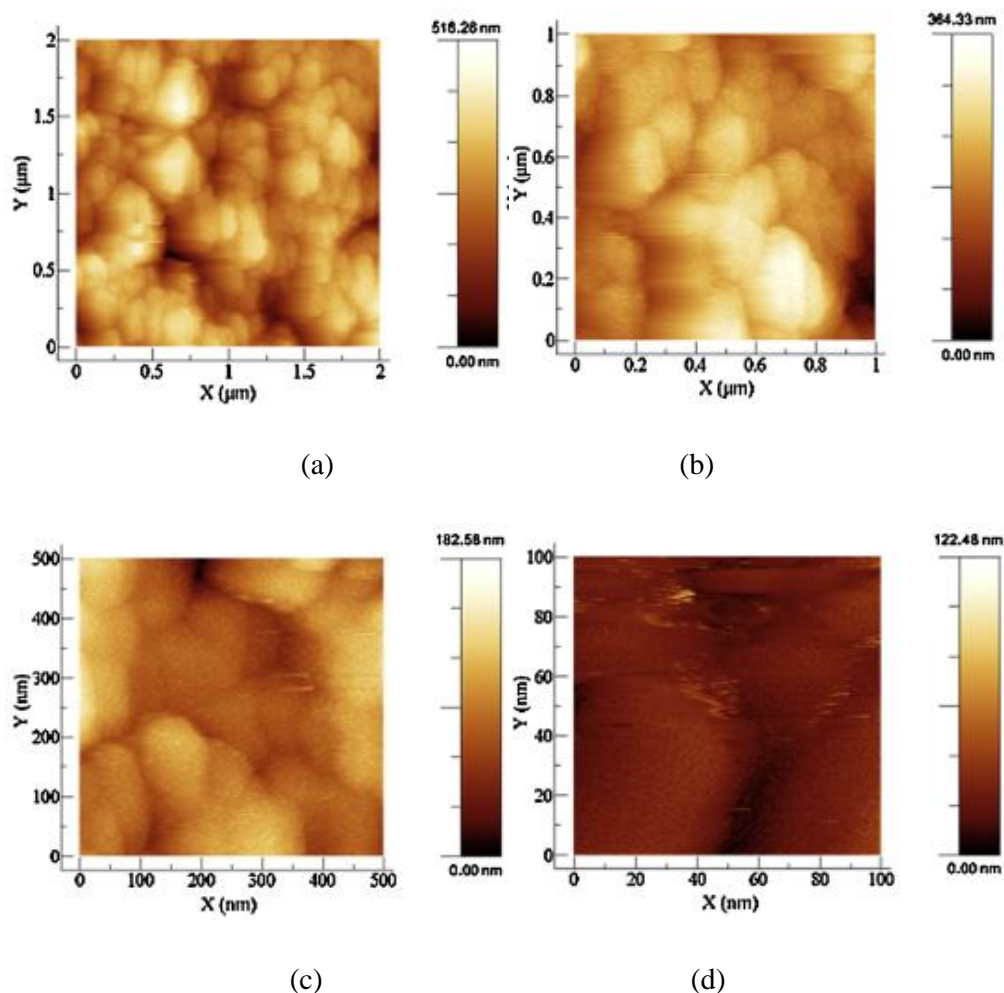


Figure 2.12: AFM images of palladium nanoparticles at different areas.

## 2.5 DEPOSITION OF Al DOPED ZnO FILMS BY SPUTTERING

To prepare AZO films, commercially available aluminium (2 wt. %) doped zinc oxide target (4 N purity) was used. ~75 nm thin film on glass substrates was formed at room temperature using pulsed dc magnetron sputtering by applying a RF power of 100 W (Advanced Energy, Pinnacle Plus) (High RF power will increase the resistivity of the film [223]). The base pressure was maintained at  $5 \times 10^{-3}$  mbar during sputtering by flowing 27 sccm of high purity argon gas. During the deposition period (12 min), substrates were rotated with a speed of 3 rpm to achieve uniform film thickness. The substrates were placed at a distance of ~8 cm and at an optimized angle of  $50^\circ$  with respect to the target normal. After deposition, the AZO films were annealed at  $400^\circ\text{C}$  for 3 h in air ambient.

## 2.6 SURFACE MODIFICATION OF Al DOPED ZnO FILMS BY CHEMICAL DIP METHOD

The palladium nanoparticles were prepared in the same manner as is discussed in section 2.1. For surface modification with Pd nanoparticles, the oxide films were dipped in a dispersed solution of metal nanoparticle in ethanol for 5s (Figure 2.13), followed by drying at 50°C in an oven.

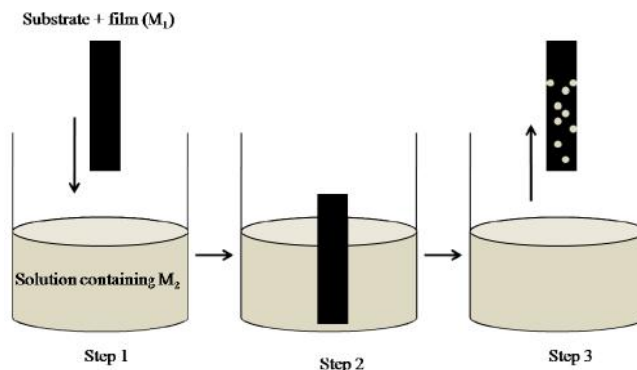


Figure 2.13: Schematic of chemical dip method.

## 2.7 EXPERIMENTAL ANALYSIS OF AZO:Pd FILM

### 2.7.1 GIXRD

The GIXRD patterns were obtained by using  $\text{CuK}_\alpha$  radiation at a fixed  $3^\circ$  grazing incidence angle. The detector scan was performed from  $20^\circ$  to  $80^\circ$  that was sufficient to capture all important palladium peaks. The XRD patterns (as shown in Figure 2.14) reveal the polycrystalline grain structure (of surface modified AZO), and the most preferred (002) orientation is shown by the presence of the most intense reflection around  $34.3^\circ$  (JCPDS card: 760704).

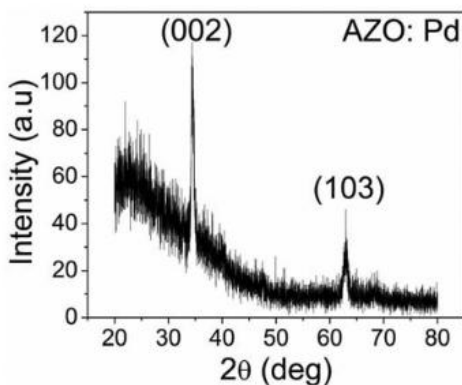
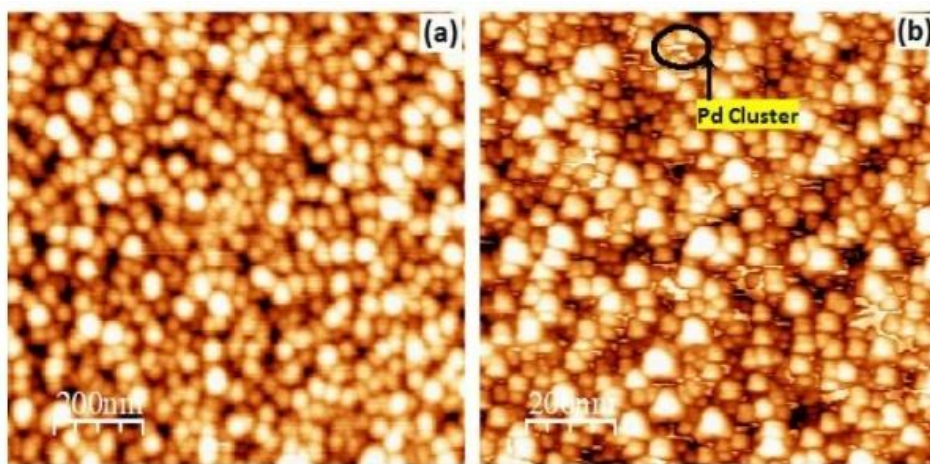


Figure 2.14: GIXRD of Pd modified AZO nanofilm (AZO:Pd)

Zinc oxide crystallizes in hexagonal crystal system (wurtzite) and the grains are oriented along c-axis, which is an energetically stable configuration [224-225]. No Pd peaks are observed in the XRD pattern of Pd modified AZO, and this probably implies that the concentration of Pd on the surface is small.

### 2.7.2 AFM (Atomic Force Microscopy)

The AFM topography of unmodified AZO surface and Pd modified AZO surface is shown in Figure 2.15(a) and 2.15(b) respectively. An overall uniformity of the surface morphology of both surfaces can be seen from the AFM images.



**Figure 2.15:** AFM topography (scale length 200 nm) (a) unmodified AZO surface  
(b) Pd nanoparticle modified AZO surface

The average AZO grain size is ~27-29 nm. In Figure 2.15(b), the appearance of some clusters in the valleys between granular hills is attributed to the presence of palladium nanoparticles. Such clusters are absent in the unmodified topography (Figure 2.15(a)). The huge number of such clusters distributed over the undulating AZO granular morphology provides the catalytic surface area for enhanced solid-gas interaction.

## **CHAPTER 3**

**Fabrication of sensor device and  
electrical measurements**





## CHAPTER 3

### FABRICATION OF SENSOR DEVICE AND ELECTRICAL MEASUREMENTS

#### 3.1 RESISTIVE DEVICE FABRICATION BASED ON:

##### 3.1.1 Pure palladium nanofilm device with interdigitated electrodes

Three simple steps (Figure 3.1) prepared palladium based sensing device. Step 1 includes drawing parallel electrodes (silver paint) using a fine needle manually across the edges of palladium film (film is prepared in section 2.3). Step 2 contains drawing lines perpendicular to these parallel electrodes. More such lines are drawn carefully (along with drying so that they do not conjoin) to form a mesh like design which are called interdigitated electrodes (step 3) so as to cover almost all sections of the sensing film. The separation between any two parallel silver electrodes was less than 1 mm.

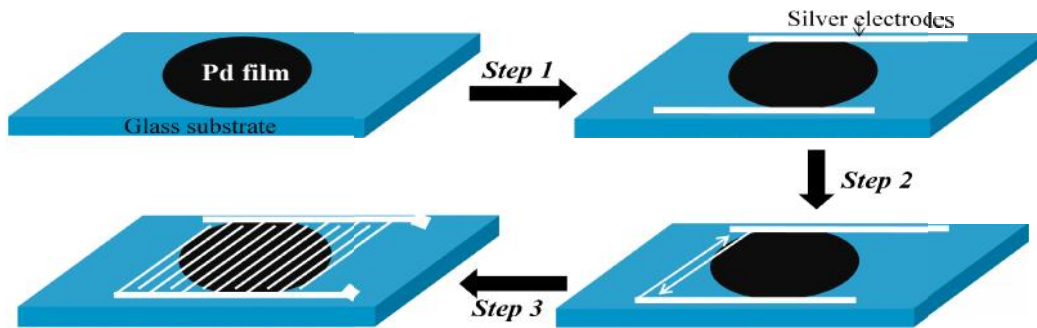


Figure 3.1: Schematic of sensor device (pure Pd).

The two opposite ends of interdigitated electrodes were then connected to the multimeter using thin copper wires to record the change in resistance of the film (Figure 3.2).

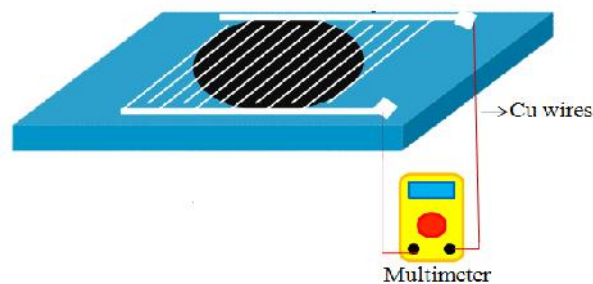


Figure 3.2: Sensing device connected to digital multimeter.

### 3.1.2 AZO:Pd nanofilm device with two parallel electrodes

The fabrication of AZO:Pd device includes the similar steps as discussed in Figure 3.1. The only difference is that in this case, two parallel electrodes were drawn on the surface of the prepared AZO:Pd films (as discussed in section 2.6) [Figure 3.3]. The total (AZO:Pd) device area was  $\sim 5\text{mm} \times 5\text{mm}$ , and the separation between the two parallel silver paste electrodes was  $\sim 2\text{ mm}$ . The two opposite ends of interdigitated electrodes were then coupled with the multimeter using thin copper wires to record the change in resistivity of the film (in a similar manner as shown in Figure 3.2). The arrangement of AZO grains and Pd NPs is shown as displayed by AFM images in section 2.7.2.

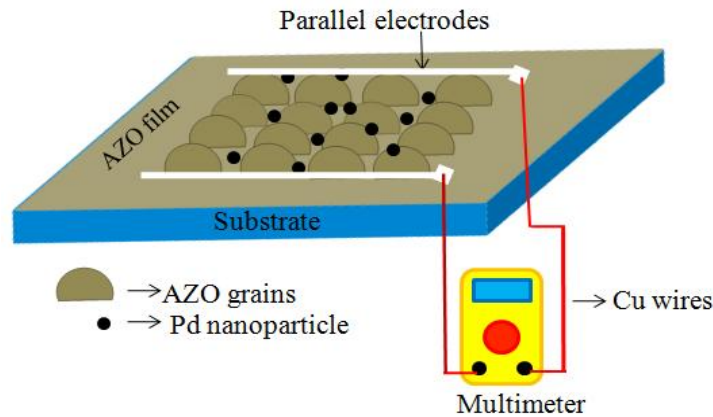


Figure 3.3: Schematic of sensor device (AZO:Pd).

### 3.2 IMPORTANCE OF SUBSTRATE

Substrate is a platform onto which a thin layer of nanomaterial is deposited. A large range of substrates exists like Teflon, glass, Quartz, alumina, plastics, silicon *etc.* Selection of substrate is in accordance with the application of deposited material. Thin films of thickness less than micrometers loses tendency to withstand the stresses due to temperature and pressure. Thus, a support is needed to withstand these stresses. The supporting material should be porous, hard (resistant to fracture), corrosion resistant, fast adhesion, isotropic, stability, free of contaminants and organic components, moisture free, porous or non-porous (application dependent), *etc.* Substrates are categorized as interfering substrate and non-interfering substrates. Substrates such as glass are non-interfering substrates, as it does not interfere with the electrical, optical or mechanical properties of deposited film. In case of interfering substrates, the orientation and crystallinity of substrate readily affects the

morphology and crystallinity of deposited film [226-228]. Sometimes it becomes important to use interfering substrates to modify the properties of the film for particular applications.

Many substrates are reported to prepare palladium thin films like glass [217,229-235],  $\text{Al}_2\text{O}_3$  [214], Silicon [236-238], GaAs [239], alumina [240-241] etc. In this work, palladium nanoparticles are deposited on clean glass substrate (non-interfering substrate) to display overall effect of palladium in hydrogen sensing (no contribution from substrate). A simple low cost glass substrate could reduce the overall price of commercial sensor. The pure Pd nanoparticle based sensors have efficient performance at low temperatures ( $<60^\circ\text{C}$ ) [97,242]. To improve the response of palladium based sensor device at high temperatures also, palladium was decorated on the surface of AZO (Aluminium doped Zinc Oxide) (interfering conducting base). AZO surfaces are stable at high temperatures and their conducting properties could help in maintaining the sensor response of palladium film. Consequently, the Pd decorated AZO devices are useful for both low and relatively high temperature applications. Moreover, this temperature range of application can be further controlled by suitable choice of substrate and catalytic nanoparticle.

### **3.3 SENSOR SETUP AND ELECTRICAL MEASUREMENTS**

A basic gas sensor setup is demonstrated in Figure 3.4. The testing chamber is connected to a gas inlet and gas outlet for the entry and exit of gases respectively. The gas cylinders that are bridged with mass flow controllers and mass flow meters provide the gases to flow in the testing chamber. Mass flow controller is a device that controls the flow of specific gas in a chamber at particular flow rates. Heater provides the wide range of temperature and pressure gauge maintains the desired pressure of gases inside the chamber. The sensing device is placed in this chamber and the electrical change in device is recorded on a sensitive multimeter.

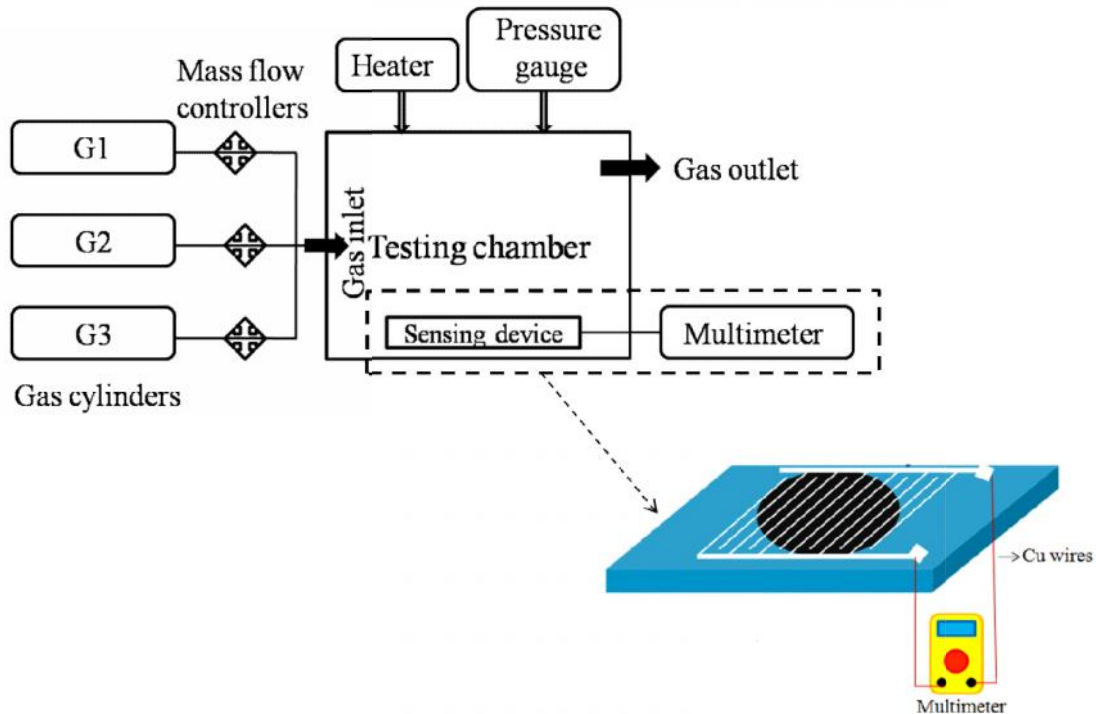


**Figure 3.4:** Block diagram of sensor setup.

In this study, the prepared sensing device (based on Pd NPs and AZO:Pd) was placed inside the sensing chamber. High purity gases (negligible moisture content (<2 ppm)) like hydrogen, methane, and air [hydrogen gas (H<sub>2</sub>) 99.998 vol. %; methane gas (CH<sub>4</sub>) 99.99 vol. %; and air (oxygen ~20 vol. % and nitrogen ~80 vol. %)] were sent into the sensing chamber using mass flow controllers and mass flow meters (Digiflow, USA). For recording the data, Agilent digital multimeter (Agilent U1252A) and Keithley Pico ammeter (Model 6487, M/S Keithley Instruments) were used. The main chamber is placed co-axially inside a resistively heated furnace with a 4 cm constant temperature zone. A copper-constantan thermocouple coupled with a precise temperature controller ( $\pm 1^\circ\text{C}$  accuracy) is used to monitor the temperature.

Basically, sensor response data is represented as the relative response of sensing device. The electrical sensor response can be plotted in many ways depending on the properties of material. For example, Current vs Voltage (I-V) at constant temperature, Voltage vs Temperature (V-T) at constant current, Resistance vs Time at constant voltage, Response% vs Time at constant gas concentrations etc.

In this study, the hydrogen gas response of prepared resistive sensor devices was determined by plotting device resistance (hydrogen gas loaded) versus exposure time graphs. Since the

electrical properties of palladium film changes when it is exposed to reducing or oxidizing gas [243]. Thus, the response study of palladium based films was carried out as resistance-time plots.

The sensor parameters were computed as follows:

- Sensitivity:** Sensitivity is the ability of the sensor of how fast the output (say for example, electrical quantity such as volts or resistance) changes in response to the change in the input parameter. Sensitivity of a resistive gas sensor is calculated by the following formula:

$$\text{Sensitivity} = \frac{\text{change in resistance (gas loaded)}}{\text{resistance (no gas)}}$$

Or

$$\text{Response \%} = \frac{R_a - R_g}{R_a} \times 100, \quad \text{at constant voltage.}$$

where  $R_a$  is the resistance of device in air (no test gas loaded) and  $R_g$  is the resistance of device when test gas is loaded (Figure 3.5)

- Response time:** Response time is the time taken by sensor to reach 90% of saturation value.

From Figure 3.5, response time is given by  $t_2-t_1$

- Recovery time:** Recovery time is time taken by sensor to reach 90% of its baseline value.

From Figure 3.5, recovery time is given by  $t_3-t_4$

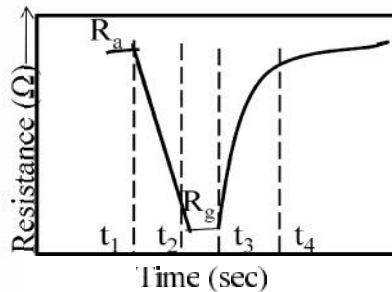


**Figure 3.5:** General response pattern

For a commercial sensor, the response time and recovery time should be very low (<1 second)

- 4. Selectivity:** Selectivity means that the sensor is unresponsive to the gases other than test gas. If a contribution to the sensor signal comes from another gas, the sensor reading will provide a false measurement.
- 5. Reproducibility:** It is the ability of sensor to produce same results after repeated use at constant gas concentration. For a reproducible sensor, response pattern should be same as shown in Figure 3.6.

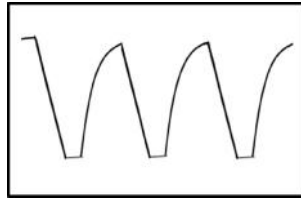


**Figure 3.6:** Reproducible sensor response.

- 6. Long-term stability:** Stability is a degree to which sensor results remains constant with time. Long-term stability is very important as sensor performance should not vary within minutes, hours or days. Generally, it happens that the material used to fabricate sensor degrades with time that changes its mechanical, electrical or chemical properties. Sometimes environmental conditions and storage conditions (improper isolation from environment) could also degrade the sensor device.

## **CHAPTER 4**

### **Hydrogen response results and discussions**





## CHAPTER 4

### HYDROGEN RESPONSE RESULTS AND DISCUSSIONS

In this study, the test gases used were hydrogen and methane, and nitrogen/air were considered as carrier gases. Study in nitrogen was done to understand the hydrogen sensing mechanism of sensor device in an unreactive atmosphere and study in air was conducted to reveal the potentiality of the sensor device for real field applications. Methane sensing was done to check the selectivity of palladium sensor device for hydrogen detection.

#### 4.1. RESPONSE STUDIES OF PURE Pd NPs DEVICES IN H<sub>2</sub>/N<sub>2</sub> AMBIENT

For understanding the hydrogen sensing behavior of prepared palladium films, these films were exposed to a range of hydrogen concentrations (0.1%, 0.2%, 0.3%, 0.4%, 0.5% and 1%) in nitrogen ambient at different temperatures (35°C-75°C) (Figure 4.1).

The absorption and desorption of hydrogen gas on palladium surface changes the resistance of the palladium film. We practiced this phenomenon to obtain the sensor response. Sensor output includes the change in resistivity (whether this be an increase or decrease) of the palladium film for different concentration of hydrogen gas at different temperatures. The resistance change is calculated by subtracting the resistance at no gas and the resistance after introducing hydrogen gas. The sensor response (S) is defined as the ratio of the change in resistance in presence of hydrogen mixed with nitrogen to the initial resistance in nitrogen at a constant voltage and is expressed as:

$$S = \frac{R_n - R_h}{R_n}$$

where  $R_n$  is the resistance of device in nitrogen ambient (hydrogen unloaded) and  $R_h$  is the resistance in H<sub>2</sub>/N<sub>2</sub> ambient.

In this study, the device showed almost zero response at 30°C. So, the studies were carried out at the starting temperature of 35°C. Figure 4.1 displays excellent response patterns for all hydrogen concentrations. It is also observed expectedly that the response magnitude is decreasing with decrease in hydrogen concentration. This is because at lower hydrogen concentrations, few hydrogen atoms gets adsorbed on palladium surface which decreases the overall response of device. For each concentration, the sensor measurements were repeated

four times in cyclic manner to check the reproducibility of the response and recovery characteristics. A stable baseline resistance with little fluctuations obtained from the experiments for a week, as shown in Figure 4.1, indicates that the device has reproducible performance. The baseline stability is necessary to make the device compatible for real field applications. Further, a decrease in the baseline resistance with the increase of temperature is probably due to the thermal expansion of the Pd nano particles and decrease in the interparticle gap. The device performance deteriorated beyond 50°C and the transient response patterns at 60°C and 75°C show a continuous drift in the baseline resistance [Figure 4.1 (d)]. This behavior can be attributed to the formation of undesirable  $\beta$ -phase of PdH<sub>x</sub> and high thermal expansion is induced at temperatures beyond 50°C. Probably, the whole film morphology weakens at high temperatures and that is reflected in the baseline resistance shift with time. So, we limited our sensor study to a maximum operating temperature of 50°C.

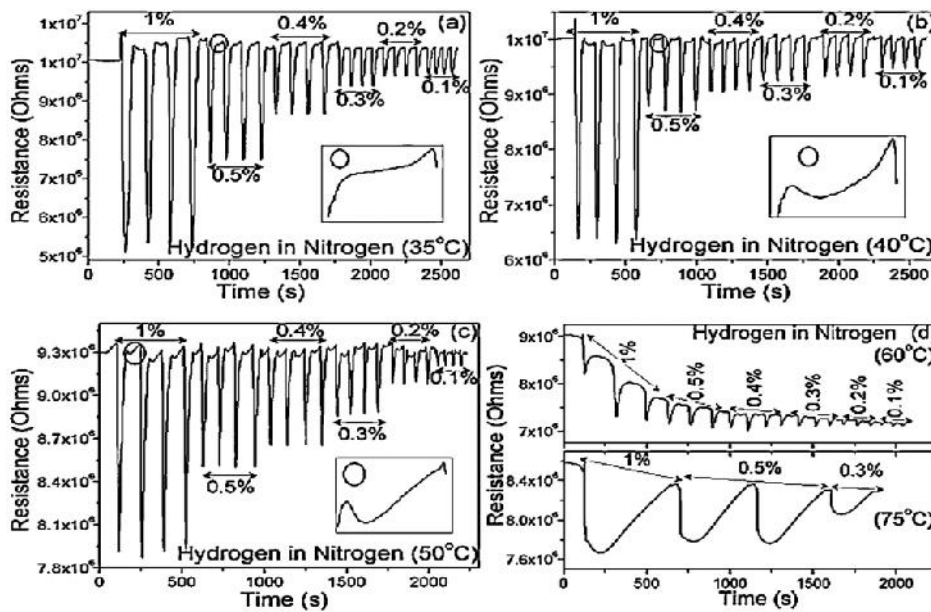


**Figure 4.1:** Transient response of palladium nanoparticle sensor in hydrogen mixed with nitrogen at (a) 35°C, (b) 40°C, (c) 50°C, and (d) 60°C and 75°C

The device shows dual response pattern to hydrogen/nitrogen mixture. At the initial stage of hydrogen exposure, the device resistance increases slowly and then suddenly drops to a low value. The initial response of the device towards hydrogen is shown in the insets of Figure 4.1 (a, b, and c). The total response is a combined effect of removal of spillover oxygen layer, increase in the resistivity of individual palladium matrix, and subsequent volume expansion of the Pd lattice.

Adsorption and desorption of hydrogen on palladium is not a single step process but has a multistep mechanism [244]. Hydrogen molecule first dissociates into hydrogen atoms and the hydrogen atoms get adsorbed on the surface sites of palladium. The hydrogen adsorption leads to the formation of non-stoichiometric palladium hydrides ( $\text{PdH}_x$ ), which changes the metallic character of palladium (increasing the resistivity of palladium) [245]. This increase in resistivity is due to the electron scattering (reduces the electronic mean free path) when hydrogen is incorporated into the palladium crystal lattice. Thus this is called electronic effect which leads to an increase in the resistance of the device. This all happens at the initial stage of hydrogen exposure. With more hydrogen exposure, a physical bonding between palladium and hydrogen results in some charge separation and formation of temporary dipoles. As a result, the lattice expands to accommodate these dipolar species. This looks like volume expansion of palladium. This is known as the geometric volume effect, which helps in reducing the inter-nanoparticle gap, and hence decreases the resistance [246] (Figure 4.2). However, the device resistance will not be close to zero due to simultaneous effect of  $\text{PdH}_x$ .

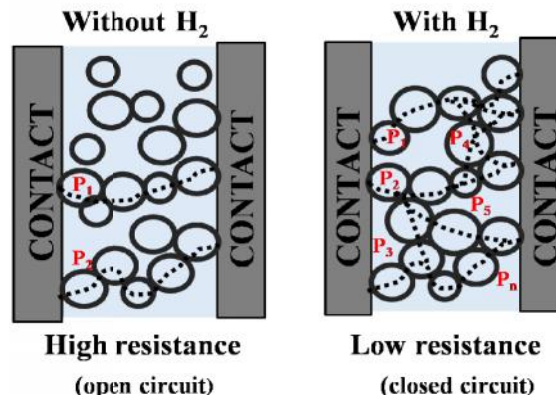


**Figure 4.2:** Schematic of geometric effect.  $P_1, P_2, \dots, P_n$  are the number of conducting pathways.

The oxygen spillover also plays role in sensing mechanism. Initially the spillover oxygen layer covers the highly reactive palladium nanoparticle surface by saturating the dangling bonds [1]. The catalytic metals gather highly reactive oxygen species from the atmosphere in order to reduce their surface activity. The schematic of oxygen spillover mechanism on palladium surface before and after hydrogen exposure is shown in Figure 4.3. Without hydrogen, the surface of palladium and the interface between two palladium nanoparticles are covered by a thick layer of charged oxygen species. The electron path is completed by this charged layer, which is the reason why we get a definite high resistance, instead of open circuit infinite resistance (Figure 4.1). The charged oxygen layer contains  $\text{O}^-$  and  $\text{O}^{2-}$  oxygen

species. The former is unsaturated with a possibility of getting saturated by accepting an electron, whereas the latter is saturated with a possibility of donating an electron to become unsaturated. This is expressed in the following equations:

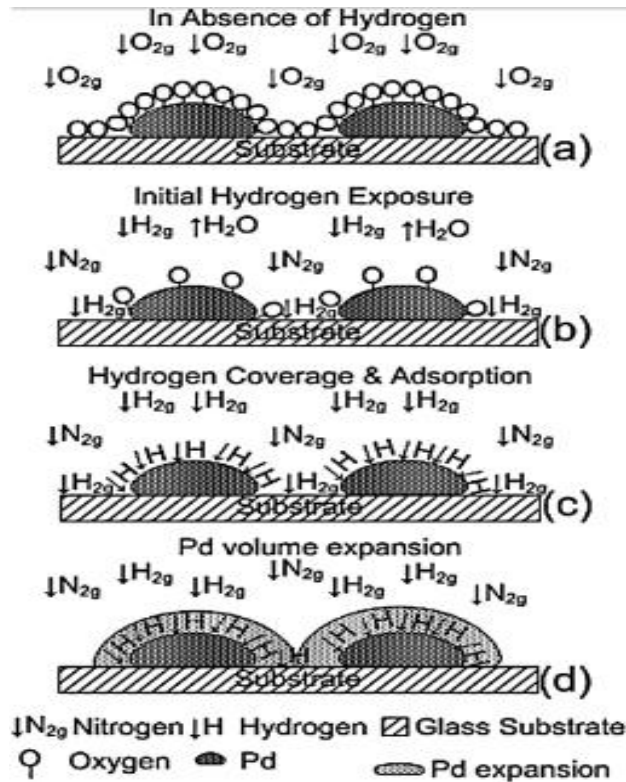
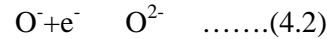
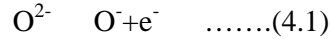
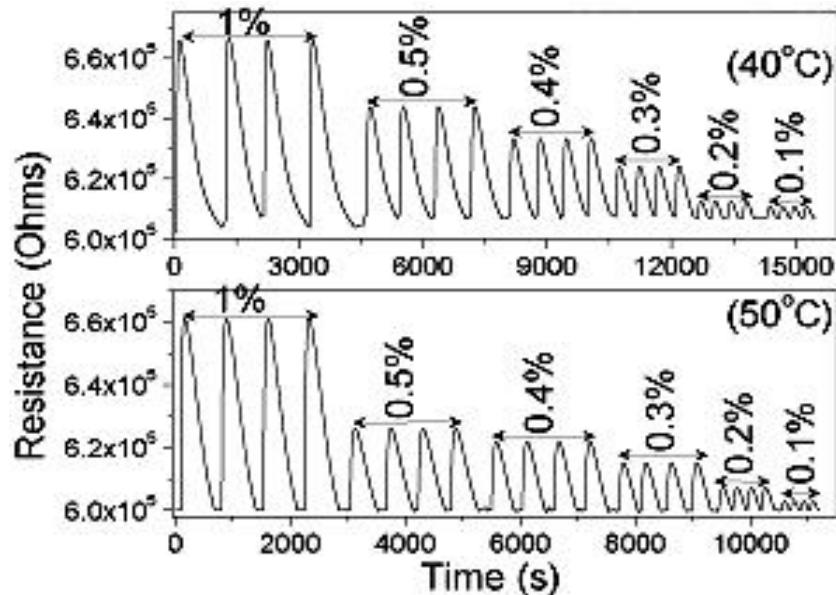


Figure 4.3: Hydrogen sensing mechanism of palladium nanoparticles.

During initial hydrogen exposure, the oxygen species are slowly removed from the palladium surface by water formation, and leaves the adsorption sites vacant. These vacant surface sites are then gradually filled by hydrogen atoms that gets adsorbed in the palladium matrix. The water formed in the molecular level will be carried away by the carrier gas (inside testing chamber) and will have negligible interference on the response because palladium has much higher affinity for hydrogen than water molecules. With time, the entire spilled over oxygen layer is removed and the surface gets saturated with hydrogen, because of adsorption of huge quantity of hydrogen atoms on the palladium matrix.

#### 4.2. RESPONSE STUDIES OF PURE Pd NPs DEVICES IN H<sub>2</sub>/air AMBIENT

A similar transient response studies were carried out in air ambient at 40°C and 50°C, since the device performance deteriorated beyond 50°C and no appreciable response was obtained below 40°C (Figure 4.4).



**Figure 4.4:** Transient response of palladium nanoparticle sensor in hydrogen mixed with air at 40°C and 50°C

Figure 4.4 displays excellent response patterns for all hydrogen concentrations (0.1%-1%). To check the reproducibility of the sensor response, the sensor measurements were repeated four times in cyclic manner for each concentration. A stable baseline resistance was also obtained. In this case, there is only increase in resistance of device when exposed to hydrogen. Initially, the palladium nanoparticles are covered by a thick oxygen layer. As the hydrogen/air mixture is introduced, hydrogen tends to extract charged oxygen species from the surface to form water, and the oxygen vacant sites are occupied by hydrogen. This leads to the formation of PdH<sub>x</sub> in the surface layers, which increase the device resistance. However, the nanoparticles are exposed to more oxygen compared to hydrogen because of higher oxygen partial pressure in the hydrogen-air mixture. So, the mechanism of sensing in air ambient is a competitive effect of forced oxygen removal by much lower percentage of hydrogen and more oxygen adsorption due to very high partial pressure of oxygen in the carrier gas. Basically, in air ambient, the resistivity change is significant, and the volume expansion is not significant due to low hydrogen adsorption. If both effects were there, the

## Chapter 4 Hydrogen response results and discussions

resistance would increase and then decrease. The response was found very fast but the recovery was delayed for each hydrogen concentration. This may be due to trapping of hydrogen atoms in the palladium during the forced oxygen removal and easy oxygen adsorption processes. The response parameters were calculated by the formulas discussed in chapter 3 and are listed in Table 4.1. The minimum response time obtained in the present study, corresponding to 90% of the saturation time required for volume expansion, is 3 s at 50°C and with 1000 ppm hydrogen in nitrogen. If we compare the sensor response of Figure 4.1 and Figure 4.4, we observe that in the inert nitrogen ambient, both response and recovery are fast relative to that in air, which is due to the fact that the adsorption as well as desorption is a one way process without any competition from the oxidizing species.

**Table 4.1:** Response (%), Response and Recovery times (for 90% change) of the palladium nanoparticle sensor for sensing hydrogen (a) mixed with nitrogen and (b) mixed with air at 50°C.

Temperature	Concentration	Hydrogen in Nitrogen			Hydrogen in Air		
		Response (%)	Response time (s)	Recovery time (s)	Response (%)	Response time (s)	Recovery time (s)
50°C	1%	15.4	10	31	10.2	40	430
	0.5%	9.1	8	24	4.39	44	340
	0.4%	7.24	7	24	3.63	44	280
	0.3%	5.11	4	20	2.51	40	234
	0.2%	2.73	3	18	1.2	41	150
	0.1%	1.15	3	10	0.48	33	82

Prior to the transient measurements with hydrogen mixed with air, the baseline resistance of the device was monitored in nitrogen and in air separately at 40°C (Figure 4.5). It was observed that the baseline resistance decreased on changing the ambient from nitrogen to air. In fact, the baseline resistance in air was ~0.1 times that in nitrogen and the reason is the oxygen spillover as discussed earlier. In an inert atmosphere, the partial pressure of oxygen is negligible. So, there is a high probability of oxygen desorption from the spillover oxygen layer on the Pd nanoparticle surface and it disturbs the continuous electrical conducting path provided by the surface adsorbed oxygen species. As a result, the observed baseline resistance in the inert ambient is relatively high.

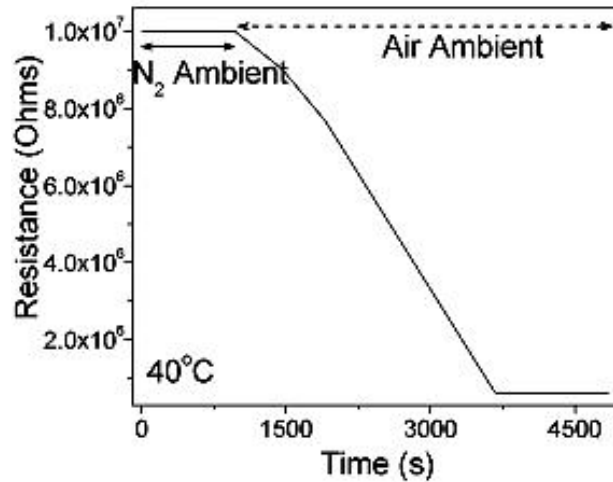


**Figure 4.5:** Shift in baseline resistance by changing the ambient atmosphere from nitrogen (N<sub>2</sub>) to air.

When the inert ambient is changed to the oxidizing atmosphere (air), sufficient oxygen is available above the sensing layer, which promotes re-adsorption of oxygen on the vacant sites of the spillover layer, due to high oxygen partial pressure. As the surface gets saturated with oxygen species, the baseline resistance drops to a lower value.

Figure 4.6 shows the comparative picture of response-recovery characteristics with the hydrogen concentrations at  $40^\circ\text{C}$  and  $50^\circ\text{C}$ . There is an increase in the magnitude of the response parameters with increase in concentration of the hydrogen gas. As per sensing mechanism, if the concentration of the sensing gas is high, the resistance change is high and the vice versa. So, the increase in percentage response at higher concentration is quite natural. However, the recovery takes longer time for higher concentration of hydrogen gas. But recovery is improved at higher temperatures due to faster desorption kinetics. At the same time, the response magnitude decreases at higher temperature due to lower gas adsorption rate above an optimum value of temperature. Thus, from these studies, it is evident that catalytic Pd nanoparticles are efficient for sensing hydrogen at lower temperatures.



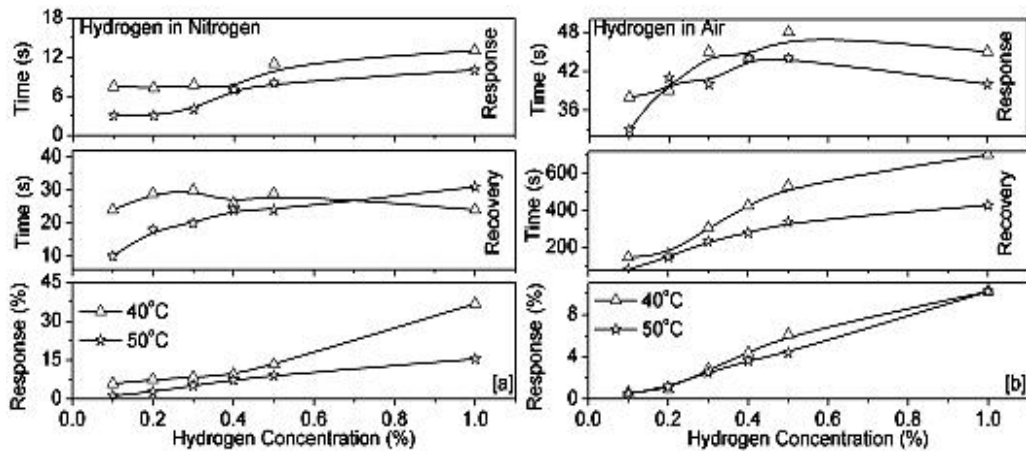


**Figure 4.6:** (%) Response, response time and recovery time of the palladium nanoparticle sensor for sensing hydrogen (a) mixed with nitrogen and (b) mixed with air.

To check the selectivity of prepared sensing device, the device was exposed to another reducing gas i.e. methane. No response for methane (1%) was observed below 75°C (Figure 4.7). A slight change in resistance was observed for methane (1%) in air at 75°C (Figure 4.7) but that was negligible compared to that shown for hydrogen. The test was conducted with 1% of methane, not beyond that as at 1% as no response was observed, so obviously lower concentration will also not respond.

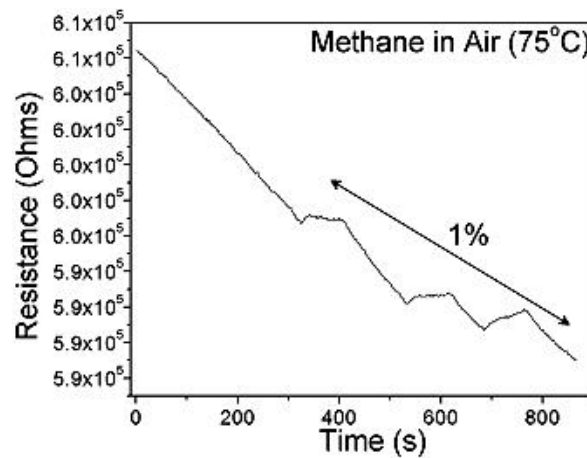


**Figure 4.7:** Response of palladium nanoparticle sensor to 1% methane in air.

In principle, heavy molecules like methane need high activation energy to show appreciable response by removing surface oxygen atoms. It can be provided at the higher temperatures. Since, our device is responding only upto 50°C. So, for low temperature operation (~50°C) the palladium nanoparticle based sensor devices are selective to hydrogen.

### 4.3 RESPONSE STUDIES OF SURFACE MODIFIED DEVICES (AZO:Pd films) IN AIR AMBIENT

To study the hydrogen response of AZO:Pd devices, these devices were exposed to different concentrations of hydrogen gas at wide range of temperature in air ambient, and the corresponding change in device resistance was recorded (Figure 4.8(a-g)). Excellent response patterns were obtained at all hydrogen concentrations as well as at all temperatures. Since, there was negligible response for hydrogen below 40°C, and hence, the sensor response was recorded in the temperature range, 40°C–150°C. The AZO layer (without Pd) showed no response to hydrogen mixed with air in the studied temperature range. So the sensitivity of the device is controlled by the catalyst palladium. The baseline resistance of the device changed with the increase in temperature, and the variation is shown in Figure 4.8(h). It can be seen from Figure 4.8(h) that during the initial rise in temperature, the device resistance decreased, and thereafter, it started to increase from ~100°C. At relatively higher temperatures (75°C–100°C), the AZO matrix undergoes semiconductor-to-metal transition and the transition is complete near ~98°C. Beyond this transition (for temperatures >100°C), the device is fully metallic. Theoretically, the resistance of semiconductors decreases with increase in temperature (due to shift in Fermi level towards conduction band) and resistance of metals increases with temperature (due to the increase in electron scattering centers).

From the response patterns shown in Figure 4.8 (a-g), it is observed that the resistance of the AZO:Pd device decreases in the presence of hydrogen. This decrease in device resistance is attributed to the generation of the electrons at all temperatures due to palladium-hydrogen interaction, which increases the device current. This decrease in resistance can also be explained by Figure 4.9. Since ZnO is a semiconductor, thus there is always the formation of a potential barrier between the grains of Al doped ZnO which directly controls the electrical conductivity of device. Any variation in this barrier will modulate the charge transport properties between the grains.

Furthermore, from AFM images (Chapter 2, Section 2.7.2), it is clear that the palladium nanoparticles or nanoclusters are present between the inter-granular valley regions, and are scattered all over the AZO surface in a discontinuous manner.

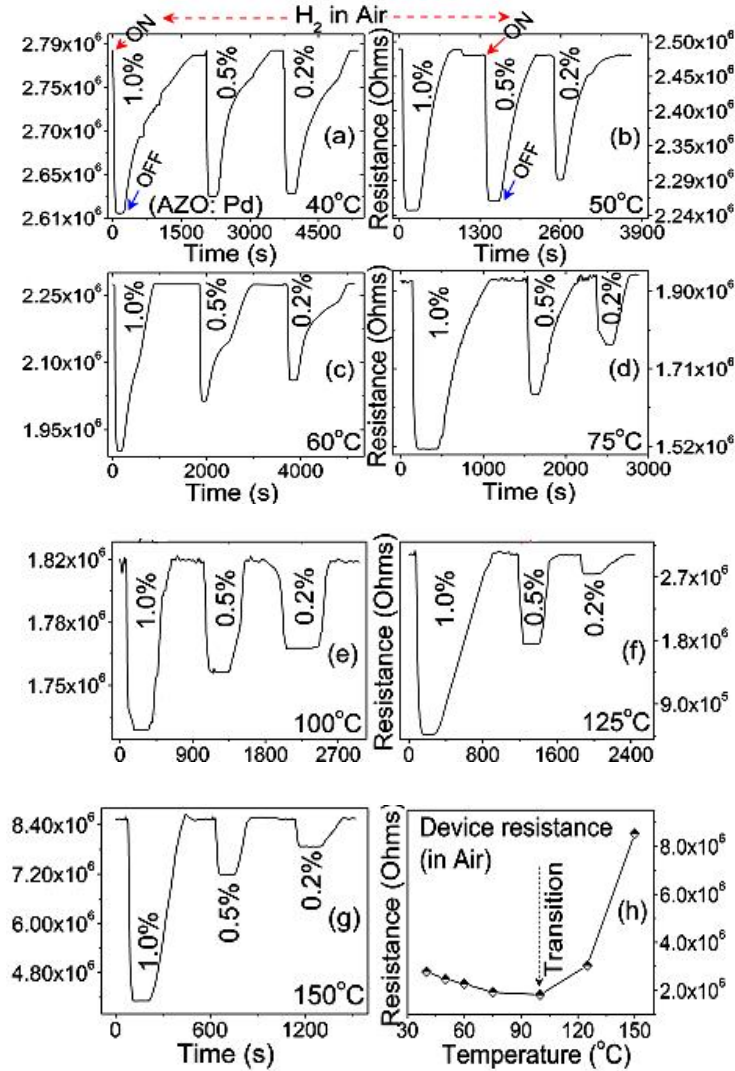


**Figure 4.8:** (a)–(g) Transient response of AZO:Pd devices in different concentrations of hydrogen mixed with air in the temperature range 40°C-150°C. (h) Variation of (baseline) device resistance with temperature in air ambient.

Thus, a parallel network of charge transport path is formed; one path is along Pd and other along AZO. Electronically, if two resistance paths are parallel, then their output resistance decreases. This is supported by following common equation.

$$\frac{1}{R_o} = \frac{1}{R_1} + \frac{1}{R_2}$$

where  $R_o$  is the output resistance.

Hence, the total conducting path between the measuring DMM leads can be considered as a series combination of two types of resistive barriers. The first type of barrier is the parallel combination of Pd and AZO, while the second type comprises of only the AZO resistance without Pd because the palladium dispersion is discontinuous. A schematic representation of the parallel paths is shown in Figure 4.9.

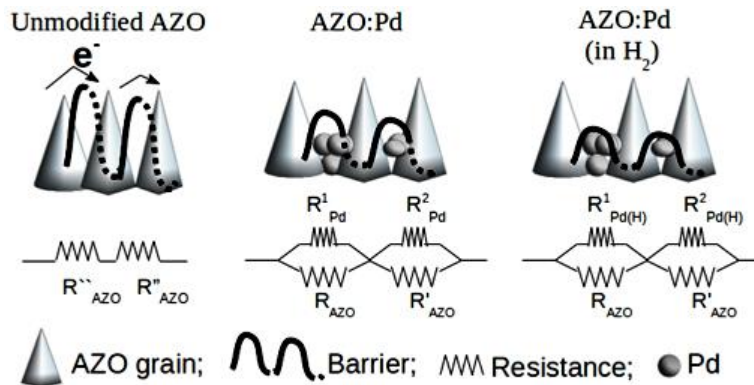


**Figure 4.9:** Sensing mechanism of AZO:Pd devices (AZO resistors are only temperature dependent, whereas Pd resistors depend both on temperature and adsorbed hydrogen).

After getting the excellent response patterns, response parameters were calculated by the formulas discussed in chapter 3 and were plotted in Figure 4.10 at different temperatures. The response parameters varies depending on the variation of conductivity of the metallic (Pd) and AZO paths at different temperatures. We observed that the response time is minimized and the (%) response maximized at two different temperature regimes ( $\sim 65^{\circ}\text{C}$  and  $\sim 135^{\circ}\text{C}$ ) (Figure 4.10 (a,c)). The response curve in Figure 4.10 (a,c) shows similar behavior. Response time is maximum at two temperature points. First maxima ( $\sim 45^{\circ}\text{C}$ ) is due to competition between electronic and geometric effect of palladium and second maxima ( $\sim 100^{\circ}\text{C}$ ) is due to the semiconductor-to-metal transition. At low temperatures, the response is dominated by the electronic effect because the amount of adsorbed hydrogen atoms is low.

The intensity of the electronic effect maximizes in the temperature range  $40^{\circ}\text{C}$  to  $50^{\circ}\text{C}$ , and in this temperature range, the geometric effect is less dominant. The electronic effect increases the resistivity of Pd due to the formation of palladium hydrides (resistivity of  $\text{PdH}_x$  is more than Pd), which reduces the electronic mean free path. So, the competition between the two effects at low temperatures prolongs the resistance saturation time (or in other words the device saturation time). As a result, the calculated response time is high.

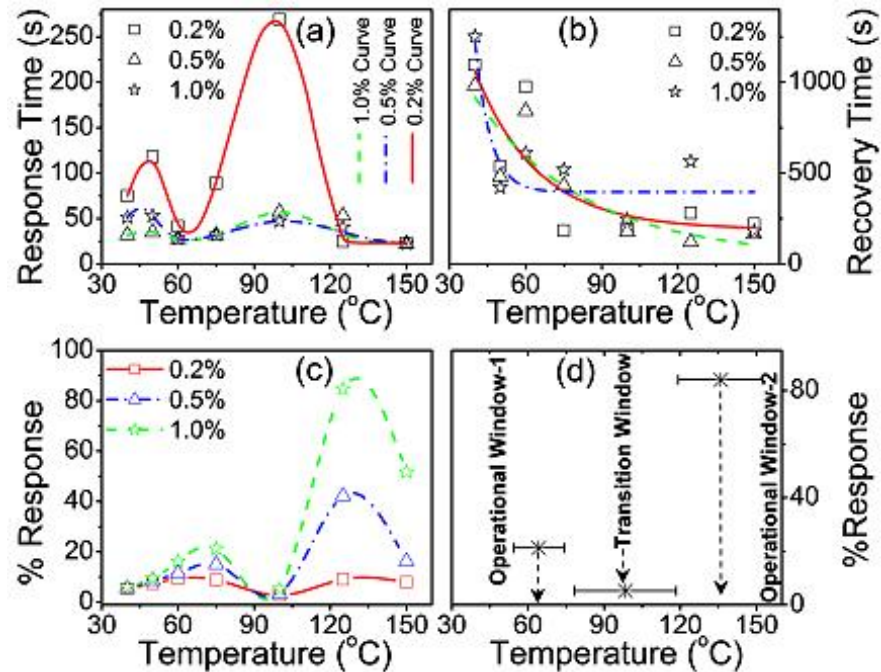


**Figure 4.10:** (a) Response time, (b) recovery time, (c) response (%), and (d) temperature windows, of AZO:Pd devices in different concentrations of hydrogen mixed with air in the temperature range 40°C–150°C.

Upon increasing the temperature further (50°C–70°C), the geometric effect becomes prominent due to higher hydrogen adsorption, and this is further aided by the thermal expansion of the metallic lattice. As a result, the electronic effect is completely masked by the geometric effect and the sensor signal quickly saturates. The calculated response time shows a minimum just after 60°C, which corresponds to the first favorable temperature window [Figure 4.10(d)]. Beyond 60°C, the thermal expansion is relatively higher, and the palladium clusters act just like catalytic centers for hydrogen dissociation, adsorption, and release of electrons. The second favorable temperature window was observed after the completion of this transition (after 120°C) [Figure 4.10(d)]. Thereafter, with the rise in temperature, the % response decreases (around 150°C), and it can be attributed to the dominance of hydrogen gas desorption over adsorption. So, any higher temperature beyond 150°C will only manifest deterioration in the hydrogen response of the device. Hence, hydrogen sensor operation beyond 150°C is not recommended for these devices.

From Figure 4.8(b), we observe that there is a complete but slow recovery of the sensor signal back to its baseline value at all the temperatures i.e. the device takes longer time to saturate (high recovery time). This is attributed to the fact that even though the generated

electrons prefer the least resistive metallic (Pd) path while crossing the parallel AZO: Pd barrier, they eventually encounter the AZO barrier, which ensures maximum hindrance to charge transport. So, the (%) response deteriorates and the sensor signal takes relatively longer time to saturate, which also maximizes the response time. The variation of recovery time with temperature is shown in Figure 4.10(b). Unlike the sensor response, the recovery time decreases exponentially with the increase of temperature. This is because the desorption rate is accelerated by the higher thermal energy at higher temperatures.

To check the reproducibility of AZO: Pd device, the experiment was performed repeatedly two times at the two temperatures (below and above the transition temperature) by varying the gas concentrations (Figure 4.11). The steady sensor performance with negligible fluctuations in baseline resistance, obtained from the repeated experiments performed for a period of five days, indicates that the device has reproducible performance with time in the studied temperature range.

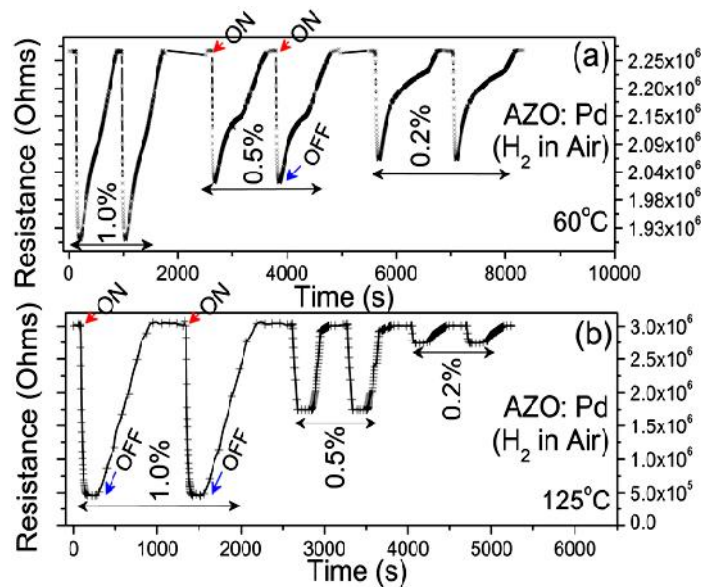


**Figure 4.11:** Repeated cycle transient response of AZO: Pd devices in different concentrations of hydrogen mixed with air at (a) 60°C (b) 125°C

To check the selectivity of prepared sensing device towards hydrogen, experiment was performed with other reducing gas methane ( $\text{CH}_4$ ) (Figure 4.12). The device showed no response to  $\text{CH}_4$  gas in the studied temperature range owing to good selectivity of device towards hydrogen.

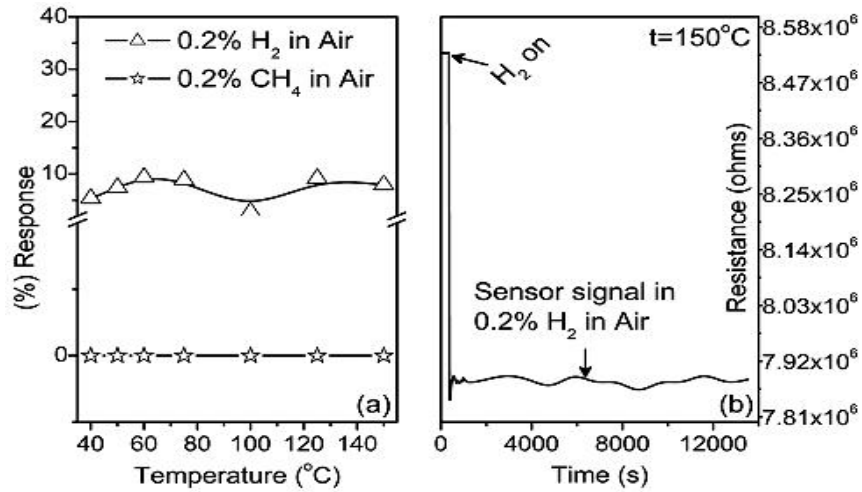


**Figure 4.12:** (a) Selectivity study of AZO:Pd devices. (b) Stability study of AZO:Pd devices.

The nil response of AZO:Pd devices toward heavy reducing CH<sub>4</sub> molecules is due to the lack of required activation energy necessary for the dissociation of CH<sub>4</sub> upto temperature 150°C.

## **CHAPTER 5**

**Adsorption kinetics on solid surfaces and  
theoretical interpretation of sensor data**

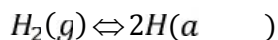




## CHAPTER 5

## ADSORPTION KINETICS ON SOLID SURFACES

The kinetics of hydrogen interaction with palladium is of great importance because of their hydrogen storage, hydrogen filtration or hydrogen sensing applications. The molecular hydrogen first dissociates into hydrogen atoms reversibly.



Once hydrogen is adsorbed on palladium surface, it reversibly diffuses into the palladium crystal lattice. Hydrogen atom tends to accommodate on interstitial tetrahedral and octahedral sites of palladium. In tetrahedral geometry, interstitial site lies at the centre of tetrahedron and in octahedral geometry, the interstitial site is located at the centre of octahedron (Figure 5.1).

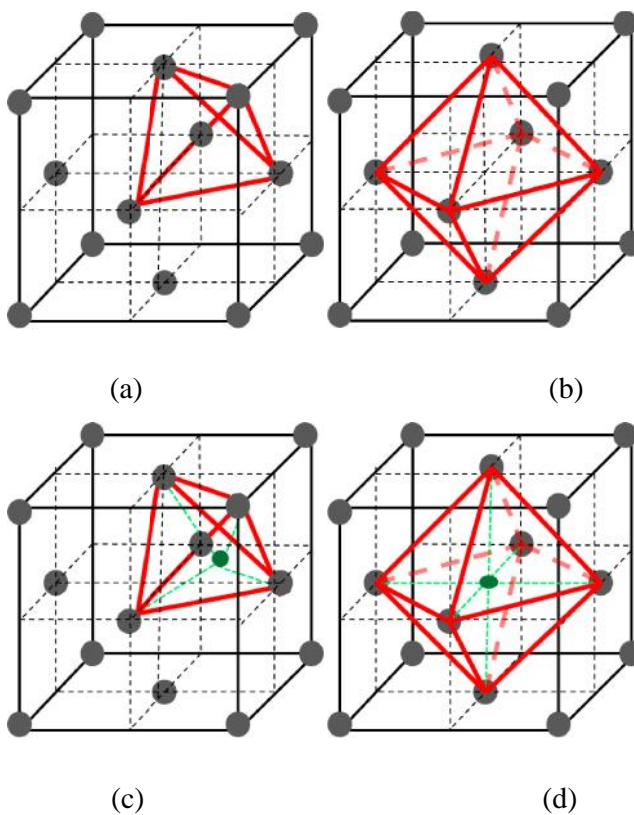


**Figure 5.1:** Schematic of (a) tetrahedral geometry, (b) octahedral geometry, (c) tetrahedral interstitial site, and (d) octahedral interstitial site. Green circle represents the interstitial site.

Occupation of hydrogen atoms in the tetrahedral and octahedral sites of palladium can be explored by radius ratio rule described as follows (Figure 5.2).

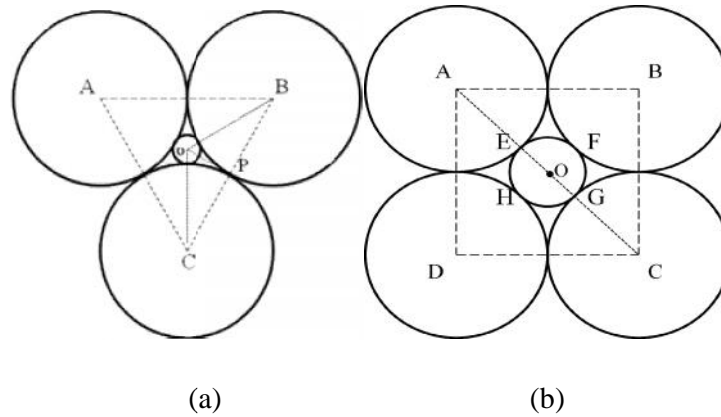


**Figure 5.2:** Schematic arrangement of host and guest atoms in (a) Tetrahedral configuration (b) Octahedral configuration.

Let  $r$  be the radius of the guest atom (hydrogen atom) and  $R$  be the radius of the host atom (palladium atom). The circle centered at  $O$  represents the host atom (hydrogen atom).

Tetrahedral site:

FCC structure has tetrahedral angle of  $109.5^\circ$  [247-248].

From Figure 5.2 (a),  $\angle OCP = 180 - (54.75 + 90) = 35.25^\circ$

Thus,  $\cos 35.25^\circ = \frac{R}{r+R}$

On solving, we get  $\frac{r}{R} = 0.225 \dots\dots\dots (5.1)$

Octahedral site:

In Figure 5.2 (b), let  $AC = x$  (say)

$AB = BC = CD = DA = a = \text{lattice constant} = 2R$

$AC = x = AE + EO + OG + GC = R + r + r + R = 2R + 2r$

Also,  $AC^2 = AB^2 + BC^2$

$\Rightarrow (2R + 2r)^2 = a^2 + a^2 = (2R)^2 + (2R)^2$

$2R + 2r = 2 \sqrt{2} R$

On solving, we get  $\frac{r}{R} = 0.414 \dots\dots\dots (5.2)$

Thus, it is concluded that the ratio of guest to host atom's size between 0.225 and 0.414 contributes towards occupation of host's tetrahedral sites by guest atom and the ratio greater than 0.414 contributes towards the occupation of host's octahedral sites by guest atom [249].

In summary,

if  $0.225 \leq \frac{r}{R} < 0.414$ , then guest atom will occupy the host's tetrahedral site.

or if  $\frac{r}{R} \geq 0.414$ , then guest atom will occupy the host's octahedral site.

Now, apply the radius ratio rule in the present system to find the scenario of hydrogen absorption in palladium (Pd) system. The radius of the hydrogen atom and Pd atom is 53 pm and 137 pm respectively [250-251]. According to the radius ratio rule,

$$\frac{r_H}{R_P} = \frac{53}{137} = 0.38$$

So it is seen that the ratio lies in the range of  $0.225 \leq \frac{r}{R} < 0.414$ . Thus, hydrogen atoms will first occupy the tetrahedral sites of Pd lattice and then will fill the empty octahedral sites (generally at high concentration of H atoms). This concludes that at  $\alpha$ -phase of palladium hydrides and hydrogen occupies tetrahedral sites whereas octahedral sites are occupied by  $\beta$ -phase of palladium hydrides.

The selective adsorption of hydrogen atoms on palladium surface depends on the surface energy of the surface planes. Pd exhibits fcc crystal structure with exposed (111), (100), (220) and (311) planes, out of which (111) and (100) are most prominent [97]. The surface energy of these planes varies as (111) < (100) [252]. The surface energy quantifies the formation of new free bonds (dangling bonds). It can be calculated by the formula given in equation (iii) [249]

The energy required per surface atom = (Energy of one bond) x (Number of bonds broken per atom)

$$\text{Surface energy, } \sigma = \frac{(e \text{ } \dots \text{ } )(\text{num } \dots \text{ } )}{s} \dots \dots \dots (5.3)$$

$$\text{Surface energy, } \sigma = \frac{1}{2} N_b \epsilon \rho_a$$

where  $\rho_a = \frac{N}{A} = \frac{N_i}{s_i}$ ,  $N_b$  is number of broken bonds and  $\epsilon$  is bond strength.

It is calculated as:

$$\gamma_1 = \frac{2\varepsilon}{\sqrt{3}a_0} = 1.15 b \quad \dots\dots(5.4)$$

$$\gamma_1 = \frac{4\varepsilon}{a_0^2} = 4 b \quad \dots\dots(5.5)$$

$$\gamma_1 = \frac{5\varepsilon}{\sqrt{2}a_0} = 3.53 b \quad \dots\dots(5.6)$$

where  $b = \frac{\varepsilon}{a_0^2}$ , and  $a_0$  is lattice parameter.

On dividing (ii) and (iii),  $\frac{\gamma_{110}}{\gamma_{100}} = 0.288 \quad \dots\dots(5.7)$

On dividing (ii) and (iv),  $\frac{\gamma_{110}}{\gamma_{111}} = 0.326 \quad \dots\dots(5.8)$

Thus we see that  $(110) > (100) > (111)$ . (100) planes have more surface energy as compared to (111) planes.

### **Solid gas interaction models (Adsorption isotherms):**

Adsorption is a significant term for adhesion. Adsorption relates the interaction of gas atoms with the surface sites only and absorption refers to the diffusion of atoms in the crystal lattice of material. The amount of gas absorbed/ adsorbed on the solid surface depends on vacant sites on the surface, gas concentration, gas partial pressure and temperature. The rate of adsorption/desorption can be expressed as following:

$$\text{Rate of adsorption} = k_1 p (1 - \theta)$$

$$\text{Rate of desorption} = k_2 \theta$$

where  $k_1$  is rate constant of adsorption and  $k_2$  is rate constant of desorption,  $p$  is gas partial pressure,  $\theta$  refers to sites occupied by gas molecules (surface coverage) and  $(1 - \theta)$  refers to vacant sites. At equilibrium, rate of adsorption = rate of desorption. Surface coverage  $\theta$ , is defined as the ratio of number of occupied adsorption sites to the total number of vacant sites. The rate of adsorption depends on the surface area of adsorbate (higher the surface area, more is the adsorption), surface coverage, vacant sites on surface and activation energy. The total volume of gas adsorbed on the solid surface can be expressed as  $V_t = V_o \theta$

Adsorption isotherm relates the behavior of gas adsorbed on solid surface as a function of partial pressure of gas at constant temperature. In the present work, the sensor response patterns were modeled by following adsorption isotherm models [253-255] to study the gas adsorption characteristics.

**Langmuir model:**

Langmuir is the basic model to study the adsorption of gas molecules on solid surface. The main assumptions of Langmuir isotherm are:

- It is based on the finite adsorption of adsorbent (gas molecules) on the monolayer homogeneous surface (i.e. all adsorption sites are equivalent) until equilibrium is reached.
- Each molecule occupies only one site and remains at the adsorbed site until it is desorbed. It means the adsorption is localized.
- The molecules adsorbed at particular adsorption site do not interact with neighboring sites.

In the present study, the formula used to fit Langmuir model is  $\Delta R = A \frac{k P_{H_2}^{\frac{1}{n}}}{1 + k P_{H_2}^{\frac{1}{n}}}$

where  $\Delta R$  is change in resistance of device,  $P_{H_2}$  is hydrogen pressure and A, k are constants.

**Freundlich model:**

Freundlich isotherm is applied for the case of multilayer heterogeneous adsorption (mainly for the rough surfaces). In real, a surface always has imperfections (especially surfaces prepared for sensing purpose). Thus it's difficult to convince that the surface is homogeneous.

The formula used to fit Freundlich model is:  $\Delta R = k_f P_{H_2}^{\frac{1}{n}}$ , where  $k_f$  is constant.

**Langmuir-Freundlich model:** The formula used to fit this model is:  $\Delta R = B \frac{k P_{H_2}^{\frac{1}{n}}}{1 + k P_{H_2}^{\frac{1}{n}}}$ , where

B is constant.

**SIPS model:** This model fits for heterogeneous surface layer adsorption. It reduces to Freundlich at high pressure and Langmuir at low pressure.

The formula used to fit SIPS model is:  $\Delta R = C \frac{kP_{H_2}^{\frac{1}{n}}}{1+kP_{H_2}^{\frac{1}{n}}}$ , where C is constant.

**TOTHmodel:** This model fits for monolayer adsorption. The limitation of both Langmuir and Freundlich is the applicability at low pressure only. Whereas, TOTH model fits for both low and high pressure of gas.

The formula used to fit TOTH model is:  $\Delta R = D \left[ \frac{kP_{H_2}^{\frac{1}{n}}}{1+kP_{H_2}^{\frac{1}{n}}} \right]^{\frac{1}{m}}$ , where D is constant.

### **Fitting of sensor data in adsorption isotherms:**

The absorption and desorption of hydrogen gas on palladium surface changes the electrical conductivity of the film. This phenomenon has been exploited to obtain the sensor response and to plot adsorption isotherms. Three isotherm models were tested for modeling the solid gas interaction (Pd-H) in the present system. The analysis of these isotherms is important in case of adsorption processes. Modeling the experimental data is an important way for predicting the mechanisms of adsorption process. In order to determine the best-fit model, the correlation coefficient (r) and coefficient of determination ( $r^2$ ) was used to evaluate the data. Co-relation coefficient signifies that how strong is the relation between the two variables. The value of  $r^2$  is important to determine which model has the best fit. For best fit, the value of  $r^2$  should be close to unity. Generally, the adsorption isotherm curve is a non-linear fit that describes the adsorption behavior at constant temperature. Co-relation coefficient is calculated by the following mathematical formula [256-257]:

$$r = \frac{n(\sum x y) - (\sum x)(\sum y)}{\sqrt{[n \sum x^2 - (\sum x)^2][n \sum y^2 - (\sum y)^2]}}$$

where n is the number of data points, x and y are the two variables related to each other. In this study, the change in resistance of palladium film with different hydrogen pressures are being observed. Thus here, “x” variable is the pressure (atmospheres) and “y” variable is the change in device resistance (ohms). As the pressure (or concentration) of gas increases, the amount of adsorption also increases.

In the present study, the hydrogen sensor response (AZO:Pd device) was furnished by using models like Langmuir, Langmuir-Freundlich (L-F), SIPS and TOTH. Theoretically, these models are governed by equations having little deviations from Langmuir-type of non-linear adsorption characteristics. In this study, we find that the fits give  $r^2$  values close to zero with L-F model at low temperatures, and SIPS model at high temperature. The data points were plotted as function of change in resistance and pressure of hydrogen gas and the model fittings were done (origin 8 software) as shown in Figure 5.3. The  $r^2$  values are shown in Table 5.1.

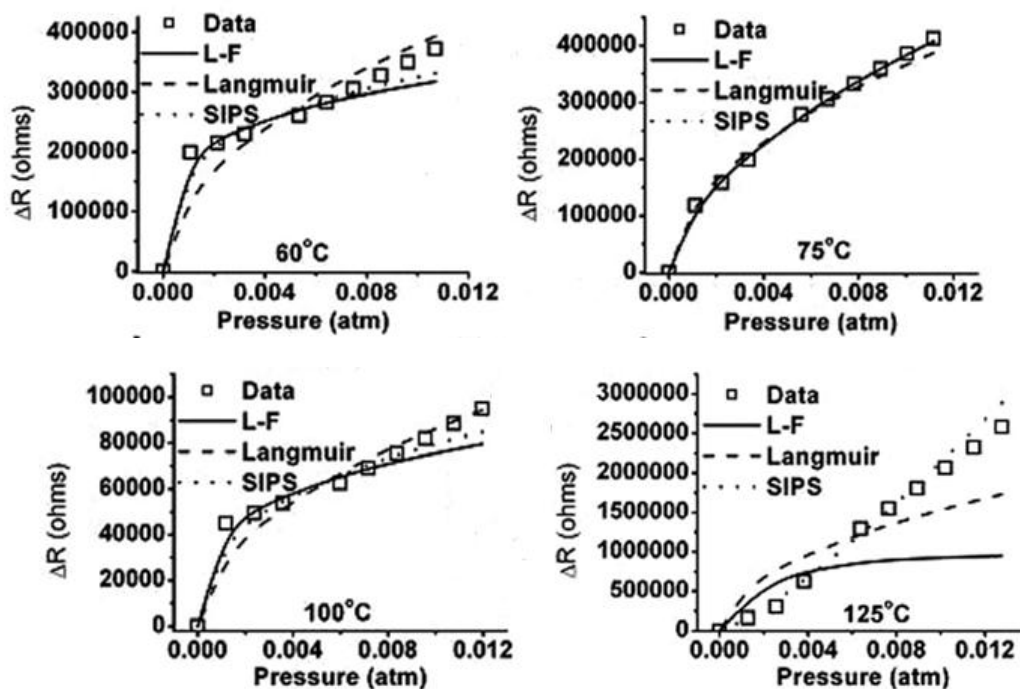


**Figure 5.3:** Adsorption isotherms for various models below and above the transition temperature ( $\sim 100^\circ\text{C}$ ).

It is observed from Figure 5.3 and Table 5.1 that the combined adsorption models like Langmuir-Freundlich (L-F) and SIPS have relatively better fit for the adsorption data. This shows that the adsorption takes place at heterogeneous surface. This is probably due to the presence of mixed metallic (Pd) and semiconducting (AZO) surfaces. L-F model has better fit at lower temperatures and SIPS models fits at higher temperature.

**Table 5.1:**  $r^2$  values of the adsorption fits. T: temperature; L: Langmuir; and F: Freundlich. (The deviation from Langmuir type with temperature is indicated in bold).

	$r^2$
--	-------



	F	L and F	L	SIPS	TOTH
40	0.194863	<b>0.998988</b>	0.492166	0.843236	0.492029
50	0.55931	<b>0.998863</b>	0.458587	0.846053	0.710593
60	0.800355	<b>0.991022</b>	0.860029	0.986269	0.85992
75	0.99812	<b>0.998133</b>	<b>0.993202</b>	<b>0.99814</b>	0.993221
100	0.98861	0.988606	0.9116	<b>0.977904</b>	0.91158
125	0.363102	0.499637	0.791433	<b>0.99559</b>	0.791812
150	0.781253	0.13014	0.893014	<b>0.92451</b>	0.893296

This is because the behavior of AZO:Pd varies with temperature (see section 4.3, Figure 4.8). With the change in temperature, the surface heterogeneity varies and hence multilayer gas adsorption occurs instead of monolayer adsorption. Other models (like F and TOTH) gave a poor fit as evident from the  $r^2$  values [Table 5.1]. Hence, F and TOTH have not been plotted and considered.

The adsorption rate also depends on the activation energy. The activation energy for the sensor response is calculated from the Arrhenius plots of Figure 5.4. The electrical output of device (resistance) is proportional to the rate of absorption of gas. The relation between activation energy and the electrical output of the device is given by:

$$\ln R = \ln R_o \pm \frac{E_a}{K} \dots\dots\dots(5.9)$$

where “R” is device resistance, “R<sub>o</sub>” is a constant with resistance dimension, “E<sub>a</sub>” is the activation energy, “T” is the temperature in Kelvin, and “K” is Boltzmann constant. Slope of this equation (1/KT) gives the value of activation energy.

The behavior of AZO:Pd is different at below and above the semiconductor-to-metal transition temperature. Thus in the presence of hydrogen, the nature of variation of E<sub>a</sub> is also different before and after transition. Figure 5.4 represents the trend of variation of activation energy below and above this transition temperature. Here, E<sub>a</sub> (low) represents the activation energy before semiconductor-to-metal transition, while E<sub>a</sub> (high) is the value after transition. The value of activation energy and slope of the curves is dependent on the temperature (Equation 5.9) and the concentration of hydrogen molecules. Before the transition, the activation energy increases with concentration of hydrogen (Figure 5.4). After transition, as

the hydrogen concentration increases, the activation energy decreases with minimum value at  $\sim 0.23$  eV at 10000 ppm of hydrogen. This is because of the scattering behavior of charge carriers at such high temperatures (transition is occurring at higher temperatures i.e.  $>90^\circ\text{C}$ ). Hence, the values of  $E_a$  (high) are higher than  $E_a$  (low) (Figure 5.4). Figure 5.4 also reveals that both the activation energies (high and low) are very close at 1.0%  $\text{H}_2$  and likely to merge at slightly higher gas concentration. Due to experimental limitation with the flow controllers and the sensor setup, studies with gas concentration higher than 1.0% could not be performed.

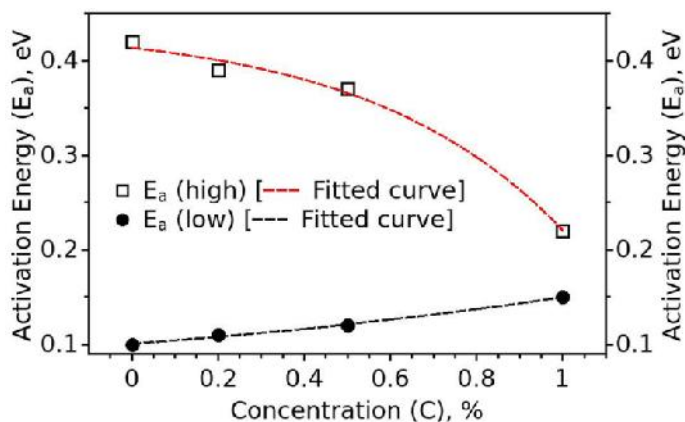


**Figure 5.4:** Variation of activation energy with hydrogen gas concentrations.

The explanation for such different behavior of activation energy before and after transition can be explained as follows:

The electrical output of AZO:Pd is a parallel network of Pd (metallic) and AZO (semiconducting) (see Section 4.3, Figure 4.9). Before the transition, AZO is a semiconductor. Since AZO did not show any hydrogen response, the metallic palladium path is mainly controlling the variation of the activation energy ( $E_a$  (low)) with the change in hydrogen concentration. The slow increase in  $E_a$  (low) with the increase in concentration is probably due to the competition between electronic and geometric effects, which are dominant at low temperature. Hence, the response barrier increases slowly. After the transition, activation energy ( $E_a$ (high)) is decreasing with concentration. On the high temperature side after the transition, both the parallel electronic paths are now metallic. Also, at high temperatures due to huge thermal expansion, the electronic and geometric effects of palladium are completely masked as expected. Moreover, the gas adsorption is high at high temperatures, which increases the stoichiometry of palladium hydrides resulting in decrease

in  $E_a(\text{high})$  value. This concentration dependent activation energy was modeled by considering simple exponential dependence (Equations 5.10(a) and (b))

$$E_{lc} = E_{oS} + E_{1S} \exp\left(\frac{C}{C_S}\right) \quad \dots\dots\dots(5.10(a))$$

$$E_{hi, h} = E_o + E_{1M} \exp\left(\frac{C}{C_M}\right) \quad \dots\dots\dots(5.10(b))$$

where the suffixes “S” and “M” with the constants just represent semiconducting and metallic domains respectively. The constants are obtained after fitting the above functions with the data [Table 5.2]. Equating equations 5.10 (a,b) gives the minimum hydrogen concentration in which the two activation energies will be similar. In the present case, the resultant equation is

$$E_{lc} = E_o + E_{1S} \exp\left(\frac{C}{C_S}\right) = E_{hi, h} = E_o + E_{1M} \exp\left(\frac{C}{C_M}\right)$$

$$\Rightarrow E_{1S} \exp\left(\frac{C}{C_S}\right) - E_{1M} \exp\left(\frac{C}{C_M}\right) = E_o - E_o \quad \dots\dots\dots (5.11)$$

The iterative solution of this Equation 5.11 yields  $C=1.113755\%$   $H_2$  and the value of activation energy at this concentration is  $E_a=0.1579989$  eV.

**Table 5.2:** Constants obtained from the activation energy versus concentration fitted curves.

$E_{oS}$	$E_{1S}$	$C_s$	$E_{oM}$	$E_{1M}$	$C_M$
0.0551272348	0.045852456	1.378317829	0.4369592689	-0.0234315806	0.4496411546

# **CHAPTER 6**

## **Summary, Conclusions and Future Scope**



### SUMMARY

The interest in hydrogen sensors arises due to the safety concerns of flammable hydrogen gas. The advancement in developing palladium and palladium-modified devices as hydrogen gas sensors has accelerated over the past two decades. Palladium based devices have shown excellent hydrogen sensing properties with high sensitivity and selectivity whose response varies with the hydrogen concentration and operating temperature.

In summary, a procedurally simple and low temperature method i.e. polyol method has been presented to prepare palladium nanoparticles. The polyol method is a simple method and acquired a good purity level of product. This is because very few chemicals were required which simplified the chemical reactions that extract few products (which can be removed easily by simple washing processes). The microscopic studies indicated that the formed palladium nanoparticles were nearly spherical in shape, which can be very useful for sensing mechanism (geometric effect of palladium hydride). UV studies showed a fair agreement as evidence to the formation of palladium nanoparticles.

Highly porous palladium (Pd) films were prepared by simple solution drop method and AZO films were prepared by sputtering technique, on glass substrates. Catalytic Pd nanoparticles modified AZO films were grown by solution dip method. Resistive sensor devices were fabricated on Pd films and AZO: Pd films by patterning silver electrodes over the films connecting the end of electrodes to a supporting multimeter. The change in conducting properties of these films upon hydrogen exposure provides the sensor response. Resistive sensor devices acquire simple electronics to extract sensor data and have simple detection mechanism. The simplicity of the device fabrication method maintained the low production cost of device. In this work, the hydrogen response studies were done with different hydrogen concentrations and different temperatures. The sensor response is different in different environments. Thus we performed the sensing test in nitrogen (inert environment) (to understand the material chemistry of sensor device) and in air (for practical application). Reproducibility, selectivity and stability test was done for both Pd and AZO: Pd devices. The mechanism of sensing hydrogen has been explained using the concepts of oxygen spill over, increase in resistivity and volume expansion of Pd nano particles in presence of hydrogen. The response in nitrogen ambient is a combined effect of resistivity and volume change, while in air ambient only resistivity change is the dominant mechanism. The performance of

the Pd device deteriorates at higher temperatures (beyond 50°C). An appreciably fast response of 3 s and 33 s were obtained with 0.1% hydrogen in nitrogen & in air, respectively at 50°C for Pd devices. Although the response in air ambient was relatively slow as compared to that in nitrogen, there is a scope of further refinement of material parameters, like shape, size, and composition, to improve the sensor performance.

The experimental results for AZO:Pd devices were found to be promising for efficient and selective hydrogen sensing at low temperature as well as high temperature (below 150°C). A suitable sensing mechanism highlighting the operational temperature zones has been proposed. A theoretical approach towards the surface gas adsorption was discussed with the help of adsorption isotherm models. These model fittings were applied to the data obtained for AZO:Pd device only because it is the most effective sensor. Heterogeneous gas adsorption was observed theoretically from the fitted isotherms, below and above the transition temperature (~100°C). In brief, decoration of palladium nanoparticles over AZO surface showed better performance in terms of response and operational temperature range.

### CONCLUSIONS

The major outcomes of this research work can be summarized as follows:

- ❖ Porous palladium nanofilms and AZO:Pd films were prepared to fabricate the resistive hydrogen sensing devices.
- ❖ Palladium device showed high sensitivity and fast response characteristics towards hydrogen (at concentrations 0.1%-1%) between the temperatures 35°C to 50°C in nitrogen/air ambient.
- ❖ The absorption and desorption of hydrogen gas on palladium surface changes the resistance of the film. We exploited this phenomenon to obtain the sensor response.
- ❖ Pd sensor device also showed good reproducibility and selectivity towards hydrogen at room temperatures. Selectivity and stability is always a prime concern for a sensor device.
- ❖ The sensing performance deteriorated above 50°C. But the sensor response in a limited temperature region was not acceptable. Thus to apply our device to higher temperature applications also, palladium nanoparticles were well decorated over the AZO (Aluminium doped Zinc Oxide) surfaces and were tested.

- ❖ The AZO:Pd devices showed clear and stable response patterns at wide range of temperatures i.e. from 40°C to 150°C.
- ❖ AZO:Pd devices also showed high sensitivity and lowest response time at both low (64°C) and relatively high temperature (130°C).
- ❖ The device is reproducible at both these favorable operating temperatures and is also stable at its highest operating temperature 150°C.
- ❖ Table 1 demonstrates the comparative picture of both the sensing devices at their best operating temperatures (maximum response). Response % is maximized for AZO:Pd devices at all hydrogen concentrations (in air ambient) as compared to pure Pd device. Response time is also improved (minimised) for AZO:Pd devices. However, the recovery is quite slow relative to the response pattern, and further studies are necessary to understand and improve recovery characteristics.
- ❖ It is observed from Table 1 that the palladium device showed good performance in the low temperature regime and showed no response at high temperature regime. But AZO:Pd device displayed sensor response at high temperature regime also with maximum response at 60°-65°C (low temperature zone) as well as at 125°-130°C (high temperature zone).
- ❖ Thus, we succeeded in preparing a selective hydrogen sensing device that is compact, low cost, highly sensitive, reproducible, stable, has low detection limit and also works in wide temperature range. It is always desirable for any commercial gas sensor to meet all these requirements, which is quite challenging.



Table 6.1: Comparative picture of the devices

		Low temperature regime	High temperature regime
<b>Pure Pd device</b> (35°C-75°C)	Temperature	<b>50°C</b>	<b>NO RESPONSE</b>
	Response %	<b>1.15 15.4</b> (0.1% 1% H <sub>2</sub> /N <sub>2</sub> ) <b>0.48 10.2</b> (0.1% 1% H <sub>2</sub> /air)	
	Response time (s)	<b>10 s 3 s</b> (0.1% 1% H <sub>2</sub> /N <sub>2</sub> ) <b>40 s 33 s</b> (0.1% 1% H <sub>2</sub> /air)	
	Recovery time (s)	<b>31 s 10 s</b> (0.1% 1% H <sub>2</sub> /N <sub>2</sub> ) <b>430 s 82 s</b> (0.1% 1% H <sub>2</sub> /air)	
<b>AZO:Pd device</b> (40°C-150°C)	Temperature	<b>60°-65°C</b>	<b>125°-135°C</b>
	Response %	<b>9.3 16.2</b> (0.2% 1% H <sub>2</sub> /air)	<b>9.15 84.7</b> (0.2% 1% H <sub>2</sub> /air)
	Response time (s)	<b>41.5 s 28 s</b> (0.2% 1% H <sub>2</sub> /air)	<b>25 s 40 s</b> (0.2% 1% H <sub>2</sub> /air)
	Recovery time (s)	<b>975 s 612 s</b> (0.2% 1% H <sub>2</sub> /air)	<b>281 s 565 s</b> (0.2% 1% H <sub>2</sub> /air)

## **FUTURE SCOPE**

The future scope of this research work will include the possible solutions to improve the response parameters and to extend the operational temperature range. This could probably open the door for hydrogen-sensing applications in the harsh environments also. We also noticed that the response of sensor device in air ambient is relatively slow as compared to that in nitrogen. Thus, there is a scope of further engineering of material parameters, like shape, size, and composition, to improve the sensor performance. In analogy to Pd decorated ZnO, either Pd can be switched to other catalytic metal to decorate on the ZnO or by switching to other oxide surfaces. Nonetheless, the fabricated AZO:Pd devices are quite suitable for hydrogen sensing below 150°C and such simplicity adopted in device fabrication could place these devices into a relevant region in the field of gas sensors.

## **REFERENCES**



## References

---

- [1] Goldsmith J.R., Jonsson E., "*Health effects of community noise*", American journal of public health, vol. 63, pp. 782-793, Sep. 1973.
- [2] Seo H., Aihara S., Watabe T., Ohtake H., Kubota M., Egami N., "*Color Sensors with Three Vertically Stacked Organic Photodetectors*", Journal of Applied Physics, vol. 46, pp. 45-49, Jan. 2007.
- [3] Michel J., Liu J., Kimerling L.C., "*High-performance Ge-on-Si photodetectors*", Nature Photonics, vol. 4, pp. 527-534, Jul. 2010.
- [4] Lau K.T., Baldwin S., Toole M.O., Shepherd R., Yerazunis W.J., Izuo S., Ueyama S., Diamond D., "*A low-cost optical sensing device based on paired emitter-detector light emitting diodes*", Analytica Chimica Acta, vol. 557, pp. 111-116, Jan. 2006.
- [5] Klipstein P.C., Livneh Y., Glozman A., Grossman S., Klin O., Snapi N., Weiss E., "*Modeling InAs/GaSb and InAs/InAsSb Superlattice Infrared Detectors*", Journal of Electronic Materials, vol. 43(8), pp. 2984-2990, May 2014.
- [6] Tompsett M.F., Amelio G.F., Bertram W.J., Buckley R.R., McNamara W.J., Mikkelsen J.C., Sealer D.A., "*Charge-coupled imaging devices: Experimental results*", Electron Devices, IEEE Transactions, vol. 18, pp. 992-996, Nov. 1971.
- [7] Gregory J.A., Smith A.M., Pearce E.C., Lambour R.L., Shah R.Y., Clark H.R., Warner K., Osgood R.M., Woods D.F., DeCew A.E., Forman S.E., Mendenhall L., DeFranzo C.M., Dolat V.S., Loomis A.H., "*Development and application of spherically curved charge-coupled device imagers*", Applied Optics, vol. 54, pp. 3072-3082, Mar. 2015.
- [8] Ma T.Y., Lin C.Y., Hsu S.W., Hu C.W., Hou T.W., "*Automatic brightness control of the handheld device display with low illumination*", Proc. 2012 IEEE International Conference, Computer Science and Automation Engineering, vol. 2, pp. 382-385, May 2012.
- [9] Bilro L., Alberto N., Pinto J.L., Nogueira R., "*Optical sensors based on plastic fibers*" Sensors, vol. 12, pp. 12184-12207, Sep. 2012.

## References

---

- [10] Perry M., Saafi M., Fusiek G., Niewcza P., “*Hybrid optical-fibre/geopolymer sensors for structural health monitoring of concrete structures*”, Smart Materials and Structures, vol. 24 (4), pp. 045011 (1-9), Feb. 2015.
- [11] Baroncini V.H., Martelli C., Da Silva M.J., Morales R.E., “*Single-and Two-Phase Flow Characterization Using Optical Fiber Bragg Gratings*”, Sensors, vol. 15(3), pp. 6549-6559, Mar. 2015.
- [12] Liu X., Liu N., Liu M., Tao Z., Kuang W., Ji X., Nathan A., “*Graphene nanomesh photodetector with effective charge tunnelling from quantum dots*”, Nanoscale, vol. 7(9), pp. 4242-4249, Jan. 2015.
- [13] Yan L., Zhang Y., Zhang X., Zhao J., Wang Y., Zhang T., Jiang Y., Gao W., Yin J., Zhao J., William, W. Y., “*Single layer graphene electrodes for quantum dot-light emitting diodes*”, Nanotechnology, vol. 26(13), pp. 135201, Mar. 2015.
- [14] Kim S.J., Choi K., Lee B., Kim Y., Hong B.H., “*Materials for Flexible, Stretchable Electronics: Graphene and 2D Materials*”, Annual Review of Materials Research, vol. 45, pp. 63-84, Jul. 2015.
- [15] Ho P.H., Liou Y.T., Chuang C.H., Lin S.W., Tseng C.Y., Wang D.Y., Chen C.C., Hung W.Y., Wen C.Y., Chen C.W., “*Self-Crack-Filled Graphene Films by Metallic Nanoparticles for High-Performance Graphene Heterojunction Solar Cells*”, Advanced Materials, vol. 27(10), pp. 1724-1729, Mar. 2015.
- [16] Joseph D., Mayhew R., Aksay I.A., “*Graphene materials and their use in dye-sensitized solar cells*”, Chemical reviews, vol. 114(12), pp. 6323-6348, May 2014.
- [17] Lukin M., Walsworth R.L., “*High sensitivity solid state magnetometer*”, U.S. Patent No. 8,947,080. Washington, DC: U.S. Patent and Trademark Office, Feb. 2015.
- [18] Takagi H., Noda J., Ueno T., Kanazawa N., Nakamura Y., Inoue M., “*Monolithic Structure and Multiaxis Magnetic Sensing with Magnonic Crystals*” Electronics and Communications in Japan, vol. 97, pp. 11-16, Oct. 2014.
- [19] Yang Y., Lin L., Zhang Y., Jing Q., Hou T.C., Wang Z.L., “*Self-powered magnetic sensor based on a triboelectric nanogenerator*”, ACS nano, vol. 6, pp. 10378-10383, Oct. 2012.

## References

---

- [20] Brown P., Beek T., Carr C., Brien H.O., Cupido E., Oddy T., Horbury T.S., “*Magnetoresistive magnetometer for space science applications*”, Measurement Science and Technology, vol. 23, pp. 025902 (1-11), Jan. 2012.
- [21] Gopinadhan K., Shin Y.J., Jalil R., Venkatesan T., Geim A.K., Neto A.H.C., Yang H., “*Extremely large magnetoresistance in few-layer graphene/boron-nitride heterostructures*”, Nature communications, vol. 6, pp. 8337 (1-7), Sep. 2015.
- [22] Luomahaara J., Vesterinen V., Grönberg L., Hassel J., “*Kinetic inductance magnetometer*”, Nature Communications, vol. 5, pp. 4872(1-16), Jan. 2014.
- [23] Nakano T., Takasu S., Tamura O., Kobayashi T., Tanaka Y., “*Temperature Characteristics of Platinum–Cobalt Resistance Thermometers Based on the ITS-90 Above 14 K*”, International Journal of Thermophysics, vol. 35, pp. 1044-1054, Jun. 2014.
- [24] Arenas O., Al Alam E., Thevenot A., Cordier Y., Jaouad A., Aimez V., Maher H., Ares R., Boone F., “*Integration of Micro Resistance Thermometer Detectors in AlGaIn/GaN Devices*”, Electron Devices Society, vol. 2(6), pp. 145-148, Nov. 2014.
- [25] Dolkar K., Kapoor N.V., Singh N.V., Suri V., “*A comparative study on the recording of temperature by the clinical mercury thermometer and digital thermometer*”, Journal of Nursing and Midwifery Research, vol. 9(1), pp. 40-46, Jan. 2013.
- [26] Zhang Y., Jahns T.M., “*Power electronics loss measurement using new heat flux sensor based on thermoelectric device with active control*”, Industry Applications, IEEE Transactions, vol. 50(6), pp. 4098-4106, Dec. 2014.
- [27] Trelewicz J.R., Longtin J.P., Hubble D.O., Greenlaw R.J., “*High-Temperature Calibration of Direct Write Heat Flux Sensors from 25°C to 860°C Using the In-Cavity Radiation Method*”, Sensors, vol. 15(1), pp. 358-364, Jan. 2015.
- [28] He S., Mench M.M., Tadigadapa S., “*Thin film temperature sensor for real-time measurement of electrolyte temperature in a polymer electrolyte fuel cell*”, Sensors and Actuators A: Physical, vol. 125(2), pp. 170-177, Jan. 2006.
- [29] Bhatt H.D., Vedula R., Desu S.B., Fralick G.C., “*La<sub>(1-x)</sub>Sr<sub>x</sub>CoO<sub>3</sub> for thin film thermocouple applications*”, Thin Solid Films, vol. 350(1), pp. 249-257, Aug. 1999.

## References

---

- [30] Toramaru A., Maeda K., “*Mass and style of eruptions in experimental geysers*”, Journal of Volcanology and Geothermal Research, vol. 257, pp. 227-239, May 2013.
- [31] Zhang H., Xiao X., Su T., Gu X., Jin T., Du L., Tang J., “*A novel thermocouple microelectrode for applications in SECM and variable temperature electrochemistry*”, Electrochemistry Communications, vol. 47, pp. 71–74, Jul. 2014.
- [32] Xie W., Liu B., Xiao S., Li H., Wang Y., Cai D., Wang D., Wang L., Liu Y., Li Q., Wang T., “*High performance humidity sensors based on CeO<sub>2</sub> nanoparticles*”, Sensors and Actuators B: Chemical, vol. 215, pp. 125-132, Aug. 2015.
- [33] Chen A., Chen H.Y., Chen C., “*Use of Temperature and Humidity Sensors to Determine Moisture Content of Oolong Tea*”, Sensors, vol. 14(8), pp. 15593-15609, Aug. 2014.
- [34] Mayer J., Gossick B., “*Use of Au-Ge Broad Area Barrier As Alpha-Particle Spectrometer*”, Review of Scientific Instruments, vol. 27(6), pp. 407-408, 1956.
- [35] Broda R., Pochwalski K., Radoszewski T., “*Calculation of liquid-scintillation detector efficiency*”, International Journal of Radiation Applications and Instrumentation. Part A. Applied Radiation and Isotopes, vol. 39(2), pp. 159-164, 1988.
- [36] Sowerby B.D., “*Cerenkov detectors for low-energy gamma rays*”, Nuclear Instruments and Methods, vol. 97(1), pp. 145-149, Nov. 1971.
- [37] Niraula M., Yasuda K., Takai N., Matsumoto M., Suzuki Y., Tsukamoto Y., Ito Y., Sugimoto S., Kouno S., Yamazaki D., Agata Y., “*Surface Processing of CdTe Detectors Using Hydrogen Bromide-Based Etching Solution*”, Electron Device Letters, vol. 36(8), pp. 856-858, Jun. 2015.
- [38] Choi H., Jeong M., Kim H.S., Kim Y.S., Ha J.H., Chai J.S., “*Growth and fabrication method of CdTe and its performance as a radiation detector*”, Journal of the Korean Physical Society, vol. 66(1), pp. 27-30, Jan. 2015.
- [39] Del Sordo S., Abbene L., Caroli E., Mancini A.M., Zappettini A., Ubertini P., “*Progress in the development of CdTe and CdZnTe semiconductor radiation*



## References

---

- detectors for astrophysical and medical applications*”, *Sensors*, vol. 9(5), pp. 3491-3526, May 2009.
- [40] Navon D., Kasten R., “*Using an Advance Time Meter display as means to reduce driving speed*”, *Transportation Research Part F: Traffic Psychology and Behaviour*, vol. 35, pp. 16-27, Nov. 2015.
- [41] Klotz M., Rohling H., “*24 GHz radar sensors for automotive applications*”, Proc. in MIKON-2000, 13th International Conference on IEEE, vol. 1, pp. 359-362, 2000.
- [42] Bernardi P., Cicchetti R., Pisa S., Pittella E., Piuze E., Testa O., “*Design, realization, and test of a UWB radar sensor for breath activity monitoring*”, *Sensors*, vol. 14(2), pp. 584-596, Feb. 2014.
- [43] Shi S.Z., Zhao Z.Y., Liu Y., Chen G., Li T., Liu J. N., Yao M., “*Experimental demonstration for ionospheric sensing and aircraft detection with a HF skywave multistatic radar*”, *Geoscience and Remote Sensing Letters*, vol. 11(7), pp. 1270-1274, Jul. 2014.
- [44] Xu J., Pan Q., Tian Z., “*Grain size control and gas sensing properties of ZnO gas sensor*”, *Sensors and Actuators B: Chemical*, vol. 66(1), pp. 277-279, Jul. 2000.
- [45] Yamazoe N., “*New approaches for improving semiconductor gas sensors*”, *Sensors and Actuators B: Chemical*, vol. 5(1), pp. 7-19, Aug. 1991.
- [46] Kim J., Yong K., “*Mechanism study of ZnO nanorod-bundle sensors for H<sub>2</sub>S gas sensing*”, *The Journal of Physical Chemistry C*, vol. 115(15), pp. 7218-7224, Mar. 2011.
- [47] Mickelson W., Sussman A., Zettl A., “*Low-power, fast, selective nanoparticle-based hydrogen sulfide gas sensor*”, *Applied Physics Letters*, vol. 100(17), pp. 173110 (1-4), Apr. 2012.
- [48] Chung M.G., Kim D.H., Lee H.M., Kim T., Choi J.H., Seo D.K., Yoo J.B., Hong S.H., Kang T.J., Kim Y.H., “*Highly sensitive NO<sub>2</sub> gas sensor based on ozone treated grapheme*”, *Sensors and Actuators B: Chemical*, vol. 166, pp. 172-176, May 2012.

## References

---

- [49] Hassan J.J., Mahdi M.A., Chin C.W., Abu-Hassan H., Hassan Z., “*A high-sensitivity room-temperature hydrogen gas sensor based on oblique and vertical ZnO nanorod arrays*”, *Sensors and Actuators B: Chemical*, vol. 176, pp. 360-367, Jan. 2013.
- [50] Gardner J.W., Bartlett P.N., “*A brief history of electronic noses*”, *Sensors and Actuators B: Chemical*, vol. 18(1), pp. 210-211, Mar. 1994.
- [51] Sberveglieri G., Concina I., Comini E., Falasconi M., Ferroni M., Sberveglieri V., “*Synthesis and integration of tin oxide nanowires into an electronic nose*”, *Vacuum*, vol. 86(5), pp. 532-535, Jan. 2012.
- [52] Bitesize Bio: How to Care for Your pH Meter, Steffi Magub, 18 May 2012
- [53] <http://www.sensorland.com/HowPage037.html>
- [54] Yamazoe N., “*Toward innovations of gas sensor technology*”, *Sensors and Actuators B: Chemical*, vol. 108(1), pp. 2-14, Jul. 2005.
- [55] Lee H.J., Yook J.G., “*Recent research trends of radio-frequency biosensors for biomolecular detection*”, *Biosensors and Bioelectronics*, vol. 61, pp. 448–459, Nov. 2014.
- [56] Chuang H., Trieu M.Q., Hurley J., Taylor E.J., England M.R., Nasraway S.A., “*Pilot studies of transdermal continuous glucose measurement in outpatient diabetic patients and in patients during and after cardiac surgery*”, *Journal of diabetes science and technology*, vol. 2, pp. 595-602, Jul. 2008.
- [57] Bandodkar A.J., Jia W., Yardimci C., Wang X., Ramirez J., Wang J., “*Tattoo-Based Noninvasive Glucose Monitoring: A Proof-of-Concept Study*”, *Analytical Chemistry*, vol. 87 (1), pp. 394-398, Dec. 2014.
- [58] Cheng S., Hideshima S., Kuroiwa S., Nakanishi T., Osaka T., “*Label-free detection of tumor markers using field effect transistor (FET)-based biosensors for lung cancer diagnosis*”, *Sensors and Actuators B: Chemical*, vol. 212, pp. 329-334, Jun. 2015.
- [59] Langmuir I., “*The constitution and fundamental properties of solids and liquids. part i. solids*”, *Journal of American Chemical Society*, vol. 38 (11), pp. 2221–2295, Nov. 1916.

## References

---

- [60] Szekely J., “*Gas-solid reactions*”, Elsevier, page 36, Edition 2012.
- [61] Foo K.Y., Hameed B.H., “*Insights into the modeling of adsorption isotherm systems*”, Chemical Engineering Journal, vol. 156, pp. 2-10, Sep. 2009.
- [62] Kisliuk P., “*The sticking probabilities of gases chemisorbed on the surfaces of solids*”, Journal of Physics and Chemistry of Solids, vol. 3, pp. 95-101, Aug. 2002.
- [63] Logan R.M., Keck J.C., “*Classical theory for the interaction of gas atoms with solid surfaces*”, The Journal of Chemical Physics, vol. 49, pp. 860-876, Sep. 2003.
- [64] Cercignani C., Lampis M., “*Kinetic models for gas-surface interactions*”, Transport Theory and Statistical Physics, vol. 1, pp. 101-114, Sep. 2006.
- [65] Steele W.A., “*The physical interaction of gases with crystalline solids: I. Gas-solid energies and properties of isolated adsorbed atoms*”, Surface Science, vol. 36, pp. 317-352, Sep. 2002.
- [66] Tamaekong N., Liewhiran C., Wisitsoraat A., Phanichphant S., “*Flame-spray-made undoped zinc oxide films for gas sensing applications*”, Sensors, vol 10, pp. 7863–7873, Aug. 2010.
- [67] Lupan O., Chai G., Chow, “*Novel hydrogen gas sensor based on single ZnO nanorod*”, Microelectronic Engineering, vol. 85, pp. 2220–2225, Jul. 2008.
- [68] Musat V., Rego A.M., Monteiro R., Fortunato E., “*Microstructure and gas-sensing properties of sol–gel ZnO thin films*”, Thin Solid Films, vol. 516, pp. 1512–1515, Aug. 2008.
- [69] Wan Q., Li Q.H., Chen J.Y., Wang T.H., He X. L., Li J.P., Lin C.L., “*Fabrication and ethanol sensing characteristics of ZnO nanowire gas sensors*”, Applied Physics Letters, vol. 84, pp. 3654-3656, Apr. 2004.
- [70] Ahn M.W., Park K.S., Heo J.H., Park J.G., Kim D.W., Choi K. J., Lee J.H., Hong S.H., “*Gas sensing properties of defect-controlled ZnO-nanowire gas sensor*”, Applied Physics Letters, vol. 93, pp. 263103 (1-3), Dec. 2008.

## References

---

- [71] Xu J., Han J., Zhang Y., Sun Y.A., Xie B., “*Studies on alcohol sensing mechanism of ZnO based gas sensors*”, Sensors and Actuators B: Chemical, vol. 132, pp. 334-339, Feb. 2008.
- [72] Shishiyanu S.T., Shishiyanu T.S., Lupan, O.I. “*Sensing characteristics of tin-doped ZnO thin films as NO<sub>2</sub> gas sensor*”, Sensors and Actuators B: Chemical, vol. 107, pp. 379-386, May 2005.
- [73] Sadek A.Z., Choopun S., Wlodarski W., Ippolito S.J., Kalantar Zadeh K., “*Characterization of ZnO Nanobelt-Based Gas Sensor for H<sub>2</sub>, NO<sub>2</sub>, and Hydrocarbon Sensing*”, Sensors, vol. 7, pp. 919-924, Jun. 2007.
- [74] Xu J., Qingyi P., Jianhua Q., “*Sensing characteristics of double layer film of ZnO*”, Sensors and Actuators B: Chemical, vol. 66, pp. 161-163, Jul. 2000.
- [75] Shinde S.D., Patil G.E., Kajale D.D., Gaikwad V.B., Jain, G.H., “*Synthesis of ZnO nanorods by spray pyrolysis for H<sub>2</sub>S gas sensor*”, Journal of Alloys and Compounds, vol. 528, pp. 109-114, Jul. 2012.
- [76] Endres H.E., Göttler W., Hartinger R., Drost S., Hellmich W., Müller G, Braumühl C.B., Krenkow A., Perego C., Sberveglieri G., “*A thin-film SnO<sub>2</sub> sensor system for simultaneous detection of CO and NO<sub>2</sub> with neural signal evaluation*”, Sensors and Actuators B, vol. 36, pp. 353–357, Oct. 1996.
- [77] Wang B., Zhu L.F., Yang Y.H., Xu N.S., Yang, G.W. “*Fabrication of a SnO<sub>2</sub> nanowire gas sensor and sensor performance for hydrogen*”, The Journal of Physical Chemistry C, vol. 112, pp. 6643-6647, Apr. 2008.
- [78] Huang X., Liu J., Pi Z., Yu Z., “*Detecting pesticide residue by using modulating temperature over a single SnO<sub>2</sub>-based gas sensor*”, Sensors, vol. 3, pp. 361-370, Sep. 2003.
- [79] Chowdhuri A., Gupta V., Sreenivas K., Kumar R., Mozumdar S., Patanjali P.K., “*Response speed of SnO<sub>2</sub>-based H<sub>2</sub>S gas sensors with CuO nanoparticles*”, Applied Physics Letters, vol. 84, pp. 1180-1182, Mar. 2004.
- [80] Phani A.R., “*X-ray photoelectron spectroscopy studies on Pd doped SnO<sub>2</sub> liquid petroleum gas sensor*”, Applied physics letters, vol. 71, pp. 2358-2360, Jul. 1997.

## References

---

- [81] Hidalgo P., RCastro.H., Coelho A.C., Gouvea D., “*Surface segregation and consequent SO<sub>2</sub> sensor response in SnO<sub>2</sub>-NiO*”, Chemistry of materials, vol. 17, pp. 4149-4153, Jul. 2005.
- [82] Gardeshzadeh A.R., Raissi B., Marzbanrad E., Mohebbi H., “*Fabrication of resistive CO gas sensor based on SnO<sub>2</sub> nanopowders via low frequency AC electrophoretic deposition*”, Journal of Materials Science: Materials in Electronics, vol. 20, pp. 127-131, Apr. 2008.
- [83] Barbi G.B., Santos J.P., Serrini P., Gibson P.N., Horrillo M.C., Manes L., “*Ultrafine grain-size tin-oxide films for carbon monoxide monitoring in urban environments*”, Sensors and Actuators B: Chemical, vol. 25, pp. 559-563, Jan. 2002.
- [84] Batzill M., “*Surface science studies of gas sensing materials: SnO<sub>2</sub>*”, Sensors, vol. 6, pp. 1345-1366, Oct. 2006.
- [85] Choi Y.J., Hwang I.S., Park J.G., Choi K.J., Park J.H., Lee J.H., “*Novel fabrication of an SnO<sub>2</sub> nanowire gas sensor with high sensitivity*”, Nanotechnology, vol. 19, pp. 095508 (1-4), Feb. 2008.
- [86] Gong J., Li Y., Hu Z., Zhou Z., Deng Y., “*Ultrasensitive NH<sub>3</sub> gas sensor from polyaniline nanograin enched TiO<sub>2</sub> fibers*”, The Journal of Physical Chemistry C, vol. 114, pp. 9970-9974, May 2010.
- [87] Zhu Y., Shi J., Zhang Z., Zhang C., Zhang X., “*Development of a gas sensor utilizing chemiluminescence on nanosized titanium dioxide*”, Analytical Chemistry, vol. 74, pp. 120-124, Nov. 2001.
- [88] Karunagaran B., Uthirakumar P., Chung S. J., Velumani S., Suh E.K., “*TiO<sub>2</sub> thin film gas sensor for monitoring ammonia*”, Materials Characterization, vol. 58, pp. 680-684, Sep. 2007.
- [89] Chaudhari G.N., Bambole D.R., Bodade A.B., Padole P.R., “*Characterization of nanosized TiO<sub>2</sub> based H<sub>2</sub>S gas sensor*”, Journal of materials science, vol. 41, pp. 4860-4864, May 2006.

## References

---

- [90] Garzella C., Comini E., Tempesti E., Frigeri C., Sberveglieri G., "*TiO<sub>2</sub> thin films by a novel sol-gel processing for gas sensor applications*", Sensors and Actuators B: Chemical, vol. 68, pp. 189-196, Aug. 2000.
- [91] Lu H.F., Li F., Liu G., Chen Z.G., Wang D.W., Fang H.T., Cheng H.M., "*Amorphous TiO<sub>2</sub> nanotube arrays for low-temperature oxygen sensors*", Nanotechnology, vol. 19, pp. 405504 (1-7), Aug. 2008.
- [92] Favier F., Walter E.C., Zach M.P., Benter T., Penner R.M., "*Hydrogen sensors and switches from electrodeposited palladium mesowire arrays*", Science, vol. 293, pp. 2227-2231, Sep. 2001.
- [93] Beutel T.W., Dettling J.C., Hollobaugh D.O., Mueller T.W., "*Catalytic oxidizing the carbon monoxide and hydrocarbons to carbon dioxide and water, and reduction of nitrogen oxides (NO<sub>x</sub>) to nitrogen; platinum and palladium ratio of bottom washcoat layer is 7: 5 and Pt: Pd ratio of top washcoat layer is 3: 1; fuel efficiency; catalytic converter for diesel engines.*", U.S. Patent 7,576,031, issued Aug. 2009.
- [94] JarvisM., AdamsK.M., "*Method for converting exhaust gases from a diesel engine using nitrogen oxide absorbent*", U.S. Patent 6,182,443, issued Feb. 2001.
- [95] HarrisonB., Cooper B.J., Wilkins A. J. J., "*Control of nitrogen oxide emissions from automobile engines*", Platinum Metals Review, vol. 25, pp. 14, 1981.
- [96] Uemiya S., Sato N., Ando H., Kikuchi E., "*The water gas shift reaction assisted by a palladium membrane reactor*", Industrial & Engineering Chemistry Research, vol. 30, pp. 585-589, 1991.
- [97] Gupta D., Dutta D., Kumar M., Barman P.B., Sarkar C.K, Basu S., Hazra S.K., "*A low temperature hydrogen sensor based on palladium nanoparticles*", Sensors and Actuators B, vol. 196, pp. 215-222, Feb. 2014.
- [98] <http://en.wikipedia.org/wiki/Palladium#Characteristics>
- [99] Guo M., Liu S., Zhou X., Lv M., Chen S., Xiao D., "*A Simple Hydrophilic Palladium(II) Complex as a Highly Efficient Catalyst for Room Temperature Aerobic Suzuki Coupling Reactions in Aqueous Media*", Molecules, vol. 19, pp. 6524-6533, May 2014.

## References

---

- [100] Corral J.A., López M.I., Esquivel D., Mora M., Sanchidrián C.J., Romero-Salguero F.J., “*Preparation of Palladium-Supported Periodic Mesoporous Organosilicas and their Use as Catalysts in the Suzuki Cross-Coupling Reaction*”, *Materials*, vol. 6, pp. 1554-1565, Apr. 2013.
- [101] Heck R.F., “*The arylation of allylic alcohols with organopalladium compounds: A new synthesis of 3-aryl aldehydes and ketones*”, *Journal of American Chemical Society*, vol. 90, pp. 5526–5531, 1968.
- [102] Heck R.F., “*The addition of alkyl- and aryl palladium chlorides to conjugated dienes*”, *Journal of American Chemical Society*, vol. 90, pp. 5542–5546, 1968.
- [103] Okumura K., Tomiyama T., Moriyama S., Nakamichi A., Niwa M., “*Enhancement in the Catalytic Activity of Pd/USY in the Heck Reaction Induced by H<sub>2</sub> Bubbling*”, *Molecules*, vol. 16, pp. 38-51, Dec. 2010.
- [104] Astruc D., “*Palladium nanoparticles as efficient green homogeneous and heterogeneous carbon-carbon coupling precatalysts: a unifying view*”, *Inorganic Chemistry*, vol. 46, pp. 1884–94, Dec. 2007.
- [105] Widenhoefer R.A., Buchwald S.L., “*Formation of palladium bis(amine) complexes from reaction of amine with palladium tris(o-tolyl) phosphine mono(amine) complexes*”, *Organometallics*, vol. 15, pp. 3534–3542, 1996.
- [106] Borkowski T., Subik P., Trzeciak A.M., Wołowicz S., “*Palladium(0) Deposited on PAMAM Dendrimers as a Catalyst for C–C Cross Coupling Reactions*”, *Molecules*, vol. 16, pp. 427-441, Jan. 2011.
- [107] Djakovitch L., Batail N., Genelot M., “*Recent Advances in the Synthesis of N-Containing Heteroaromatics via Heterogeneously Transition Metal Catalysed Cross-Coupling Reactions*”, *Molecules*, vol. 16, pp. 5241-5267, Jun. 2011.
- [108] Alia S.M., Duong K., Liu T., Jensen K., Yan Y., “*Palladium and Gold Nanotubes as Oxygen Reduction Reaction and Alcohol Oxidation Reaction Catalysts in Base*”, *ChemSusChem*, vol. 7, pp. 1739–1744, Apr. 2014.

## References

---

- [109] Adams C.P., Walker K.A., Obare S.O., Docherty K.M., “*Size-Dependent Antimicrobial Effects of Novel Palladium Nanoparticles*”, *PloS One*, vol. 9, pp. 85981(1-15), Jan. 2014.
- [110] Cotton J.B., “*The Role of Palladium in Enhancing Corrosion Resistance of Titanium*”, *Platinum Metals Review*, vol. 11, pp. 50-52, Apr. 1967.
- [111] Tang J., Zuo Y., “*Study on corrosion resistance of palladium films on 316L stainless steel by electroplating and electroless plating*”, *Corrosion science*, vol. 50, pp. 2873-2878, Oct. 2008.
- [112] Graham T., “*On the occlusion of hydrogen gas by metals*”, *Proceedings of the Royal Society of London*, vol. 16, pp. 422-427, 1867.
- [113] Steele M.C., Hile J.W., MacIver B.A., “*Hydrogen sensitive palladium gate MOS capacitors*”, *Journal of Applied Physics*, vol. 47, pp. 2537-2538, 1976.
- [114] Lundström I., Shivaraman S., Svensson C., Lundkvist L., “*A hydrogen-sensitive MOS field-effect transistor*”, *Applied Physics Letters*, vol. 26, pp. 55-57, 1975.
- [115] Sathananthan S., Dravid V.P., Fan S.W., “*Hydrogen-sensing characteristics of palladium-doped Zinc Oxide nanostructures*”, *Nanoscape*, vol. 6(1), pp. 6-11, 2009.
- [116] Chen Z.H., Jie J.S., Luo L.B., Wang H., Lee C.S., Lee S.T., “*Applications of silicon nanowires functionalized with palladium nanoparticles in hydrogen sensors*”, *Nanotechnology*, vol. 18, pp. 345502 (1-5), Jul. 2007.
- [117] Cherevko S., Kulyk N., Fu J., Chung C.H., “*Hydrogen sensing performance of electrodeposited conoidal palladium nanowire and nanotube arrays*”, *Sensors and Actuators B: Chemical*, vol. 136(2), pp. 388-391, Mar. 2009.
- [118] Noh J.S., Lee J.M., Lee W., “*Low-dimensional palladium nanostructures for fast and reliable hydrogen gas detection*”, *Sensors*, vol. 11(1), pp. 825-851, Jan. 2011.
- [119] Khanuja M., Varandani D., Mehta B.R., “*Pulse like hydrogen sensing response in Pd nanoparticle layers*”, *Applied Physics Letters*, vol. 91, pp. 253121(1-3), Dec. 2007.
- [120] Salomons E., “*On the lattice gas description of hydrogen in palladium: a molecular dynamics study*”, *Journal of Physics: Condensed Matter*, vol. 2(4), pp. 845, 1990.



## References

---

- [121] Kishore S., Nelson J.A., JAdair.H., .Eklund P.C, “*Hydrogen storage in spherical and platelet palladium nanoparticles*”, Journal of alloys and compounds, vol. 389, pp. 234-242, Mar. 2005.
- [122] Lischka M., Grob A., “*Hydrogen on palladium: A model system for the interaction of atoms and molecules with metal surfaces*”, Recent Developments in Vacuum Science and Technology, vol. 37, pp. 111-132, 2003.
- [123] Oriani R.A., “*The physical and metallurgical aspects of hydrogen in metals*”, Fusion Technology, vol. 26(4), pp. 235-266, 1994.
- [124] Falco M.D., Luigi Marrelli, Gaetano Iaquaniello, “*Membrane Reactors for Hydrogen Production Processes*”, vol. 264(11), pp. 65, 2011.
- [125] Khanuja M., Mehta B.R., Agar P., Kulriya P.K., Avasthi D.K., “*Hydrogen induced lattice expansion and crystallinity degradation in palladium nanoparticles: Effect of hydrogen concentration, pressure, and temperature*”, Journal of Applied Physics, vol. 106, pp. 093515 (1-8), Nov. 2009.
- [126] Formo E., Lee E., Campbell D., Xia Y., “*Functionalization of electrospun TiO<sub>2</sub> nanofibers with Pt nanoparticles and nanowires for catalytic applications*”, Nano Letters, vol. 8(2), pp. 668-672, Jan. 2008.
- [127] Kanungo J., Saha H., Basu S., “*Pd sensitized porous silicon hydrogen sensor- influence of ZnO thin film*”, Sensors and Actuators B: Chemical, vol. 147, pp. 128–136, May 2010.
- [128] Wang H.T., Kang B.S., Ren F., Tien L.C., Sadik P.W., Norton D.P., Pearton S.J., Lin J. “*Hydrogen-selective sensing at room temperature with ZnO nanorods*”, Applied Physics Letters, vol. 86, pp. 243503, Jun. 2005.
- [129] Wu C.C., Wu C.I., Sturm J.C., Kahn A., “*Surface modification of indium tin oxide by plasma treatment: An effective method to improve the efficiency, brightness, and reliability of organic light emitting devices*”, Applied Physics Letters, vol. 70(11), pp. 1348-1350, 1997.

## References

---

- [130] Mo D., Ye D., “*Surface study of composite photocatalyst based on plasma modified activated carbon fibers with TiO<sub>2</sub>*”, *Surface and Coatings Technology*, vol. 203(9), pp. 1154-1160, Jan. 2009.
- [131] Liqiang J., Baiqi W., Baifu X., Shudan L., Keying S., Weimin C., Honggang F., “*Investigations on the surface modification of ZnO nanoparticle photocatalyst by depositing Pd*”, *Journal of Solid State Chemistry*, vol. 177(11), pp. 4221-4227, Nov. 2004.
- [132] Liqiang J., Dejun W., Baiqi W., Shudan L., Baifu X., Honggang F., Jiazhong S., “*Effects of noble metal modification on surface oxygen composition, charge separation and photocatalytic activity of ZnO nanoparticles*”, *Journal of Molecular Catalysis A: Chemical*, vol. 244(1), pp. 193-200, Feb. 2006.
- [133] Bera A., Basak D., “*Pd-nanoparticle-decorated ZnO nanowires: ultraviolet photosensitivity and photoluminescence properties*”, *Nanotechnology*, vol. 22, pp. 265501(1-7), May 2011.
- [134] Kashif M., Ali M.E., Usman Ali S.M., Hashim U., Abd Hamid S.B., “*Impact of hydrogen concentrations on the impedance spectroscopic behavior of Pd-sensitized ZnO nanorods*”, *Nanoscale Research Letters*, vol. 8(68), pp. 1-9, 2013.
- [135] Lu Y., Li J., Han J., Ng H.T., Binder C., Partridge C., Meyyappan M., “*Room Temperature Methane Detection Using Palladium Loaded Single-Walled Carbon Nanotube Sensors*”, *Chemical Physics Letters*, vol. 391, pp. 344–348, Jun. 2004.
- [136] Wang D., Ma Z., Dai S., Liu J., Nie Z., Engelhard M.H., Kou R., “*Low-temperature synthesis of tunable mesoporous crystalline transition metal oxides and applications as Au catalyst supports*”, *The Journal of Physical Chemistry C*, vol. 112, pp. 13499-13509, Aug. 2008.
- [137] Tian J., Wang J., Hao J., Du H, Li X., “*Toluene sensing properties of porous Pd-loaded flower-like SnO<sub>2</sub> microspheres*”, *Sensors and Actuators B*, vol. 202, pp. 795–802, Jun. 2014.

## References

---

- [138] Haridas H., Chowdhuri H., Sreenivas H., Gupta V., “Enhanced LPG response characteristics of SnO<sub>2</sub> thin film based sensors loaded with Pt clusters”, International Journal On Smart Sensing And Intelligent Systems, vol. 2, pp. 503-514, Sep. 2009.
- [139] Sadek A.Z., Choopun S., Wlodarski W., Ippolito S.J., Kalantar-zadeh K., “Characterization of ZnO nanobelt-based gas sensor for H<sub>2</sub>, NO<sub>2</sub>, and hydrocarbon sensing”, Sensors, vol. 7(6), pp. 919-924, Jun. 2007.
- [140] Traversa E., Di Vona M.L., Licoccia S., Sacerdoti M., Carotta M.C., Crema L., Martinelli G., “Sol-gel processed TiO<sub>2</sub>-based nano-sized powders for use in thick-film gas sensors for atmospheric pollutant monitoring”, Journal of sol-gel science and technology, vol. 22(1-2), pp. 167-179, 2001.
- [141] Chaudhari G.N., Bambole D.R., Bodade A.B., Padole P.R., “Characterization of nanosized TiO<sub>2</sub> based H<sub>2</sub>S gas sensor”, Journal of materials science, vol. 41(15), pp. 4860-4864, May 2006.
- [142] Nitta M., Ohtani S., Haradome M., “Temperature dependence of resistivities of SnO<sub>2</sub>-based gas sensors exposed to CO, H<sub>2</sub>, and C<sub>3</sub>H<sub>8</sub> gases”, Journal of Electronic Materials, vol. 9(4), pp. 727-743, 1980.
- [143] Chekin F., “Sol-gel synthesis of palladium nanoparticles supported on reduced graphene oxide: an active electrocatalyst for hydrogen evolution reaction”, Bulletin of Materials Science, vol. 38(4), pp. 887-893, Aug. 2015.
- [144] Chen D.H., He X.R., “Synthesis of nickel ferrite nanoparticles by sol-gel method”, Materials Research Bulletin, vol. 36(7), pp. 1369-1377, Jun. 2001
- [145] Vafae M., Ghamsari M.S., “Preparation and characterization of ZnO nanoparticles by a novel sol-gel route”, Materials Letters, vol. 61(14), pp. 3265-3268, Dec. 2006.
- [146] Banerjee S., Loza K., Meyer-Zaika W., Prymak O., Epple M., “Structural evolution of silver nanoparticles during wet-chemical synthesis”, Chemistry of Materials, vol. 26(2), pp. 951-957, Jan. 2014.
- [147] Suresh S., “Wet chemical synthesis of Tin Sulfide nanoparticles and its characterization”, International Journal of Physical Sciences, vol. 9(17), pp. 380-385, Sep. 2014.

## References

---

- [148] Manikandan A., Kennedy L.J., Bououdina M., Vijaya J.J., “*Synthesis, optical and magnetic properties of pure and Co-doped ZnFe<sub>2</sub>O<sub>4</sub> nanoparticles by microwave combustion method*”, Journal of Magnetism and Magnetic Materials, vol. 349, pp. 249-258, Jan. 2014.
- [149] Franco A., de Oliveira Lima E.C., Novak M.A., Wells P. R., “*Synthesis of nanoparticles of Co<sub>x</sub>Fe<sub>(3-x)</sub>O<sub>4</sub> by combustion reaction method*”, Journal of magnetism and magnetic materials, vol. 308(2), pp. 198-202, Jan. 2007.
- [150] Lam C., Zhang Y.F., Tang Y.H., Lee C.S., Bello I., Lee S.T., “*Large-scale synthesis of ultrafine Si nanoparticles by ball milling*”, Journal of crystal growth, vol. 220(4), pp. 466-470, Dec. 2000.
- [151] Wang Y., Li Y., Rong C., Liu J.P., “*Sm–Co hard magnetic nanoparticles prepared by surfactant-assisted ball milling*”, Nanotechnology, vol. 18(46), 465701 (1-4), Oct. 2007.
- [152] Barth J.V., Costantini G., Kern K., “*Engineering atomic and molecular nanostructures at surfaces*”, Nature, vol. 437(7059), pp. 671-679, Sep. 2005.
- [153] Daraio C., Jin S., “*Synthesis and Patterning Methods for Nanostructures Useful for Biological Applications*”, Book chapter, Nanotechnology for Biology and Medicine, pp. 27-44, 2012.
- [154] Xiong Y., McLellan J.M., Chen J., Yin Y., Li Z.Y., Xia Y., “*Kinetically controlled synthesis of triangular and hexagonal nanoplates of palladium and their SPR/SERS Properties*”, Journal of American Chemical Society, vol. 127, pp. 17118-17127, 2005.
- [155] Nguyen V.L., Nguyen D.C., Hirata H., Ohtaki M., Hayakawa T., Nogami M., “*Chemical synthesis and characterization of palladium nanoparticles*”, Advances in Natural Sciences: Nanoscience and Nanotechnology, vol. 1, pp. 035012–035016, Nov. 2010.
- [156] Wang W., Cao G., “*Synthesis and structural investigation of Pd/Ag bimetallic nanoparticles prepared by the solvothermal method*”, Journal of Nanoparticle Research, vol. 9(6), pp. 1153-1161, Jan. 2007.

## References

---

- [157] Li D., Komarneni S., “*Nanoparticles of Pd: synthesis by microwave-solvothermal method and optical properties*”, *Journal of Nanoscience and Nanotechnology*, vol. 8(8), pp. 3930-3934, Aug.2008.
- [158] Nadagouda M.N., Varma R.S., “*Green synthesis of silver and palladium nanoparticles at room temperature using coffee and tea extract*”, *Green Chemistry*, vol. 10, pp. 859-862, Jul. 2008.
- [159] Ilias S.H., Kok K.Y., Ng I.K., Saidin N.U., “*Electrochemical Synthesis and Characterization of Palladium Nanostructures*”, *Journal of Physics: Conference Series*, vol. 431, pp. 012003 (1-6), 2013.
- [160] Deshmukh K.M., Qureshi Z.S., Bhatte K.D., Venkatesan K.A., Srinivasan T.G., Vasudeva Rao P.R., Bhanage B.M., “*One-pot electrochemical synthesis of palladium nanoparticles and their application in the Suzuki reaction*”, *New Journal of Chemistry*, vol. 35, pp. 2747-2751, 2011.
- [161] Zhang P., Sham T.K., “*Fabrication of thiol-capped Pd nanoparticles: An electrochemical method*”, *Applied Physics Letters*, vol. 82, pp.1778-1780, Mar. 2003.
- [162] Shendage S.S., Patil U.B., Nagarkar J.M., “*Electrochemical synthesis and characterization of palladium nanoparticles on nafion-graphene support and its application for Suzuki coupling reaction*”, *Tetrahedron letters*, vol. 54, pp. 3457-3461, Apr. 2013.
- [163] Guo P., Wei Z., Ye W., Qin W., Wang Q., Guo X., Lu C., Zhao X. S., “*Preparation and characterization of nanostructured Pd with high electrocatalytic activity*”, *Colloids and Surfaces A: Physicochemical and Engineering Aspects*, vol. 395, pp. 75-81, Feb. 2012.
- [164] Zhang H., Jin M., Xiong Y., Lim B., Xia Y., “*Shape-Controlled Synthesis of Pd Nanocrystals and Their Catalytic Applications*”, *Accounts of chemical research*, vol. 46(8), pp. 1783-1794, Nov. 2012.
- [165] Gugliotti L.A., Feldheim D.L., Eaton B.E., “*RNA-mediated metal-metal bond formation in the synthesis of hexagonal palladium nanoparticles*”, *Science*, vol. 304, pp. 850–852, 2004.

## References

---

- [166] Schlotterbeck U., Aymonier C., Thomann R., Hofmeister H., Tromp M., Richter-ing W., Mecking S., “*Shape-Selective Synthesis of Palladium Nanoparticles Stabilized by Highly Branched Amphiphilic Polymers*”, *Advanced Functional Materials*, vol. 14(10), pp. 999-1004, Oct. 2004.
- [167] Xiong Y., Chen J., Wiley B., Xia Y., Aloni S., Ying Y., “*Understanding the role of oxidative etching in the polyol synthesis of Pd nanoparticles with uniform shape and size*”, *Journal of American Chemical Society*, vol. 127, pp. 7332–7333, May 2005.
- [168] Niu W.X., Li Z.Y., Shi L.H., Liu X.Q., Li H.J., Han S., Chen J., Xu G.B., “*Seed-mediated growth of nearly monodisperse palladium nanocubes with controllable sizes*”, *Crystal Growth and Design*, vol. 8, pp. 4440–4444, Sep. 2008.
- [169] Lee Y.W., Kimab M., Han S.W., “*Shaping Pd nanocatalysts through the control of reaction sequence*”, *Chemical Communications*, vol. 46, pp. 1535–1537, Jan. 2010.
- [170] Park B.K., Jeong S., Kim D., Moon J., Lim S., Kim J.S., “*Synthesis and size control of monodisperse copper nanoparticles by polyol method*”, *Journal of colloid and interface science*, vol. 311(2), pp. 417-424, Jul. 2007.
- [171] Tsuji M., Hashimoto M., Nishizawa Y., Tsuji T., “*Synthesis of gold nanorods and nanowires by a microwave–polyol method*”, *Materials Letters*, vol. 58(17), pp. 2326-2330, Jul. 2004.
- [172] Kim D., Jeong S., Moon J., “*Synthesis of silver nanoparticles using the polyol process and the influence of precursor injection*”, *Nanotechnology*, vol. 17(16), pp. 4019-4024, Jul. 2006.
- [173] Chen J., Herricks T., Geissler M., Xia Y., “*Single-crystal nanowires of platinum can be synthesized by controlling the reaction rate of a polyol process*”, *Journal of the American Chemical Society*, vol. 126(35), pp. 10854-10855, Aug. 2004.
- [174] Chen J., Herricks T., Xia Y., “*Polyol synthesis of platinum nanostructures: control of morphology through the manipulation of reduction kinetics*”, *Angewandte Chemie*, vol. 117(17), pp. 2645-2648, Mar. 2005.

## References

---

- [175] Park B.K., Jeong S., Kim D., Moon J., Lim S., Kim J.S., “*Synthesis and size control of monodisperse copper nanoparticles by polyol method*”, Journal of colloid and interface science, vol. 311(2), pp. 417-424, Jul. 2007.
- [176] Banerjee S., Dasgupta K., Kumar A., Ruz P., Vishwanadh B., Joshi J.B., Sudarsan V., “*Comparative evaluation of hydrogen storage behavior of Pd doped carbon nanotubes prepared by wet impregnation and polyol methods*”, International Journal of Hydrogen Energy, vol. 40(8), pp. 3268-3276, Mar. 2015.
- [177] Kim S.K., Kim C., Lee J.H., Kim J., Lee H., Moon S.H., “*Performance of shape-controlled Pd nanoparticles in the selective hydrogenation of acetylene*”, Journal of Catalysis, vol. 306, pp. 146–154, Oct. 2013.
- [178] Cerritos R.C., Balcázar M.G., Ramírez R.F., García J.L., Arriaga L.G., “*Morphological Effect of Pd Catalyst on Ethanol Electro-Oxidation Reaction*”, Materials, vol. 5, pp. 1686-1697, Sep. 2012.
- [179] Hao D., Zhao S.X., Min S.C., Chao H., Chuan X.Z., Chen L., Yuan T., Ke, W. D., Jun G.H., “*Synthesis of monodisperse palladium nanocubes and their catalytic activity for methanol electrooxidation*”, Chinese Physics B, vol. 19(10), pp. 106104 (1-5), 2010.
- [180] Sun Y., Frenkel A.I., Isseroff R., Shonbrun C., Forman M., Shin K., Koga T., White H., Zhang L., Zhu Y., Rafailovich M. H., Sokolov J.C., “*Characterization of Palladium Nanoparticles by Using X-ray Reflectivity, EXAFS, and Electron Microscopy*”, Langmuir, vol. 22, pp. 807-816, Dec. 2005.
- [181] Lin R., Freemantle R.G., Kelly N.M., Fielitz T.R., Obare S.O., Ofoli R.Y., “*In situ immobilization of palladium nanoparticles in microfluidic reactors and assessment of their catalytic activity*”, Nanotechnology, vol. 21, pp. 325605 (1-8), Jul. 2010.
- [182] Xu L., Wu X.C., Zhu J.J., “*Green preparation and catalytic application of Pd nanoparticles*”, Nanotechnology, vol. 19, pp. 305603 (1-6), Jun. 2008.
- [183] Wu M.L., Chen D.H., Huang T.C., “*Preparation of Pd/Pt bimetallic nanoparticles in water/AOT/isooctane microemulsions*”, Journal of Colloid and Interface Science, vol. 243(1), pp. 102-108, Nov. 2001.

## References

---

- [184] Yuan Z., Jiang D., Naftel S.J., Sham T.K., Puddephatt R.J., “*Dimethylpalladium(II) Complexes as Precursors for Chemical Vapor Deposition of Palladium*”, *Chemistry of Materials*, vol. 6 (11), pp. 2151–2158, Nov. 1994.
- [185] Panigrahi S., Kundu S., Ghosh S., Nath S., Pal T., “*General method of synthesis for metal nanoparticles*”, *Journal of nanoparticle Research*, vol. 6(4), pp. 411-414, 2004.
- [186] Vancova M., Slouf M., Langhans J., Pavlova E., Nebesarova J., “*Application of colloidal palladium nanoparticles for labeling in electron microscopy*”, *Microscopy and Microanalysis*, vol. 17(05), pp. 810-816, Sep.2011.
- [187] He G., Song Y., Kang X., Chen S., “*Alkyne-functionalized palladium nanoparticles: Synthesis, characterization, and electrocatalytic activity in ethylene glycol oxidation*”, *Electrochimica Acta*, vol. 94, pp. 98–103, Apr. 2013.
- [188] Li J.G., Tsai C.Y., Kuo S.W., “*Fabrication and Characterization of Inorganic Silver and Palladium Nanostructures within Hexagonal Cylindrical Channels of Mesoporous Carbon*”, *Polymers*, vol. 6, pp. 1794-1809, Jun. 2014.
- [189] Jana N.R., Wang Z.L., Pal T., “*Redox Catalytic Properties of Palladium Nanoparticles: Surfactant and Electron Donor-Acceptor Effects*”, *Langmuir*, vol. 16, pp. 2457-2463, Feb. 2000.
- [190] Lu W., Wang B., Wang K., Wang X., Hou J.G., “*Synthesis and characterization of crystalline and amorphous palladium nanoparticles*”, *Langmuir*, vol. 19, pp. 5887-5891, May 2003.
- [191] Cookson J., “*The Preparation of Palladium Nanoparticles*”, *Platinum Metals Review*, vol. 56 (2), pp. 83–98, 2012.
- [192] Hankare P.P., Mali A.V., Burungale S.H., Delekar S.D., Garadkar K.M., “*Synthesis, characterization and application of eco-friendly and recyclable heterogeneous palladium catalyst*”, *Journal of Chemical & Pharmaceutical Research*, vol. 6(2), pp. 668-672, 2014.
- [193] Shen X.S., Wang G.Z., Hong X., Zhu W., “*Shape-controlled synthesis of palladium nanoparticles and their SPR/SERS properties*”, *Chinese Journal of Chemical Physics*, vol. 22(4), pp. 440-446, 2009.



## References

---

- [194] Cargnello M., Wieder N. L., Canton P., Montini T., Giambastiani G., Benedetti A., Raymond J. Gorte, Fornasiero P., “*A versatile approach to the synthesis of functionalized thiol-protected palladium nanoparticles*”, *Chemistry of Materials*, vol. 23(17), pp. 3961-3969, Aug. 2011.
- [195] Chen S., Huang K., Stearns J.A., “*Alkanethiolate-protected palladium nanoparticles*”, *Chemistry of materials*, vol. 12(2), pp. 540-547, Jan. 2000.
- [196] Rai P., Yu Y.T., “*Citrate-Assisted One-Pot Assembly of Palladium Nanoparticles onto ZnO Nanorods for CO Sensing Application*”, *Materials Chemistry and Physics*, vol. 142, pp. 545–548, 2013.
- [197] Xiong Y., Chen J., Wiley B., Xia Y., Aloni S., Yin Y., “*Understanding the role of oxidative etching in the polyol synthesis of Pd nanoparticles with uniform shape and size*”, *Journal of the American Chemical Society*, vol. 127(20), pp. 7332-7333, May 2005.
- [198] Ghosh S.K., Pal T., “*Interparticle coupling effect on the surface plasmon resonance of gold nanoparticles: from theory to applications*”, *Chemical Reviews*, vol. 107(11), pp. 4797-4862, Nov. 2007.
- [199] Haes A.J., Van Duyne R.P., “*A nanoscale optical biosensor: sensitivity and selectivity of an approach based on the localized surface plasmon resonance spectroscopy of triangular silver nanoparticles*”, *Journal of the American Chemical Society*, vol. 124(35), pp. 10596-10604, Aug. 2002.
- [200] Xiong Y., Chen J., Wiley B., Xia Y., Yin Y., Li Z.Y., “*Size-dependence of surface plasmon resonance and oxidation for Pd nanocubes synthesized via a seed etching process*”, *Nano letters*, vol. 5(7), pp. 1237-1242, Jun. 2005.
- [201] Willets K.A., Van Duyne R.P., “*Localized surface plasmon resonance spectroscopy and sensing*”, *Annual Review of Physical Chemistry*, vol. 58, pp. 267-297, May 2007.
- [202] Zeng S., Yu X., Law W. C., Zhang Y., Hu R., Dinh X. Q., Ho-Pui Ho, Yong K. T., “*Size dependence of Au NP-enhanced surface plasmon resonance based on*

## References

---

- differential phase measurement*”, Sensors and Actuators B: Chemical, vol. 176, pp. 1128-1133, Jan. 2013.
- [203] Xomeritakis G., Lin Y.S., “*CVD synthesis and gas permeation properties of thin palladium/alumina membranes*” American Institute of chemical Engineers, vol. 44 (1), pp. 174–183, Jan. 1998
- [204] Seo H.K., Ansari S.G., Al-Deyab S.S., Ansari Z.A., “*Glucose sensing characteristics of Pd-doped tin oxide thin films deposited by plasma enhanced CVD*”, Sensors and Actuators B: Chemical, vol. 168, pp. 149–155, Jun. 2012.
- [205] Korotcenkov G., Brinzari V., Boris Y., Ivanov M., Schwank J., Morante J., “*Influence of surface Pd doping on gas sensing characteristics of SnO<sub>2</sub> thin films deposited by spray pyrolysis*”, Thin Solid Films, vol. 436(1), pp. 119-126, Jul. 2003.
- [206] Kordas K., Leppavuori S., Uusimaki A., George T.F., Nanai L., Vajtai R., Bali K., Bekesi J., “*Palladium thin film deposition on polyimide by CW Ar<sup>+</sup> laser radiation for electroless copper plating*”, Thin Solid Films, vol. 384(2), pp. 185-188, Mar. 2001.
- [207] Ilias S., Su N., Udo-Aka U.I., King F.G., “*Application of electroless deposited thin-film palladium composite membrane in hydrogen separation*”, Separation science and technology, vol. 32(1-4), pp. 487-504, 1997.
- [208] Weber M.J., Mackus A.J., Verheijen M.A., Longo V., Bol A.A., Kessels W.M., “*Atomic layer deposition of high-purity palladium films from Pd(hfac)<sub>2</sub> and H<sub>2</sub> and O<sub>2</sub> plasmas*”, The Journal of Physical Chemistry C, vol. 118(16), pp. 8702-8711, Apr. 2014.
- [209] Kapica R., Redzyna W., Tyczkowski J., “*Characterization of Palladium-based Thin Films Prepared by Plasma-enhanced Metalorganic Chemical Vapor Deposition*”, Materials Science, 18(2), 128-131, 2012.
- [210] Ten Eyck G.A., Senkevich J.J., Tang F., Liu D., Pimanpang S., Karaback T., Wang G.C., Lu T.M., Jezewski C., Lanford W.A., “*Plasma-Assisted Atomic Layer Deposition of Palladium*”, Chemical Vapor Deposition, vol. 11, pp. 60-66, Jan. 2005.
- [211] Al-zaidi Q.G., Suhail A.M., Al-azawi W.R., “*Palladium-doped ZnO thin film hydrogen gas sensor*”, Applied Physics Research, vol. 3(1), pp. 89-99, May 2011.

## References

---

- [212] Patil K.R., Hwang Y.K., Kim M.J., Chang J.S., Park S.E., “*Preparation of thin films comprising palladium nanoparticles by a solid–liquid interface reaction technique*”, Journal of colloid and interface science, vol. 276(2), pp. 333-338, Aug. 2004.
- [213] Zhao H.B., Xiong G.X., Baron G.V., “*Preparation and characterization of palladium-based composite membranes by electroless plating and magnetron sputtering*”, Catalysis Today, vol. 56, pp. 89–96, Feb. 2000.
- [214] Salcedo K.L., Rodríguez C.A., Perez F.A., Riascos H., “*Morphological Study of Palladium Thin Films Deposited By Sputtering*”, Journal of Physics: Conference Series, vol. 274, pp.012120-012126, 2011.
- [215] Joshi R.K., Krishnan S., Yoshimura M., Kumar A., “*Pd nanoparticles and thin films for room temperature hydrogen sensor*”, Nanoscale research letters, vol. 4(10), pp. 1191-1196, Oct. 2009.
- [216] Vicinanza N., Svenum I.H., Naess L.N., Peters T.A., Bredesen R., Borg A., Venvik H.J., “*Thickness dependent effects of solubility and surface phenomena on the hydrogen transport properties of sputtered Pd77% Ag23% thin film membranes*”, Journal of Membrane Science, vol. 476, pp. 602-608, Feb. 2015.
- [217] Samavat F., Mahmoodi F., Ahmad P.T., Samavat M.F., Tavakoli M.H., Hadidchi S., “*Effect of Annealing Temperature on the Optical Properties of Palladium Thin Film*”, Open Journal of Physical Chemistry, vol. 2, pp. 103-106, May 2012.
- [218] Singh U., Jha N., Kapoor A., “*Characterization of Palladium thin film deposited by pulsed laser deposition*”, International Conference on Applications of Optics and Photonics, International Society for Optics and Photonics, pp. 80010W-80010W, May 2011.
- [219] Ramírez L.A., Feroa Y., Rodríguez D., Otaño W., Cabrera C.R., “*Palladium Nanostructures Synthesis by Sputtering Deposition on HOPG Surface*”, ECS Transactions, vol. 28(7), pp. 1-7, 2010.
- [220] Charles Kittel, “*Introduction to solid state physics*”, edition 8, John Wiley & sons, pp.40-41

## References

---

- [221] Mote V.D., Purushotham Y., Dole B.N., “*Williamson-Hall analysis in estimation of lattice strain in nanometer-sized ZnO particles*”, Journal of Theoretical and Applied Physics, vol. 6(1), pp. 1-8, Jul. 2012.
- [222] Monshi A., Foroughi M. R., Monshi M.R., “*Modified Scherrer equation to estimate more accurately nano-crystallite size using XRD*”, World Journal of Nano Science and Engineering, vol. 2(03), pp. 154, Sep. 2012.
- [223] Seo J.K., Ko K.H., Cho H.J., Choi W.S., “*Synthesis and Characterization of Al-Doped Zinc Oxide Films by an Radio Frequency Magnetron Sputtering Method for Transparent Electrode Applications*”, Transactions on Electrical And Electronic Materials, vol. 11(1), pp. 29-32, Feb. 2010.
- [224] Lee H.S., Lee J.Y., Kim T.W., Kim D.W., Cho W.J., “*Formation mechanism of preferential c-axis oriented ZnO thin films grown on p-Si substrates*”, Journal of Materials Science, vol. 39(10), pp. 3525-3528, May 2004.
- [225] Lu J.G., Ye Z.Z., Zeng Y.J., Zhu L.P., Wang L., Yuan J., Zhao B.H., Liang Q.L., “*Structural, optical, and electrical properties of (Zn,Al)O films over a wide range of compositions*”, Journal of Applied Physics, vol. 100, pp. 073714 (1-11), 2006.
- [226] Pocuca M., Brankovic Z., Brankovic G., Vasiljevic-radovic D., “*Influence of substrate orientation on the morphology and orientation of LaNiO<sub>3</sub> thin films*”, Journal of microscopy, vol. 232(3), pp. 585-588, Nov. 2008.
- [227] Schuster F., Weisz S., Hetzl M., Winnerl A., Garrido J.A., Stutzmann M., “*Influence of substrate material, orientation, and surface termination on GaN nanowire growth*”, Journal Applied Physics, vol. 116, pp. 054301, Aug. 2014.
- [228] Beck G., Bachmann C., Bretzler R., Kmeth R., “*Epitaxial and non-epitaxial platinum, palladium and silver films on yttrium-stabilised zirconia*”, Materials Chemistry and Physics, vol. 158, pp. 107–114, May 2015.
- [229] Yalamanchili K., Kostanic I.N., Nazer M., Pozo de Fernandez M., McCay M.H. “*Electrical and optical responsivity of thin palladium films during hydrogen exposure*”, In MRS Proceedings, vol. 1098, pp. 1098-HH08, Cambridge University Press, Jan. 2008.

## References

---

- [230] Velásquez P., Castañer R., de la Casa-Lillo M.A., Sánchez-López M.M., Mallavia R., Moreno I., Gutiérrez A., Mateos F., "*Surface and optical characterization of yttrium hydride films deposited on regular glass to be used as switchable mirrors*", *Surface and interface analysis*, vol. 34(1), pp. 311-315, Aug. 2002.
- [231] Cavalcanti G.O., Fontana E., Oliveira S.C., "*Hydrogen detection using surface plasmon resonance in palladium films*", In *Microwave and Optoelectronics Conference (IMOC), 2009 SBMO/IEEE MTT-S International*, pp. 312-315, Nov. 2009.
- [232] Shin K.S., Cho Y.K., Kim K.L., Kim K., "*Electroless Deposition and Surface-Enhanced Raman Scattering Application of Palladium Thin Films on Glass Substrates*", *Bull. Korean Chem. Soc*, vol. 35(3), pp. 743, 2014.
- [233] Kürschner J., Wagner S., Pundt A., "*Delamination-supported growth of hydrides in Pd thin films studied by electrochemical hydrogenography*", *Journal of Alloys and Compounds*, vol. 593, pp. 87-92, Apr. 2014.
- [234] Wagner S., Pundt A., "*Conduction mechanisms during the growth of Pd thin films: Experiment and model*", *Physical Review B*, vol. 78(15), pp. 155131, Oct. 2008.
- [235] Yoshimura K., Nakano S., Uchinashi S., Yamaura S., Kimura H., Inoue A., "*A hydrogen sensor based on Mg-Pd alloy thin film*" *Measurement science and technology*, vol. 18(11), pp. 3335, Sep. 2007.
- [236] Ruffino F., Grimaldi M.G., "*Island-to-percolation transition during the room-temperature growth of sputtered nanoscale Pd films on hexagonal SiC*", *Journal of Applied Physics*, vol. 107(7), pp. 074301, Apr. 2010.
- [237] Joshi, R.K., Krishnan, S., Yoshimura, M., & Kumar, A., "*Pd nanoparticles and thin films for room temperature hydrogen sensor*", *Nanoscale research letters*, vol. 4(10), pp. 1191-1196, Jul. 2009.
- [238] Siviero G., Bello V., Mattei G., Mazzoldi P., Battaglin G., Bazzanella N., Checchetto R., Miotello A., "*Structural evolution of Pd-capped Mg thin films under H<sub>2</sub> absorption and desorption cycles*", *International Journal of Hydrogen Energy*, vol. 34(11), pp. 4817-4826, 2009.

## References

---

- [239] England C.D., Engel B. N., Falco C.M., “*Preparation and structural characterization of epitaxial Co/Pd (111) superlattices*”, Journal of Applied Physics, vol. 69(8), pp. 5310-5312, Apr. 1991.
- [240] Keuler J.N., Lorenzen L., “*Developing a heating procedure to optimise hydrogen permeance through Pd-Ag membranes of thickness less than 2.2  $\mu\text{m}$* ”, Journal of Membrane Science, vol. 195(2), pp. 203-213, Jan. 2002.
- [241] Sun G.B., Hidajat K., Kawi S., “*Ultra thin Pd membrane on  $\gamma\text{-Al}_2\text{O}_3$  hollow fiber by electroless plating: high permeance and selectivity*”, Journal of membrane science, vol. 284(1), pp. 110-119, Nov. 2006.
- [242] Noh J.S., Lee J.M., Lee W., “*Low-Dimensional Palladium Nanostructures for Fast and Reliable Hydrogen Gas Detection*”, Sensors, vol. 11, pp. 825-851, Jan. 2011.
- [243] Kumar R., Varandani D., Mehta B.R., Singh V.N., Wen Z., Feng X., Mullen K., “*Fast response and recovery of hydrogen sensing in Pd-Pt nanoparticle-graphene composite layers*”, Nanotechnology, vol. 22, pp. 275719(1-7), May 2011.
- [244] Johansson M., Skúlason E., Nielsen G., Murphy S., Nielsen R.M., Chorkendorff I., “*Hydrogen adsorption on palladium and palladium hydride at 1 bar*”, Surface Science, vol. 604, pp. 718-729, Feb. 2010.
- [245] Flanagan T.B., Oates W.A., “*The Palladium-Hydrogen System*”, Annual Review of Materials Science, vol. 21, pp 269-304, Aug. 1991.
- [246] Zhao M., Nagata S., Shikama T., Inouye A., Yamamoto S., & Yoshikawa M., “*Surface electronic properties of discontinuous Pd films during hydrogen exposure*”, Japanese Journal of Applied Physics, vol. 50, pp. 01BE08 (1-4), Jan. 2011.
- [247] Brittin W.E., “*Valence angle of the tetrahedral carbon atom.*” Journal of Chemical Education, vol. 22, pp. 145, 1945.
- [248] Afanasyeva V.A., Glinskaya L.A., Klevtsova R.F., Sheludyakova L.A., “*Crystal and molecular structure of  $[\text{Au}(\text{Cl}_4\text{H}_2\text{N}_4)][\text{H}_3\text{O}](\text{ClO}_4)_4$* ”, Journal of Structural Chemistry, vol. 46, pp. 131-136, 2005.

## References

---

- [249] Cao G., "Nanostructures and nanomaterials: Synthesis, properties and materials" Imperial College Press, pp. 18-20.
- [250] Huber H., Klotzbücher W., Ozin G.A., Vander Voet A., "Binary Dioxygen Complexes of Nickel, Palladium, and Platinum,  $M(O_2)$  and  $(O_2)M(O_2)$ , in Low Temperature Matrices", Canadian Journal of Chemistry, vol. 51, pp. 2722-2736, 1973.
- [251] Hall H., "The theory of photoelectric absorption for x-rays and  $\gamma$ -rays", Reviews of Modern Physics, vol. 8, pp. 358, 1936.
- [252] Ghetta V., "Materials issues for Generation IV systems" Springer, pp. 407-408.
- [253] Toth E.J., "Adsorption: Theory, Modeling, and Analysis", Marcel Dekker, Inc., New York, 2002.
- [254] Sips R., "On the structure of a catalyst surface", Journal of Chemical Physics, vol. 18, pp. 1024, 1950.
- [255] Chen X., "Modeling of Experimental Adsorption Isotherm Data", Information, vol. 6(1), pp. 14-22, Jan. 2015.
- [256] A book by Rummel R.J., "Understanding correlation", Department of Political Science, University of Hawaii, Chapter 3, 1976.
- [257] Lohninger H., "Teach/Me Data Analysis", Springer-Verlag, Berlin-New York-Tokyo, 1999, ISBN 3-540-14743-8.

## LIST OF PUBLICATIONS

### International Journals:

1. **D.Gupta**, D.Dutta, M. Kumar, P.B. Barman, C.K. Sarkar, S. Basu, S.K.Hazra, “A low temperature hydrogen sensor based on palladium nanoparticles” *Sensors and Actuators B* **196** (2014) 215-222.
2. **D.Gupta**, D.Dutta, M.Kumar, P.B. Barman, T.Som, S.K.Hazra, “Temperature dependent dual hydrogen sensor response of Pd nanoparticle decorated Al doped ZnO surfaces” *Journal of Applied Physics* **118** (2015) 164501(8pp)
3. **D.Gupta**, D.Dutta, P.B.Barman, S.Basu, S.K. Hazra, “A review on palladium with low dimensional configurations for chemical gas sensor applications” *Sensor Letters* **14** (2016) 211-233.

### Conferences (National/International):

1. **D.Gupta**, P.B.Barman, and S.K.Hazra, “Hydrogen response of porous palladium nano-films” Advanced Materials and Radiation Physics (AMRP-2015): 4th National Conference on Advanced Materials and Radiation Physics, 1675, *AIP Publishing*, 2015.
2. **D.Gupta**, P.B.Barman, S.K.Hazra, “Effect of silver on the shape of palladium nanoparticles” International conference on condensed matter physics (ICC-2015)
3. **D.Gupta**, P.B.Barman, S.K.Hazra, “Synthesis of palladium nanoparticles for selective hydrogen sensing” Abstract accepted in international conference on Electron Microscope Society of India (EMSI-2014)